Title
Engineering and Reverse Engineering of the Yeast Regulatory Network

Author
Mace, Kieran George

Publication Date
2021

Peer reviewed|Thesis/dissertation

Engineering and Reverse Engineering of the Yeast Regulatory Network

by
Kieran Mace

DISSERTATION
Submitted in partial satisfaction of the requirements for degree of
DOCTOR OF PHILOSOPHY

in

Biological and Medical Informatics

in the

GRADUATE DIVISION
of the
UNIVERSITY OF CALIFORNIA, SAN FRANCISCO

Approved:

DocuSigned by:
Hana El-Samad
52F8E320792C4C4...

Hana El-Samad

Chair

DocuSigned by:
David Pincus
DocuSigned by:4F2...

David Pincus

DocuSigned by:
Matt Thomson
DocuSigned by:4B...

Matt Thomson

DocuSigned by:
Joe DeRisi
50AE848EEDE2449...

Joe DeRisi

Committee Members

Acknowledgements

I have received a great deal of support and assistance throughout the writing of this dissertation.

I would first like to thank my supervisor Professor Hana El-Samad whose expertise was invaluable in formulating the research questions and methodology. Your insightful feedback pushed me to sharpen my thinking and brought my work to a higher level. Thank you for inspiring me to “really prove” things. Before your mentorship, I was often satisfied with an approximate answer to questions. You taught me what it really means to have scientific rigor.

I would also like to thank my mentor, thesis committee member, and friend Professor David Pincus who inspired me to take on a second project, stayed up with me for many late nights to get our experiments working, and provided incredible guidance in experimental design and scientific reporting. I could not have done this without you.

I am also thankful for my thesis committee members Professor Joe DeRisi and Matt Thomson who offered valuable guidance throughout my studies. You provided me with the tools I needed to choose the right direction and successfully complete my dissertation. Thank you for the constant motivation and for your belief in me. It carried me through the hardest hours.

I also would like to thank other professors and administrators for giving me the guidance I needed to navigate graduate school, especially Leor Weinberger, Tanja Kortemme, Patricia Babbitt, Ryan Hernandez, Julia Molla, and Rebecca Dawson.

In addition, I would like to acknowledge my colleagues from my lab and program. Getting a PhD is challenging, and your friendship, encouragement, and support carried me when I was at a loss. Thanks to Andrés Aranda-Díaz, Ignacio Zuleta, Lucien Bogar, Ophelia Venturelli, and Patrick Harrigan for teaching me about synthetic biology, cloning, automation, and wet lab work. Chapter 2 of this work is a reprint of a paper of which Andrés is a co-first author. Thank you to Raj Bhatnagar, Graham Heimberg, and Mike Chevalier for helping me think deeply about systems biology, gene expression, and mathematical modeling. Thanks to Susan Chen, Alain Bonny, João Fonseca and Ben Heineike for teaching me about yeast and microscopy and RNA-seq. Thank you to Pradeep Bandaru, Brian O'Donovan, John Hawkins, Veronica Pessino, and Christina Homer for being amazing friends.

Finally, I would like to thank my family for their love, support, and wise counsel. Specifically, I want to recognize my incredible wife Katie, brother and best friend Connor, loving and supporting parents Michele, Nicholas, Deidre, and David, and my newly born daughter Arden. You have and always will be there for me. You are the best part of my life. I love you all.

Contributions

Chapter 2 contains reprinted or adapted material from the following previously published manuscript:

Aranda-Díaz A, Mace K, Zuleta I, Harrigan P, El-Samad H. Robust Synthetic Circuits for Two-Dimensional Control of Gene Expression in Yeast. ACS Synth Biol. 2017 Mar 17;6(3):545-554. doi: 10.1021/acssynbio.6b00251. Epub 2016 Dec 27. PMID: 27930885; PMCID: PMC5507677.

Chapter 3 contains reprinted or adapted material from the following previously published manuscript:

Mace K, Krakowiak J, El-Samad H, Pincus D (2020) Multi-kinase control of environmental stress responsive transcription. PLOS ONE 15(3): e0230246. https://doi.org/10.1371/journal.pone.0230246

Engineering and Reverse Engineering of the Yeast Regulatory Network

Kieran Mace

Abstract

Complex emergent biological behavior requires coordinated activity among an entire genome's biomolecules. Cells respond to changes in environmental conditions by activating signaling pathways and gene expression programs to maintain homeostasis. Here, we first present a synthetic tool that can either dynamically regulate the expression levels of two genes independently or regulate the log mean and variance of a single gene's expression. We then present the use of similar tools to perturb and produce a large dataset of perturbed, whole genome, gene expression measurements to explore the relationship between environmental stresses, kinase signaling, and global gene expression in *S. Cerevisiae*. With these data, we reconstructed canonical stress pathways, identified examples of crosstalk among pathways, and implicated numerous kinases in novel environment-specific roles. Specifically, we investigated how individual kinases tuned the magnitude of induction of the environmental stress response (ESR) in environment-specific ways. Our findings suggest that the ESR integrates inputs from multiple sensory kinases to modulate gene expression and growth control.

Table of Contents

List of Figures

List of Tables

List of Abbreviations

AD: activation domain

DBD: DNA binding domain

hER: human estrogen receptor

hPR: human progesterone receptor

LBD: lipid binding domain

TR: transcriptional regulator

YFP: yellow fluorescent protein.

Chapter 1

Introduction

Emergent behavior occurs when relatively simple entities interact in a system to produce complex phenomena unrevealed at the level of the individual entity. Many fields are dedicated to investigating emergent behavior from complex systems, including ecology (species), anthropology and sociology (humans), physiology (organs), morphology (cells), and neurology (neurons). This dissertation focuses on systems biology, a domain of complex biological systems, defined here as the study of subcellular systems in which distinct biomolecular entities, such as genes and proteins, interact to produce an emergent behavior or functionality at the level of the cell.

Among the many functions a cell routinely performs (such as cell division, structural integrity, motility, metabolism, etc), here we focus on the homeostatic gene regulatory pathways of the model organism Saccharomyces Cerevisiae (budding yeast). Homeostasis can be defined as the optimal internal physiological state for a cell to function (live). Deviations from homeostasis can cause significant issues for the cell's growth rate, and major deviations outside of the homeostatic range may result in cell death. Stress occurs when the external environment challenges a cell's homeostasis. All organisms have evolved behaviors and abilities to adapt to and mitigate the effects of environmental stress (and therefore maintain homeostasis). This set of behaviors is generally referred to as the stress response. As a relatively immotile single-celled

organism, yeast cannot evade environmental stress and therefore must resist stress by modifying its internal physiology. Examples of such modification include producing more protein chaperones in high temperatures to maintain protein integrity, storing glycogen, synthesizing glycerol, synthesizing salt pumps in hyperosmotic environments to maintain osmolarity, and slowing growth and increasing glucose absorption when carbon sources are limited to maintain overall metabolism.

A cell's internal physiology can be changed by altering the relative abundance of genes and their associated proteins inside the cell. This change in relative protein composition allows the cell to allocate appropriate focus to the biological processes most relevant to tasks at hand (maintaining homeostasis, survival, growth, etc.). The mechanism that produces gene transcripts (RNA) from the hereditary material (DNA) is called transcription or gene expression, and the cell's ability to dynamically tune each gene's relative abundance is called gene regulation. A modern sequencing technology known as RNA-seq and the computational techniques collectively called bioinformatics have made it possible to routinely assess the relative activity of genes inside a population of cells. Fortunately, previous research has provided functional descriptions to for majority of yeast genes, making it one of the best understood species in biology, making it a great candidate for genetic modification and engineering.

In order to support, refute, or validate a scientific hypothesis, scientists must conduct experiments to gather data and compare findings against competing hypotheses. Studies can be subdivided into two forms – observational studies, where data is passively collected, and experimental studies, where the scientist administers some treatment or perturbation and collects the data resulting from that perturbation. While

observational studies have great strengths, they lack the ability to cleanly demonstrate causation due to confounding factors. We utilize synthetic biological circuits as a mechanism to create perturbations in biological systems, which is critical in determining causal associations between biomolecules and emergent cellular phenomena.

In Chapter 2 we develop synthetic modules that use different arrangements of two transcriptional regulators to achieve either concurrent and independent control of the expression of two genes, or decoupled control of the mean and variance of a single gene. We use these modules to perturb the expression levels of the cell cycle gene SIC1. In Chapter 3 we inactivate kinase signaling pathways in the context of various environmental stresses to determine their contribution in activating the transcriptional stress response, identifying novel interactions between kinases and operons.

Chapter 2

Robust Synthetic Circuits for Two-Dimensional Control of Gene Expression in Yeast

2.1 ABSTRACT

Cellular phenotypes are the result of complex interactions between many components. Understanding and predicting the system level properties of the resulting networks requires the development of perturbation tools that can simultaneously and independently modulate multiple cellular variables. Here, we develop synthetic modules that use different arrangements of two transcriptional regulators to achieve either concurrent and independent control of the expression of two genes, or decoupled control of the mean and variance of a single gene. These modules constitute powerful tools to probe the quantitative attributes of network wiring and function.

2.2 INTRODUCTION

Functional outputs of cellular networks rely on intricate interactions between their component genes and proteins. A systems-level understanding of the operation of these networks requires probing the individual roles of these components and then mapping their quantitative interactions.

Assessing the roles of individual genes has traditionally relied on gene deletions, knockdowns, and over expression. Combinatorial perturbations of mean gene expression, such as genome-wide epistasis studies based on deletions[1] and knockdowns[2] have led to important discoveries about the relationship between different genes and their concerted impact on functional phenotypes. These technologies are very informative about the specific arrangements of these genes with respect to each other in a network (e.g. their position in series or in parallel) and their involvement in particular biological processes (such as membership in a macromolecular complex). However, this information is often insufficient to predict how perturbations of these genes, especially concurrent perturbations, quantitatively affect network output or complex activity. To do so, technologies that provide simultaneous, graded and independent perturbations to multiple genes are needed[3,4].

Methods for graded perturbations of single genes include synthetic hormone inducible transcription circuits[5–8], repurposed bacterial systems[9–12], yeast galactose-inducible promoters[13] and plant-derived light-inducible transcription factors[14,15]. These technologies perturb the mean expression of a gene under study and conclusions are drawn from the ensuing changes in the mean behavior of a functional phenotype.

However, single cell studies have indicated that cell-to-cell variability, or noise[16,17], in gene expression has dramatic relevance to many phenotypes in a variety of biological systems[18–23]. Systematic mapping of the contribution of noise in a given gene to network function has awaited the development of perturbation methods to simultaneously and independently control the mean and variance of gene expression.

Mutations in promoters[24,25] and ribosome competing RNAs[26] allow for modulation of noise but not independently from the mean, with low noise levels correlating with high mean expression levels[24]. Strategies that achieve different noise levels for the same mean include propagating noise through transcriptional cascades[27,28]. While successful, these approaches do not provide the flexibility needed to achieve the desired quantitative, predictable, tunable and dynamical noise modulation. A system with such properties has only been described in bacteria by modulating bias and frequency of a genetic switch[29].

In this work, we demonstrate how different arrangements of two simple inducible synthetic Transcriptional Regulators (TRs) can address the challenges of dual gene activation, as well as mean and variance control of gene expression. Specifically, two inducible TRs arranged *in parallel* can drive the simultaneous and independent expression of two genes, while their arrangement *in series* can decouple mean and variability of a single gene in a substantial dynamic range. Together, these circuits provide a versatile and robust technology to elucidate the quantitative relationships between genes and the causal impact of their expression noise on cellular function.

2.3 RESULTS

2.3.1 A 2D-parallel circuit is a quantitative tool for simultaneously perturbing two cellular variables

The inducible activation of human hormone receptors has been previously exploited to modulate the activity of synthetic TRs in mammalian cell lines. In these constructs, the ligand binding domain (LBD) of either the human estradiol[30] or progesterone[31,32]

receptors (hER and hPR, respectively) is fused to the Gal4p DNA binding domain (GAL4-DBD) and to the viral VP16 activation domain. Both the apo-receptor and the ligand-bound TRs interact with Hsp90 and other auxiliary proteins, which regulate the nuclear localization and activity of the TR[33,34]. In the absence of hormone, the TRs are localized in the cytoplasm. When the inducing hormone binds the LBD of one of these chimeric TRs, the complex translocates to the nucleus and controls expression from promoters containing Gal4p binding sites[6]. An estradiol-responsive variant of these TRs has also been implemented in *S. cerevisiae*[5–8] to control the galactose regulon. More recently, the Gal4p DBD was replaced by the DBD of the mouse transcription factor Zif268[35], successfully targeting the TR to only one promoter engineered to contain the corresponding binding motifs. These inducible circuits each provided quantitative graded control of the expression of one gene.

To simultaneously and independently control the expression level of two different genes, we constitutively expressed two chimeric TRs in the same cell. The first is an estradiol-responsive TR in which the GAL4-DBD is fused to the hER-LBD and the transcription factor Msn2p activation domain (MSN2-AD) (GEM, **Fig 2.1a, upper**). The second TR is a new recombinant protein consisting of the ZIF268-DBD, the hPR-LBD and the MSN2-AD (ZPM, **Fig 2.1a, bottom**). Estradiol-bound GEM translocates into the nucleus and binds and activates transcription from promoters that contain Gal4p binding sites, such as pGAL1, which contains four dimeric Gal4 binding sites[36,37]. Similarly, progesterone-bound ZPM activates transcription from pZ, a modified pGAL1 promoter containing three dimeric Zif268 binding sites but lacking Gal4p binding sites[35] (**Fig 2.1b, Supplementary Information**).

To characterize the dynamics of this 2D-parallel circuit, we used automated high-throughput flow cytometry[38] to monitor the time-resolved expression of a yellow fluorescent protein (YFP) under the transcriptional control of either pZ or pGAL1. We co-cultured two strains each containing both the GEM and ZPM constructs driving YFP. We could differentiate the two co-cultured strains by labeling the strain containing the pGAL1-YFP reporter with a constitutively expressed red fluorescent protein (mKate2) expressed from the TDH3 promoter (**Fig 2.1c**). In this scheme, we are able to control for well-to-well variability in hormone concentration and assess gene expression elicited by the two inducible TRs on equal footing using the same fluorescent protein.

In cultures stimulated with estradiol and progesterone, we observed exclusive and graded gene expression corresponding to action of the two TRs (**Fig 2.1d**), suggesting that there is little detectable cross-activation between the two systems. Cells containing both constructs, one driving expression of YFP and the other driving expression of mKate2 confirmed their simultaneous and independent operation (**Fig 2.4**). Furthermore, induction of either or both TRs activity did not cause any growth defects (**Supplementary Table 1**).

To quantify promoter activity, we calculated the expression rate of pGAL1-YFP and pZ-YFP as the growth-corrected change in fluorescence[38] (See **Methods**). The steady state expression rate of pGAL1-YFP as a function of estradiol shows that GEM activity has a graded dependence on estradiol and is largely independent of progesterone at all tested concentrations (**Fig 2.1e** and **Supplementary Fig 2.6 and 2.7, left panels**). Likewise, pZ-YFP expression rate at steady-state has graded dependence on progesterone and slight inhibition by estradiol at very high concentrations (**Fig 2.1f** and **Supplementary Fig**

2.6 and 2.7, right panels), consistent with previous observations on human hormone receptors [39].

Close examination of the outputs of the GEM and ZPM circuits indicated that ZPM achieves a higher steady state expression rate than GEM at saturating doses of the hormones (**Fig 2.1e-f and Supplementary Fig 2.8a**). Furthermore, ZPM reaches its maximal activity faster than GEM, as quantified by the time it takes to achieve half-maximum expression (**Supplementary Fig 2.8b-c**). These differences are quantitative but reproducible. In order to dissect the contribution of the different TR domains to these differences, we exchanged either the DBD or the LBD in the GEM construct. First, we replaced the GAL4-DBD with the ZIF268-DBD. This new chimeric TR (ZEM), which still responds to estradiol but now activates pZ-YFP expression, exhibited higher expression rates but similar activation times when compared to the original GEM construct (**Supplementary Fig 2.9**). Secondly, we replaced the hER-LBD with the hPR-LBD. This modified version of the GEM construct (GPM) is now responsive to progesterone, but activates pGAL1-YFP expression. GPM exhibited similar expression rates but faster responses when compared to the original GEM (**Supplementary Fig 2.10**). Taken together, these results suggest that the hormone-LBD pair is the major contributor to the differences in the timescale of induction, whereas the DBD-promoter pair is the major contributor to differences in maximal expression rate.

To characterize the 2D-parallel circuit under different operating conditions, we measured circuit output in three scenarios: varying cell densities, different growth media and time-varying induction levels. We found that as cell density increased over time, the expression rates of both ZPM and GEM slowly declined (**Supplementary Fig 2.11a-b**). By contrast,

when we matched the culture dilution rate to that of the population proliferation rate, thereby keeping the number of cells in the culture constant, the expression rates of both constructs remained constant for hours after the addition of hormone inputs (**Supplementary Fig 2.11c-d)**. In agreement, in a separate experiment, in cultures originally inoculated at different densities, GEM and ZPM also showed different expression rates for different densities, with decreasing expression with increasing density (**Supplementary Fig 2.12**). We next investigated the differential impact of growth in YPD versus minimal (SDC) media. In SDC, the 2D parallel circuit maintained inducibility and component independence, but exhibited a quantitatively different dose response than that in YPD (**Supplementary Fig 2.13**). These results highlight the quantitative dependence of this synthetic circuit on experimental conditions, a feature that is likely to hold for most synthetic constructs, therefore motivating their thorough characterizations under appropriate operating conditions for practical applications. Finally, we probed the ability of the 2D circuit to be switched off for applications that require a regulated pulse-like operation. In this experiment, we induced cultures with different estradiol and progesterone concentrations, and then washed out the hormones after 3.7 hours. We observed that the expression rates for both TR systems dropped to basal levels in approximately 2 hours, thereby demonstrating the reversibility of this system (**Supplementary Fig 2.14**). Taken together, these data demonstrate that the 2D-parallel circuit is tunable and reversible, as previously described for a single TR[6].

To demonstrate the capabilities of the 2D-parallel circuit, we used it to quantitatively map the dose dependent genetic interactions of positive and negative regulators of an endogenous cellular pathway, the yeast pheromone mating response, a canonical GPCR-

MAPK signaling cascade[40]. In this pathway, the binding of pheromone to a GPCR membrane receptor is transduced to the cell through a series of phosphorylation events that ultimately activate the transcription factor Ste12p and result in the subsequent expression of various proteins required for mating. Many regulators tune the activity of this pathway in a dose dependent fashion. Positive regulators include the beta-gamma subunit of the G protein, Ste4p[41], which recruits the MAPKs to the membrane to initiate the phosphorylation cascade. Negative regulators of the pathway include the transcriptional repressor Dig1p[42], which binds and inhibits Ste12p; the dual-specificity phosphatase, Msg5p[43], which dephosphorylates and deactivates the MAPK Fus3p; and the GTP-binding alpha subunit of the G protein, Gpa1p[44], which sequesters and inhibits Ste4p (**Fig 2.2a**).

We built a strain containing the ZPM TR in which progesterone induces expression of an extra copy of the STE4 gene from the pZ promoter. In the same strain, we also incorporated a GEM TR with pGAL1 driving the expression of one of the negative regulators Gpa1p, Msg5p or Dig1p (**Fig 2.2**). We modulated the expression of the positive/negative regulator pairs over a large combinatorial range by varying the concentrations of the two hormones (**Supplementary Fig. 2.15**). We then measured growth rate and mating pathway activity as quantified by YFP expression rates from the Ste12p-responsive promoter of AGA1 (pAGA1-YFP[45]).

Estradiol-dependent induction of Ste4p results in graded activation of the mating response[46]. Expression of Ste4p in our strains also induced pAGA1-YFP in a progesterone dose dependent fashion (**Fig 2.2 b-c, top panels**). We could inhibit this pathway activity elicited by Ste4p over-expression through induction of the negative

regulators, with quantitative effects that depended both on the identity of the regulator and the level of Ste4p expression. The two-dimensional dose responses were similar for MSG5 and GPA1 (MSG5-STE4 and GPA1-STE4), but were markedly different for DIG1 (DIG1-STE4). Specifically, Dig1p failed to efficiently overpower Ste4p positive action except at very high induction levels, whereas Msg5p and Gpa1p could exert marked inhibition at lower Ste4p levels (**Fig 2.2 b-d top panels**, see for example the estradiol dose response for P=4.44 nM).

Activation of the mating pathway slows growth through Far1p mediated cell cycle arrest[47]. Therefore, increasing Ste4p expression without over-expressing any of the negative regulators caused corresponding decrease in growth rate (**Fig 2.2 b-c, bottom panels**, 0 estradiol). Counter-balancing over-expression of Ste4p with over-expression of either Gpa1p or Msg5p had a favorable effect on growth, culminating in a recovery to normal growth rate at concentrations of the negative regulators that abolish signaling in the pathway as evidenced by recovery of pAGA1-YFP to pre-stimulus levels (**Fig 2.2 b-c, top and bottom panels**, see as an example P=10 nM and E=100nM). The increase in the growth rate coincided with estradiol concentrations where the negative regulators started exhibiting their inhibitory action, suggesting that growth recovery is likely resulting from decreased signaling in the mating pathway, and that lack of balanced signaling, rather than over-expression of the proteins themselves, is likely to be the major contributor to growth penalty upon over-expression of positive regulators.

Interestingly, however, expression of Gpa1p and Msg5p at concentrations below those needed to overcome Ste4 induced pathway activity seemed to reproducibly penalize growth (Fig 2.2b, lower panel, see for example P=2.96 nM, E=0-2 nM). As mentioned

above, this detrimental effect on growth was reversed at supra-inhibitory Gpa1p and Msg5p levels, where growth rate now increased as a function of Gpa1p and Msg5p (Fig 2.2b, lower panel, see P=2.96 nM, E>2 nM). This non-monotonic behavior cannot be solely attributed to generic over-expression effects of these regulators, since this over-expression in the absence of Ste4p induction does not affect growth. Also, the growth recovery phase for MSG5-STE4 occurred at higher levels of estradiol than GPA1-STE4 (**Supplementary Fig. 2.16**). Finally, Dig1 over-expression did not seem to markedly affect growth. Taken together, these data suggest that intricate epistatic relationships exist between these positive and negative regulators of the mating pathway, and that quantitative mapping is needed to uncover their existence. Traditional epistatic mapping using only extreme over-expression or complete deletion would miss Gpa1p and Msg5p's effects on growth rate as well as pathway repression by Dig1p, both of which occur at intermediate levels of Ste4p and are only observed by looking at the entire dual dose responses of Figure 2. These data suggest that the 2D-parallel circuit constitutes a useful tool to perform next generation genetic rescue experiments in which a quantitative phenotype is systematically mapped as a function of its effectors. These methods are crucial for generating a systems-level understanding of biological pathways.

2.3.2 A 2D-series circuit is a versatile noise rheostat

The 2D-parallel circuit is able to independently and simultaneously modulate the first moments, or means, of two transcriptional output distributions. We now explore whether a different configuration of the ZPM and GEM modules can be used to

simultaneously control two moments (mean and variance) of the distribution of a single transcriptional output. Such a “noise rheostat” circuit would be a powerful tool for adding different amounts of noise into a cellular process and quantifying the repercussions of this noise.

We explored the behavior that would ensure from connecting the GEM and ZPM TRs in series instead of in parallel. In this circuit, the expression of ZPM is under the control of GEM and both are activated by their respective inputs (progesterone and estradiol) (**Supplementary Fig 2.17a**). Computational modeling demonstrated that this configuration allows for the same transcriptional mean output to be achieved with different combinations of GEM and ZPM activation levels (**Supplementary Fig 2.17b** and **Supplementary Note**). This phenomenon is mediated by the fact that this circuit effectively operates as a multiplier—at all combinatorial estradiol and progesterone concentrations, the mean output is the simple products of two doses responses, the first being the mean steady-state dose response of circuit output as a function of estradiol at saturating concentration of progesterone while the second is the mean steady-state dose response as a function of progesterone at a saturating concentration of estradiol. Modeling of this circuit also demonstrated that different combinations of estradiol and progesterone can produce the same mean output but with different variances. Specifically, for the same mean output, high upstream (GEM) activity and correspondingly low ZPM activity leads to low variability while low upstream (GEM) activity leads to larger variability. That is, the model predicted that different output noise levels could be achieved, with high output variance for low levels of estradiol and high levels of

progesterone and low variance for high levels of estradiol and low levels of progesterone (**Supplementary Fig 2.17b and c**).

To experimentally implement this design and verify its predictions, we built a strain in which a constitutively expressed GEM TR drives the expression of the ZPM TR from pGAL1 in response to estradiol. The ZPM TR in turn drives the expression of YFP from the pZ promoter in response to progesterone (**Fig 2.3a**). We measured the two-dimensional dose response output of this circuit for different combinations of estradiol and progesterone (**Supplementary Fig 2.18**). As expected, the output increased gradually as a function of both inputs and was highest for maximum concentrations of both estradiol and progesterone (**Fig 2.3b**). From out data, we extracted output dose response as a function of estradiol at saturating progesterone concentration, and vice versa, as a function of progesterone at saturating estradiol concentration. We then used these functions to confirm the multiplicative property of the circuit as suggested by the computational model (**Supplementary Fig 2.19, Supplementary Note)**.

Furthermore, as predicted by the model, different combinations of estradiol and progesterone yielded similar mean expression values over a substantial dynamic range (**Fig. 3b**). Gratifyingly, in agreement with the principles of the design, we also observed wide differences in the transient and steady-state fluorescence distributions for these similar means (**Fig. 3c and d**). We quantified the spread of these distributions using the squared coefficient of variation (CV^2=variance/mean^2) of fluorescence at steady state, and confirmed that different CV^2 values can be achieved for the same mean (**Fig. 3b and e**). We note here that the observation that multiple-input/single-output systems can give rise to different variances for the same mean has previously been reported[48]. Our work

exploits a similar principle to implement noise modulation, but using synthetic components that are orthogonal to the endogenous cellular circuitry.

To achieve a thorough characterization of the noise rheostat circuit, we carried out a number of experiments. In the first, we decomposed noise in the expression of the pZ promoter into its intrinsic and extrinsic[49] components by measuring, in the same cell, a second fluorescent protein (mCherry) driven by a second pZ promoter (**Fig 2.3a, Supplementary Fig 2.20 and 2.21a-b**). We observed that extrinsic, or correlated, variation accounts for the majority of the variation in fluorescence (**Fig 3f**) and is asymmetric with respect to the two estradiol and progesterone inputs (**Supplementary Fig 17c**). On the other hand, intrinsic noise in pZ is symmetric with respect to the inputs (**Supplementary Fig 2.21d**). This suggests that protein number noise in the pZ promoter itself is not a significant contribution to the cell-to-cell variation. As expected, a plot of the CV^2 associated with intrinsic noise for pZ versus mean fluorescence shows a Poisson-like structure, while the same plot for CV^2 of extrinsic noise shows a range of values for any given mean (**Fig 2.3e and Supplementary Fig 2.17e**). Finally, we compared the variability of the two promoters in the circuit using a dual-fluorophore strain containing a pGAL1-mCherry (to monitor the GEM system, **Supplementary Fig 2.22**) and a pZ-YFP (to monitor the ZPM system). Most of the variation can be attributed to the correlated component (**Supplementary Fig 2.23**). These noise trends were reproducible across experiments (**Supplementary Fig 2.24a-b**) and reporter fluorophores (**Supplementary Fig 2.24c-d**) and in qualitative agreement with the modeling predictions (**Supplementary Fig 2.17f**). Overall, our data demonstrate that the 2D-series configuration constitutes a simple circuit that can be used to achieve noise control in a robust and predictable way.

To illustrate an application of the noise rheostat circuit, we used it to assess the impact of modulating the mean and noise in the expression of the cell cycle regulator Sic1p. Sic1p is a cyclin-dependent kinase inhibitor that regulates the G1/S transition controller Cdc28-Clb complex[50]. Overexpression of wild-type Sic1p has been reported to result in cell cycle arrest in G1 and elongated bud morphology[51]. We built a strain harboring the noise rheostat construct controlling the expression of an extra copy of the SIC1 gene (**Fig 2.4a**). To measure expression levels from pZ, we included a copy of the transcriptional reporter pZ-YFP in the same strain. At high Sic1p level (*i.e.* high estradiol and progesterone doses), cells have a marked phenotypic hallmark, appearing to be bigger with elongated buds (**Fig 2.4b**).

To probe the fitness effect of increased Sic1 noise beyond the extreme Sic1 expression case, we induced expression of Sic1p with different combinations of estradiol and progesterone and measured expression levels by flow cytometry. In the experiment, we also estimated growth for the different estradiol-progesterone combinations by measuring cell density five hours after induction. As expected, we observed a monotonic decrease in growth with increased mean Sic1p expression, corroborating the idea that overexpression of this protein promotes cell cycle arrest (**Figure 4c, Supplementary Fig 2.25**). We also observed a robust wide regime in which different levels of cell-cell variability can be achieved for the same mean (**Figure 4c**). For this regime, there seemed to be a trend of increased growth with increased variability, manifesting as a positive correlation between CV^2 of Sic1p expression and growth (**dotted lines in Figure 4c, Supplementary Fig 2.26**) in a mean-independent way (**Supplementary Fig. 2.27**). That is, for two estradiol and progesterone combinations that generated the same Sic1 mean,

the population subjected to the dosage that also produced higher variability seemed to have enhanced growth rate. This counter-intuitive observation may potentially be attributed to the fact that increased variability at a given mean simultaneously increases the proportion of cells in the lowly and highly expressed tail regions of the Sic1p distribution. While cells in the high upper tail of the distribution might be growth stunted, those in the lower tail experience attenuated cell cycle arrest. Therefore, the higher growth of low-Sic1 expressing cells may supersede the effects of the slow growing, high-Sic1 expressing cells. Importantly, this effect of increased Sic1p variability is not apparent at all levels of induction. It surfaces and disappears as Sic1p levels change, highlighting the need to map phenotypes associated with cell-cell variability over a broad range of mean expression levels and noise.

2.3.3 Analysis of multiplicative behavior of mean output of the 2D-series noise rheostat circuit

Using automated flow cytometry, we measured the expression of pZ-YFP over time for different combinations of concentrations of estradiol (E) and progesterone (P). We averaged the steady state expression rate over the last 10 timepoints for each of 96 conditions. We refer to this value as the steady state output of the circuit. Now, if the circuit is multiplicative, the expression rate for a given combination of E and P, alpha(E,P), is the result of the multiplication of the individual contributions:

$$alpha(\boldsymbol{E}, \boldsymbol{P}) = \frac{alpha(\boldsymbol{E}, P_{max}) \times alpha(E_{max}, \boldsymbol{P})}{alpha(E_{max}, P_{max})}$$

Or, in terms of gains G (between 0 and 1) for the individual steps:

$$G \times alpha(E_{max}, P_{max}) = G_X \times G_Y \times alpha(E_{max}, P_{max})$$

Where

$$G_X = \frac{alpha(\boldsymbol{E}, P_{max})}{alpha(E_{max}, P_{max})}$$

and

$$G_Y = \frac{alpha(E_{max}, \boldsymbol{P})}{alpha(E_{max}, P_{max})}$$

To quantify the multiplicative behavior of the circuit (**Supplementary Fig. 2.19**), we estimated the output of the circuit for a given dose of estradiol and progesterone, alpha(E,P). As mentioned in the main text, we find that indeed the output is, as predicted by our qualitative model, multiplicative.

2.4 CONCLUSION

In this work, we present two synthetic circuits that exploit two degrees of freedom to either control two independent cellular outputs or two moments of the distribution of a single output. The TRs used here provide high dynamic range control of gene expression, while having no (for ZPM) or limited (the GAL regulon activated by GEM) off-targets and no detectable leakage in the absence of inputs. Importantly, these TRs do not impact fitness, making them suitable for the construction of circuits that operate orthogonally to the physiology of the cell. Moreover, the modularity of the hormone-inducible TRs allows for future combinations of hormone-LBD pairs to be devised and constructed, therefore expanding the number of network components that can be simultaneously manipulated.

The in-parallel circuit configuration provides a tool that could be instrumental for *in vivo* quantitative characterization of genetic interactions, including protein complexes, pathway crosstalk, and genetic rescue experiments in which a quantitative phenotype is systematically mapped as a function of its effectors. By capitalizing on this system to drive

the expression of mating pathway regulators, we showed quantitative phenotypes that could not be revealed without the ability to control the expression of two genes in a graded and simultaneous fashion. Conventional epistatic mapping using over expressions and deletions would have disregarded Dig1p as a negative regulator of the pathway. In a similar way, traditional methods would miss the differences in how Gpa1p and Msg5p rescue mating pathway induced growth arrest, which are revealed only when observing the entire dual dose response of these negative regulators and Ste4p. We anticipate this circuit to be greatly instrumental in probing the hierarchy and timing of interacting cellular pathways, for example by mapping the influence of one cellular pathway on another as a function of their relative induction delay[52,53].

The serial configuration of the two synthetic TRs allows for the modulation of noise independently of mean at low and medium expression levels, a range where variability is most physiologically relevant. This capability is primarily achieved through the presence of two dials that can be simultaneously changed to achieve the same mean, but with different consequences for output variability. The simplicity of this design and its robust operation makes it instrumental for testing the causal connections between noise and fitness, which has so far eluded systematic exploration because schemes for modulating variability, such as mutations to pathway components, are often accompanied by a change in mean, are not tunable or require changing nutritional composition of the media. The ability to compare phenotypes induced by different cell-cell variability in a signal in the context of the same population mean can bridge this gap, providing an invaluable resource for delineating the biological repercussions of molecular noise. Here, we have illustrated a simple manifestation of this point,

demonstrating that it is possible to impact population-level fitness by changing the single-cell expression level distribution of the cell cycle regulator Sic1. Much investigation is still needed to go beyond the phenomenology we report, and to extract the underlying principles of noise regulation in this system as well as its exact map to cellular physiology. However, the intricate relationship between mean Sic1 expression, its cell-cell variability, and the resulting morphological and growth phenotypes argues that a tunable noise-controlling circuit such as the one we report here is crucially needed to pinpoint interesting operational regimes of cell-cell variability and delineate the contexts in which more mechanistic investigations should be deployed.

2.5 MATERIALS AND METHODS

2.5.1 Plasmids and strains

All plasmids used in this study are listed in **Supplementary Table 2**. Plasmids were cut or PCR-amplified (pHES941) and transformed into *S. cerevisiae* with standard lithium acetate transformation protocol. The resulting yeast strains are listed in **Supplementary Table 3**. All plasmids are single-integration constructs when cut with PmeI or PCR-amplified. All constructs were built by restriction/ligation of plasmids and PCR products amplified with Elongase Enzyme Mix (Life Technologies).

The TR constructs consist of a constitutive promoter (a crippled version of the ADH1 promoter) driving the expression of the chimeric transcription factor (**Figure 1a**). The ZPM construct was built by inserting the hPR-LBD (amplified from Addgene plasmid pRR-PR-

5Z, generated in the Miller lab) flanked with BamHI and NotI sites and a small linker into a plasmid containing a BamHI and a NotI restriction site downstream of pADH1(cr) and upstream of the MSN2-AD. The Zif268-LBD (amplified from genomic DNA of an *S. cerevisiae* strain provided by David Botstein's lab) flanked by NheI and BglII restriction sites was inserted in between pADH1(cr) and the Zif268-LBD using NheI and BamHI restriction sites.

The TRs reporters were built in a similar way, inserting pGAL1 or pZ upstream of YFP or mCherry, using PspOMI and XhoI restriction sites. The pZ promoter was amplified from strains containing a pGAL1 promoter where three GAL4 binding sites were replaced by four Zif268 binding sites [6]. We mutated an extra putative GAL4 binding site (see sequence in Supplementary Text) to avoid activation of transcription from this promoter with either galactose-containing media or the GEM construct. Mating pathway and SIC1 expression plasmids were built by inserting the GPA1, MSG5, DIG1, STE4 or SIC1 ORFs in pGAL1 or pZ-containing plasmids.

The mating pathway reporter was built by inserting a pAGA1-YFP construct, flanked by PspOMI and XhoI restriction sites, into a plasmid containing a geneticin resistance cassette downstream of the insertion. This construct, including the resistance marker, was then PCR-amplified with homology regions to the CAN1 locus flanking the amplicon and transformed into yeast.

2.5.2 Media and growth conditions

Cells were inoculated from single colonies into liquid media and grown for at least 20h in exponential phase at 30ºC with constant shaking before starting experiments. Complete

media (YPD) consists of 10 g/L yeast extract, 20 g/L Bacto peptone™ (Becton Dickinson) and 0.2 g/L dextrose (Sigma-Aldrich). Complete synthetic media (SDC) consists of 6.7 g/L nitrogen base without amino acids, 2 g/L dextrose (Sigma-Aldrich) and 0.79 g/L complete supplement mixture (MP Biomedicals).

Most transformations were selected in synthetic media agar plates with the corresponding amino acid dropout. The pAGA1-YFP-tKan construct transformation was selected in YPD agar plates containing 200ug/mL G418 (Teknova).

.

2.5.3 In parallel circuit automated flow cytometry measurements

Experiments were conducted as previously described [38]. In the case of multiplexing experiments, strains containing a pTdh3-mKate2-labeled strain were mixed with a strain lacking the label in a 1:1 ratio at the start of the experiment. All cultures were taken to an initial cell density of approximately $6x10^5$ cells/mL. Cells were transferred to a 96-well plate and placed in a robotic setup that constantly diluted the cells and took samples to a coupled cell cytometer (LSRII BD) every 20 minutes. Estradiol (ß-estradiol, Sigma-Aldrich) and progesterone (Sigma-Aldrich) were added at the final concentrations indicated in the results section at time 0 and were maintained at those concentrations by replacing the samples taken by the robotic setup with fresh media containing the hormones. To match growth rate, the dilution rate of the cultures was 0.51 h^{-1}, unless otherwise noted. Data was analyzed in Matlab®.

Red fluorescence measurements for each cell were divided by the cell's side scattering value (SSC) and the 2 subpopulations: mKate2-labeled cells (high red fluorescence) and unlabeled cells (low red fluorescence) were identified. The median green fluorescence measurements (FITC) each subpopulation was taken for further analysis. Histograms were computed on volume-corrected fluorescence, by dividing each cell's fluorescence by its side scattering (SSC). Cell density was calculated as the event rate measured by the cytometer for each condition and time-point and this value was used to calculate growth rate. Changes in fluorescence over time and growth rates were used to calculate expression rates, following the equation:

$$\alpha_{cell,t} = (dlog(F_t) + dlog(N_t)) \times F_t$$

where $\alpha_{cell,t}$ is the expression rate at time t, $F_{total,t}$ is the median fluorescence at time t and N_t is the cell density at time t . Since we didn't observe large fluctuations in growth rates over time before saturation or after approximately 1h after transferring the cells to the robotic setup, the median dlog(N) value was used for all times t, unless otherwise noted. Activation time was calculated as the time to reach half the steady-state mean expression rate.

2.5.4 Noise measurements and analysis

For the in-series circuit two-color experiments, cells of two strains (containing pZ-YFP/ pZ-mCherry or pZ-YFP/ pGAL1-mCherry reporters) were grown and measured using an automated flow cytometry system as described previously. Using Matlab® we computed single-cell fluorescence summary statistics for all timepoints and combinations of estradiol and progesterone. To filter out variability due to cell cycle stage, we gated in the FSC-SSC plane to extract a subset of cells with similar characteristics for computing

intrinsic and extrinsic noise components (see **Supplementary Fig. 17**). We extracted intrinsic and extrinsic noise components using principal component analysis (PCA). For comparison, we also computed intrinsic and extrinsic components of noise using the expression used by Elowitz et al[54]:

$$\eta_{int}^2 = \frac{\langle (x-y)^2 \rangle}{2\langle x \rangle \langle y \rangle} \quad \eta_{ext}^2 = \frac{\langle xy \rangle - \langle x \rangle \langle y \rangle}{\langle x \rangle \langle y \rangle} \quad \eta_{tot}^2 = \frac{\langle x^2 + y^2 \rangle - 2\langle x \rangle \langle y \rangle}{2\langle x \rangle \langle y \rangle}$$

Where x and y are the fluorescence values of two different reporters in the cell **(Supplementary Fig. 23)**

2.5.5 Expression, density and morphology measurements for noisy expression of SIC1

Cells were grown from saturation for 5 h in exponential phase SDC at 30 ºC. 200 µL of culture (OD_{600} 0.05) were transferred to a shallow 96-well plate (Corning). Estradiol and progesterone were added at the concentrations indicated in Figure 4 and cells were left shaking at 1200 rpm and 30ºC (Thermo-shaker DTS-4, ELMI). After 5 hours, cultures were diluted 1:2 with 1X TE buffer and taken to a cytometer (LSR-II, BD Biosciences) equipped with a high throughput sampler (BD Biosciences). Data was collected in FACS DIVA and analyzed in Matlab®. Cell density was estimated from flow cytometry event rate.

Light microscopy was conducted on samples uninduced and fully induced with both hormones. 100 µL of cultures treated for 5 h were sonicated and added to glass-bottom plate pre-coated with conavalin-A. Cells were immediately imaged in a Nilon Eclipse-Ti microscope with a 40X objective.

2.5.6 Quantitative model of asymmetric noise partitioning

We built a simple 8-species/18-reaction gene expression model for the 2D-series circuit using linear propensities (**Supplementary Figure 13a**). This model is intended to be a phenomenological model that captures the ability of an in-series connection of the two TRs to produce different noise levels for the same mean expression.

Given a set of reactions describing a biochemical circuit, we can define the stoichiometry matrix *S*, propensities υ of these reactions and state vector $x = (x_1,\ldots,x_8)$. The dynamics of the system are given by

$$\dot{x} = S\upsilon = Ax + B$$

where *A* is the Jacobian of the propensities or dynamics matrix and *B* is the vector of zeroth-order inputs into the system. For any choice of parameters the steady state of the system is easily computed as $x_{ss} = -A^{-1}B$. Furthermore, since all propensities in the model are linear or constant on all species, the covariance matrix *C* of the system at steady state can be computed using the fluctuation-dissipation theorem[55] by solving the Lyapunov equation

$$AC + CA^T + S\,\mathrm{diag}\,\upsilon_{ss}\,S^T = 0$$

where υ_{ss} are the steady state propensities for each reaction. The covariance matrix diagonal elements are the variances of the individual species, which are used with the steady state mean concentrations to compute the square of the coefficient of variation (CV^2). If we assume that intrinsic noise is accounted for by counting or sampling noise, its distribution is Poisson and the associated CV^2 is the reciprocal of the mean ($1/\mu$). The extrinsic noise is the portion of the CV^2 not explained by the counting noise[56]:

$$CV^2_{total} = CV^2_{int} + CV^2_{ext} = \frac{1}{\mu} + CV^2_{ext}$$

Where CV^2_{ext} accounts for the noise contribution from translation, transcription and other upstream molecular processes that give rise to the observed abundances.

Parameters were chosen as an example to qualitatively show the asymmetry of noise partitioning (**Supplementary Figure 13b-f**).

2.6 AUTHOR CONTRIBUTIONS

The authors make the following declarations about their contributions:

Conceived and designed the experiments, analyzed the data and wrote the paper: A.A.-D., K.M., I.Z., P.H. and H.E.-S. Performed the experiments: A.A.-D., K.M., I.Z., P.H. Conceived and developed the quantitative model: I.Z.

2.7 ACKNOWLEDGEMENTS

We would like to thank Jacob Stewart-Ornstein for valuable discussion and early work on the characterization of the GEM construct. The Zif268-DBD and the modified GAL1 promoter were kindly provided by the Botstein lab. We thank Ophelia Venturelli and Michael Chevalier for useful conversations and their insight on experimental and theoretical aspects of the work, Lucien Bogar for technical assistance, as well as the rest of the El-Samad lab for feedback throughout. This work was supported by a grant from the Paul G. Allen Family Foundation and the NIGMS system biology center (P50 GM081879) to H.E.-S. The authors declare no competing financial interests.

2.8 CONFLICT OF INTEREST

The authors declare no conflicts of interest.

2.9 FIGURES

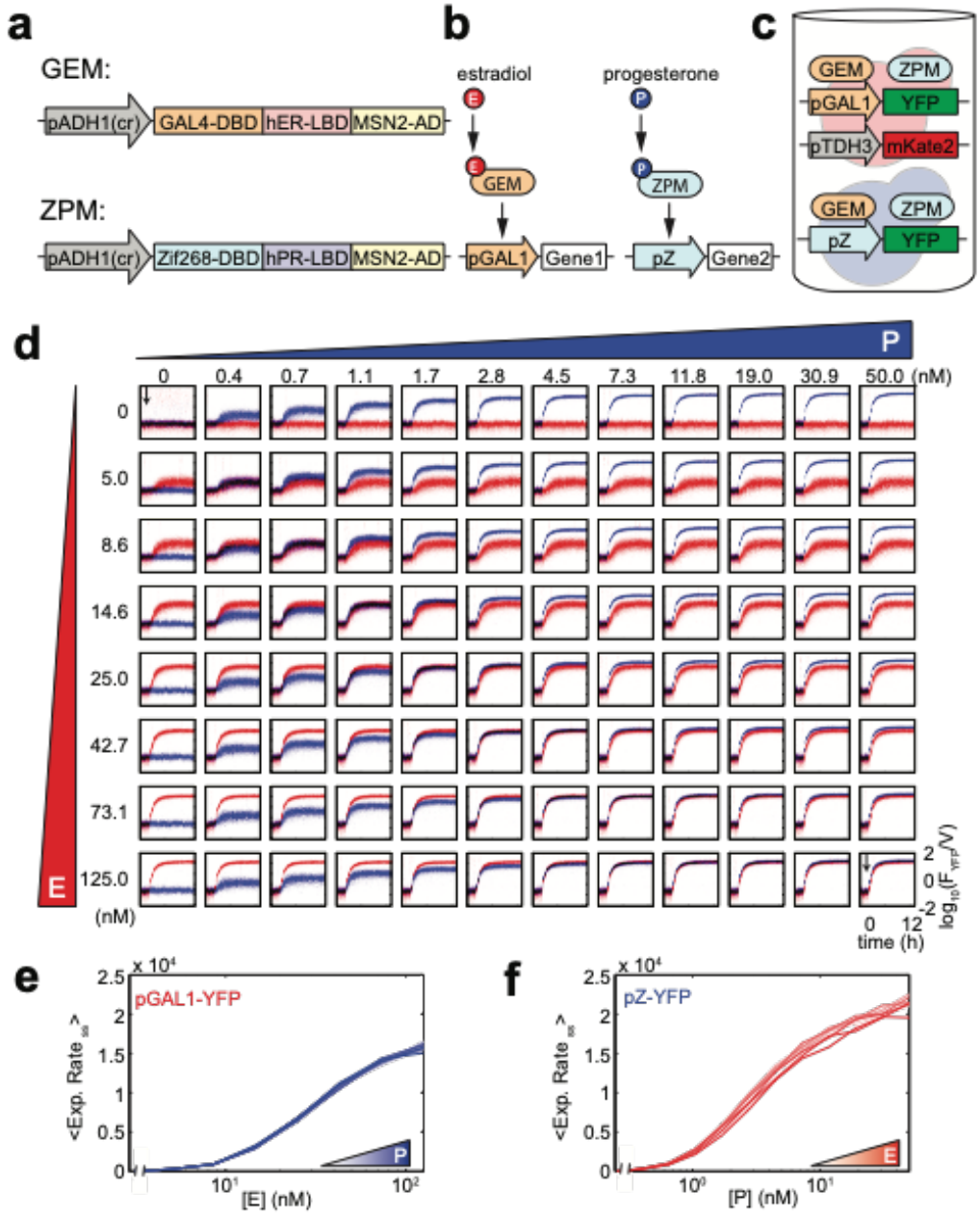
a
GEM:
pADH1(cr)
GAL4-DBD
hER-LBD
MSN2-AD
ZPM:
pADH1(cr)
Zif268-DBD
hPR-LBD
MSN2-AD
b
estradiol
progesterone
GEM
ZPM
pGAL1
Gene1
pZ
Gene2
c
GEM
ZPM
pGAL1
YFP
pTDH3
mKate2
GEM
ZPM
pZ
YFP
d
P
0
0.4
0.7
1.1
1.7
2.8
4.5
7.3
11.8
19.0
30.9
50.0 (nM)
E
0
5.0
8.6
14.6
25.0
42.7
73.1
125.0
(nM)
time (h)
e
pGAL1-YFP
<Exp. Rate ss>
[E] (nM)
f
pZ-YFP
<Exp. Rate ss>
[P] (nM)

Figure 2.1 Simultaneous and independent control of gene expression using two chimeric transcriptional regulators (TRs) in parallel.
(a) Scheme of two chimeric TRs constitutively expressed under the control of a crippled ADH1 promoter (pADH1(cr)). The TRs (GEM and ZPM) are a fusion of a DNA binding domain (Gal4p-DBD or Zif268-DBD, respectively), a human hormone receptor li-binding domain (from the estradiol or progesterone receptors, hER-LBD and hPR-LBD) and a transcriptional activation domain (Msn2p-AD). (b) Representation of the action of the TRs GEM (left) and ZPM (right) in the presence of estradiol (E) or progesterone (P), respectively. (c) Diagram of the experimental setup. Two strains were co-cultured, both expressing the GEM and ZPM constructs but alternatively containing the transcriptional reporters pGAL1-YFP (top) or pZ-YFP (bottom). A red-fluorescent protein was used to label the pGAL1-YFP-containing strain (top). Fluorescence, volume and cell counts were measured by automated flow cytometry. (d) Time-dependent distributions of pGAL1-YFP (red) and pZ-YFP (blue) fluorescence for different combinations of logarithmically spaced doses of estradiol and progesterone. Fluorescence values are volume-corrected (e) Steady-state dose response of the pGAL1-YFP reporter as a function of estradiol for different progesterone concentrations (shades of blue). (f) Steady-state dose response of the pZ-YFP reporter as a function of progesterone for different doses of estradiol (shades of red). In (e) and (f) pGAL1-YFP and pZ-YFP expression rates are averaged over progesterone or estradiol concentrations, respectively. The expression rates were also averaged from 3 to 12.3h after induction.

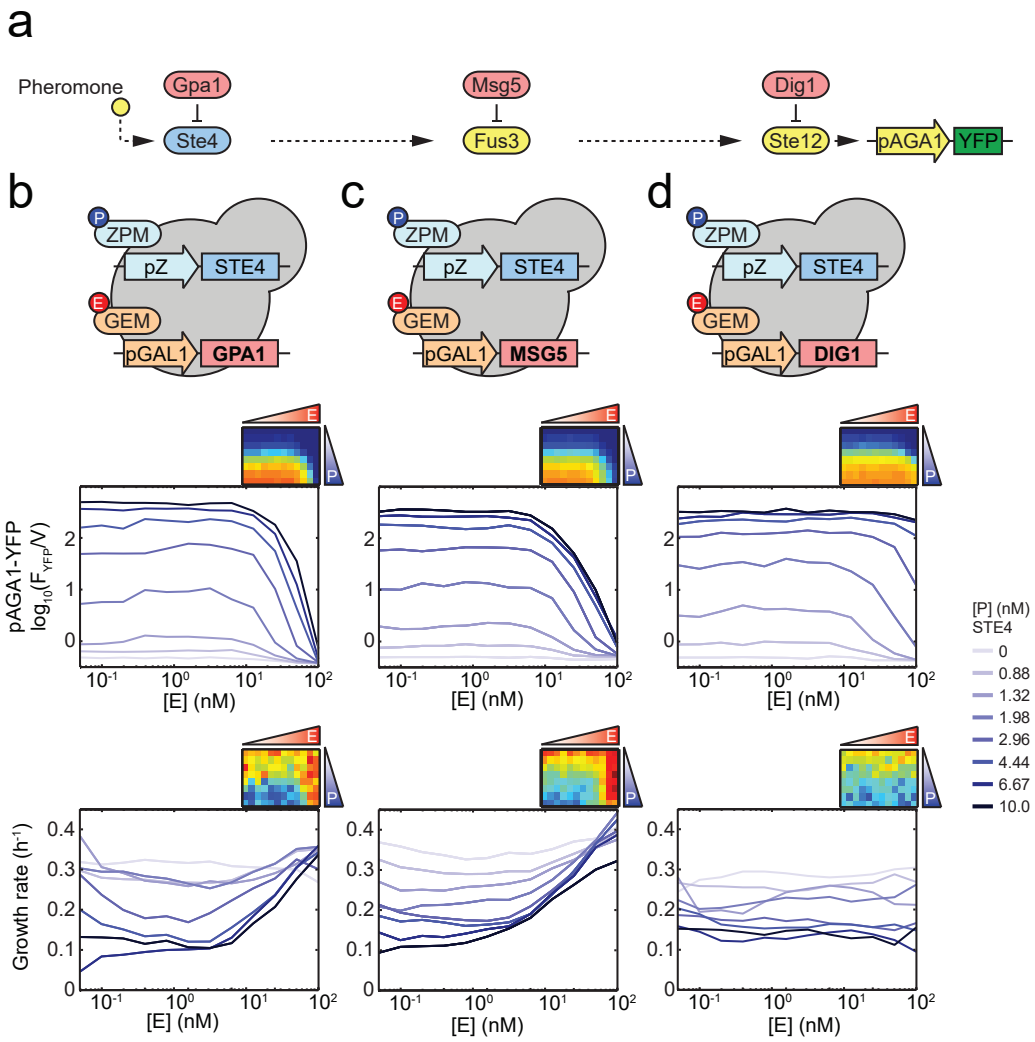
a
Pheromone
Gpa1
Ste4
Msg5
Fus3
Dig1
Ste12
pAGA1
YFP
b
c
d
P
ZPM
pZ
STE4
E
GEM
pGAL1
GPA1
MSG5
DIG1
pAGA1-YFP
log10(FYFP/V)
Growth rate (h-1)
[E] (nM)
[P] (nM)
STE4
0
0.88
1.32
1.98
2.96
4.44
6.67
10.0

Figure 2.2: A 2D-parallel circuit controlling the expression of positive and negative regulators modulates the transcriptional output of the yeast mating pathway

(a) Mating pathway signaling cascade regulators relevant to this study. A positive regulator (Ste4p) is under the control of ZPM and three negative regulators (Gpa1p, Msg5p, Dig1p) are under the control of GEM. The activity of the pathway is measured with a transcriptional reporter consisting on the AGA1 promoter driving the expression of YFP (pAGA1-YFP). (b-d) Upper panels: Schemes of the strains used in each experiment. Middle panels: Steady-state dose response of pAGA1-YFP as a function of estradiol modulating the expression of Gpa1p (b), Msg5p (c) or Dig1p (d). Different doses of progesterone (shades of blue) generate different levels of Ste4p. Fluorescence was measured after 4 hours of induction and was volume-corrected. Lower panels: Mean steady-state growth rate as a function of estradiol and progesterone (shades of blue). Insets: same data as in line graphs, shown as a heat map.

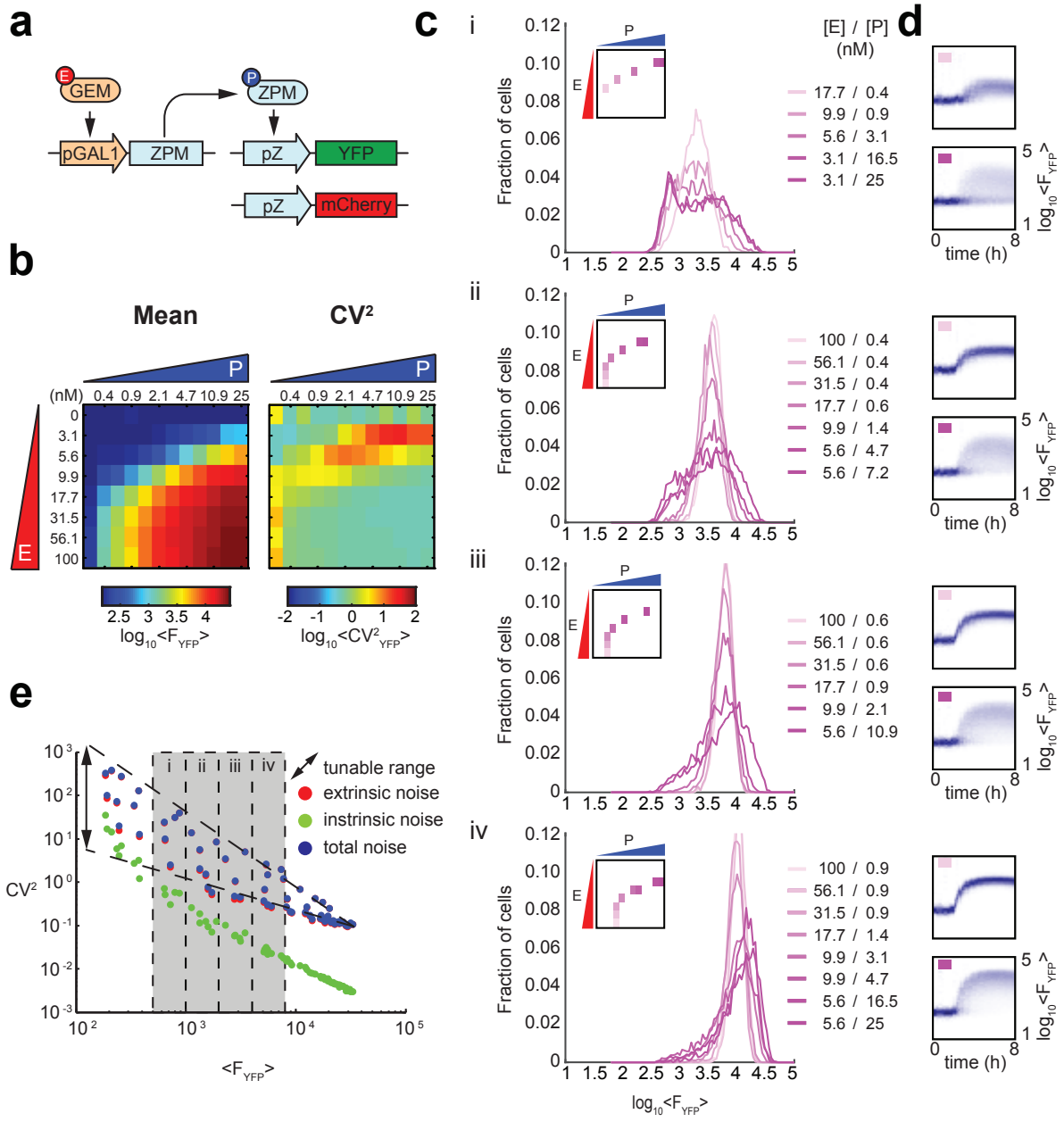
a
GEM
ZPM
pGAL1
ZPM
pZ
YFP
pZ
mCherry
b
Mean
CV²
P
(nM) 0.4 0.9 2.1 4.7 10.9 25
0
3.1
5.6
9.9
17.7
31.5
56.1
100
E
2.5 3 3.5 4
log10<FYFP>
-2 -1 0 1 2
log10<CV²YFP>
c
i
ii
iii
iv
Fraction of cells
[E] / [P] (nM)
17.7 / 0.4
9.9 / 0.9
5.6 / 3.1
3.1 / 16.5
3.1 / 25
100 / 0.4
56.1 / 0.4
31.5 / 0.4
17.7 / 0.6
9.9 / 1.4
5.6 / 4.7
5.6 / 7.2
100 / 0.6
56.1 / 0.6
31.5 / 0.6
17.7 / 0.9
9.9 / 2.1
5.6 / 10.9
100 / 0.9
56.1 / 0.9
31.5 / 0.9
17.7 / 1.4
9.9 / 3.1
9.9 / 4.7
5.6 / 16.5
5.6 / 25
log10<FYFP>
d
time (h)
e
CV²
<FYFP>
tunable range
extrinsic noise
instrinsic noise
total noise

Figure 2.3: Two TRs connected in series act as a noise rheostat circuit that decouples mean and variance

(a) Schematic of the noise rheostat. An estradiol-responsive transcriptional regulator (GEM) is used to dial the abundance of a progesterone-responsive regulator (ZPM), which in turns dials the expression of yellow- and red-fluorescent proteins (YFP and mCherry, respectively) under the control of pZ. (b) Mean and CV2 of pZ-YFP distribution for different combinations of estradiol and progesterone. (c) Steady-state pZ-YFP distributions centered at (i) 750, (ii) 1500, (iii) 3000 and (iv) 6000 arbitrary fluorescence units. For each one of these cases, the same mean of the distribution but different variance around the mean could be achieved using different combinations of estradiol and progesterone (inset). (d) Time-dependent pZ-YFP distributions for conditions in (b) that generate the minimum (upper) and maximum (lower) spread over the mean. (e) Coefficient of variation of the intrinsic (green), extrinsic (red) and total (blue) noise as a function mean fluorescence, Only conditions for which the fluorescence is greater than autofluorescence are plotted.

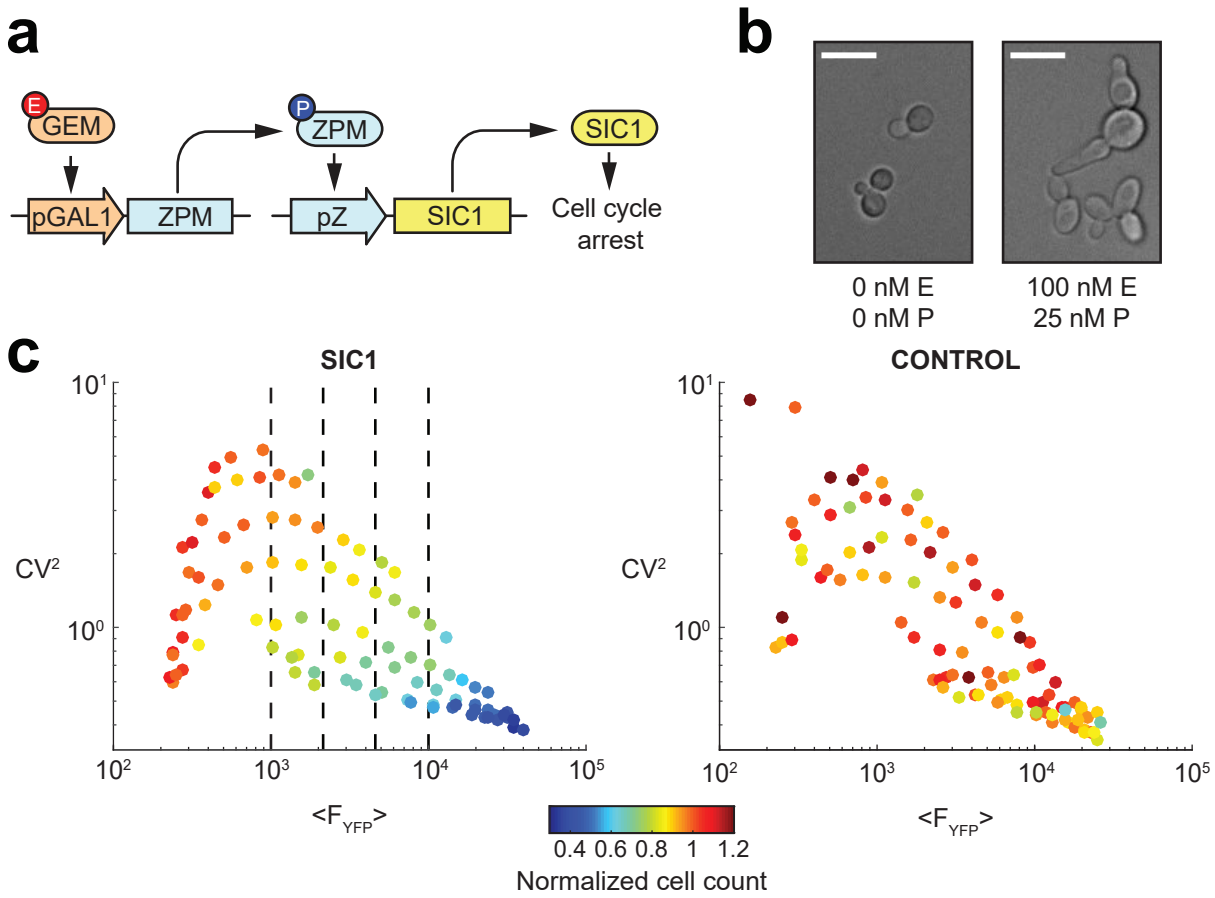

Figure 2.4: Noise rheostat circuit control of cell cycle regulator SIC1 shows effects of variability in gene expression at the same mean

(a) Cell cycle regulator SIC1 expression under the control of the noise rheostat circuit. (b) Bright field microscopy of cells harboring a SIC1 copy driven by the noise rheostat- with no or high concentration of estradiol and progesterone. Size bars: 10 μm. (c) Coefficient of variation as a function of mean of the single-cell YFP fluorescence distribution for different combinations of estradiol and progesterone in a strain containing the noise rheostat regulating the expression of SIC1 (left) and a control strain containing the noise rheostat without SIC1 construct (right). Cytometry cell counts (normalized to non-induced control) are represented in colors of dots. Data for SIC1 noise rheostat experiment represent mean of three replicates. Dotted lines show increasing cell counts with increasing CV^2 for data points with similar mean fluorescence.

2.10 SUPPLEMETARY FIGURES

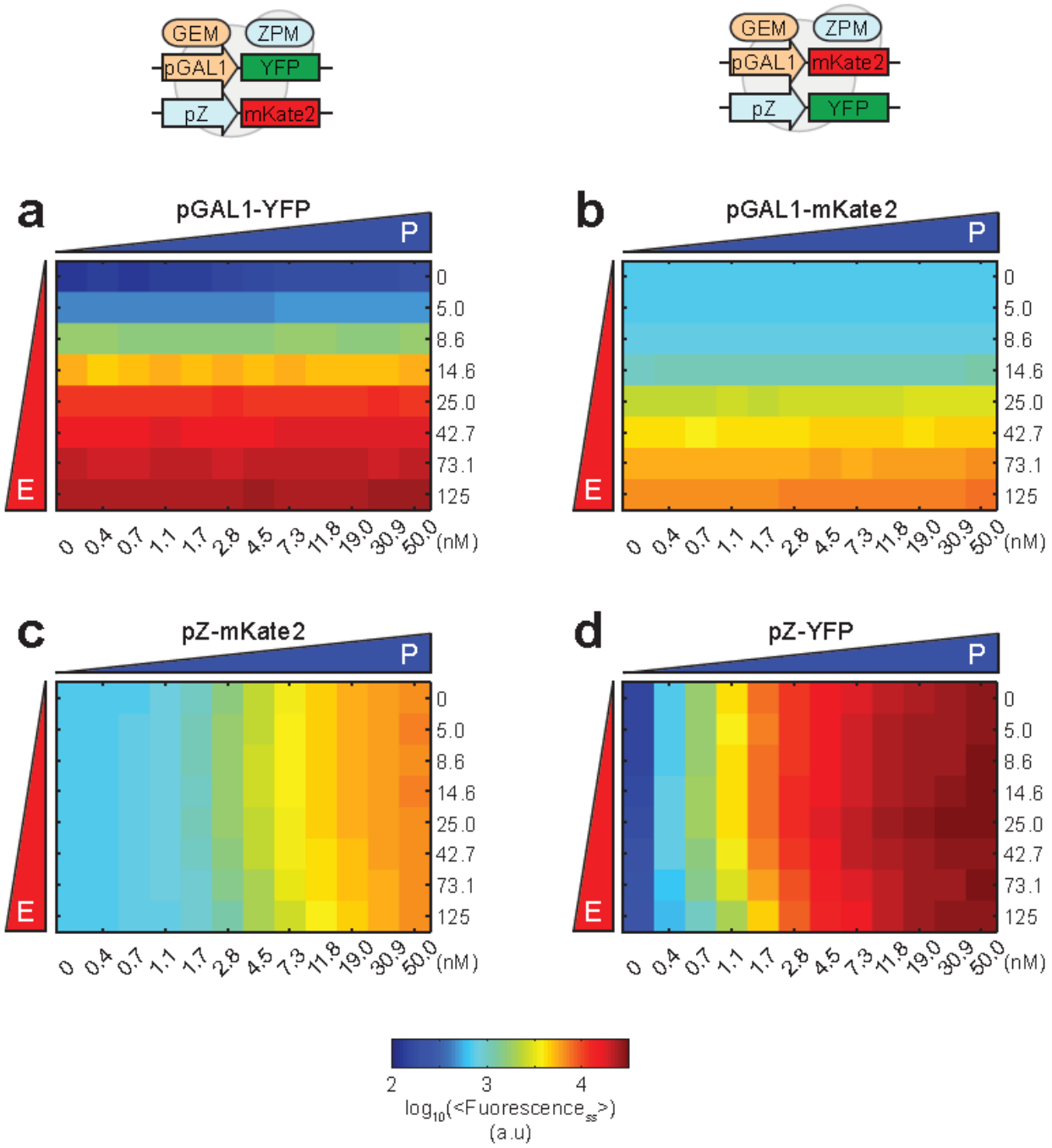

Figure 2.5: 2D-parallel circuit characterization using two reporters in the same strain

Median fluorescence output from promoters pGal1 and pZ controlling the expression of YFP or mKate2 in strains containing the 2D-parallel circuit constructs, for different combinations of estradiol (E) and progesterone (P). One strain contained the reporters pGal1-YFP (**a**) and pZ-mKate2 (**b**). The other one contained the reporters pGal1-mKate2 (**c**) and pZ-YFP (**d**). Fluorescence was measured 4 hours after induction.

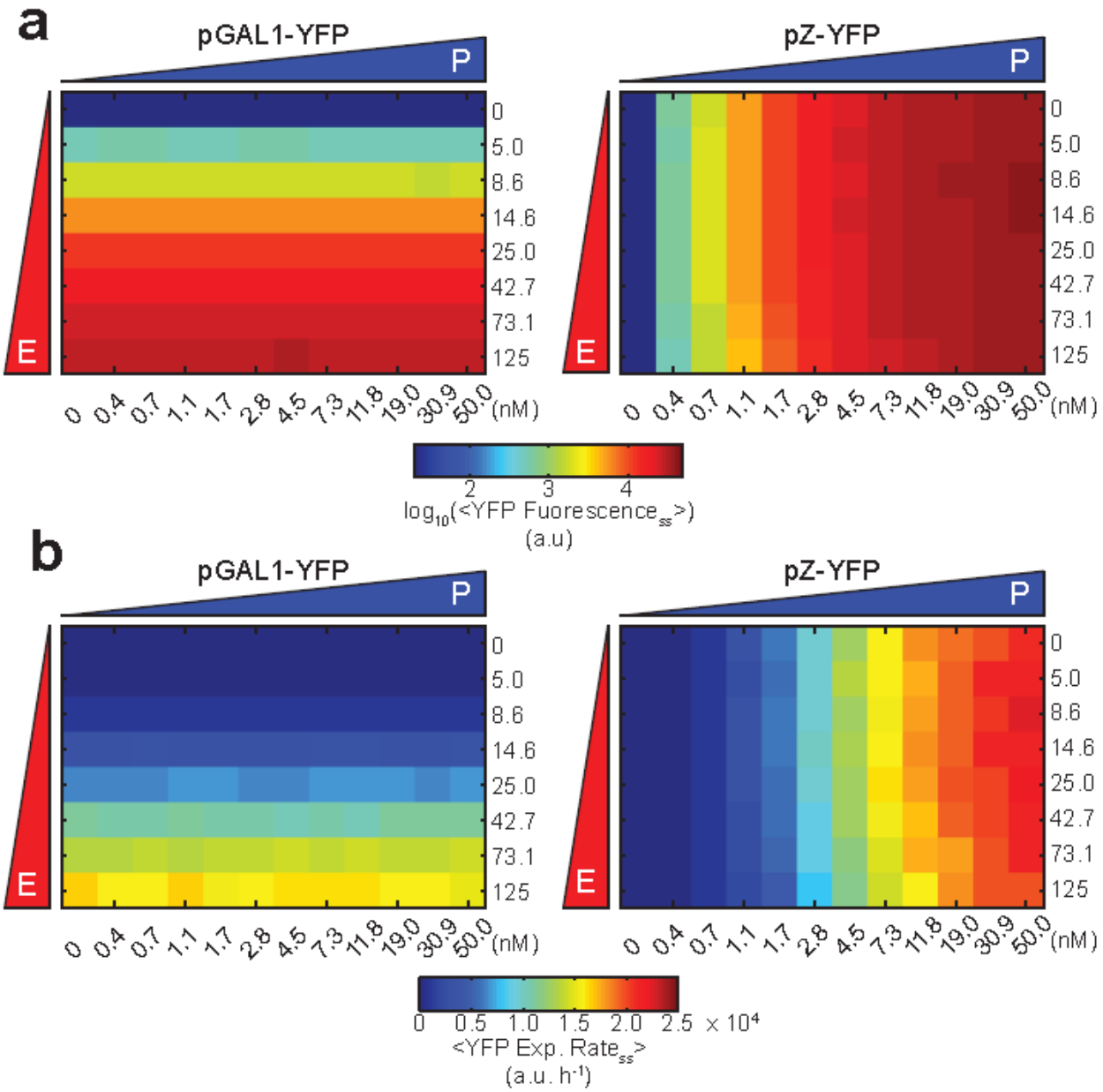

Figure 2.6: Steady-state characterization of the 2D-parallel circuit
(**a**) Median steady state YFP fluorescence and (**b**) YFP expression rate at steady state for transcriptional reporters pGAL1-YFP (**left**) and pZ-YFP (**right**) for different combinations of estradiol (E) and progesterone (P). The expression rates were averaged from 3.3 to 12.3 h after induction. Same data as in Fig. 1e and f.

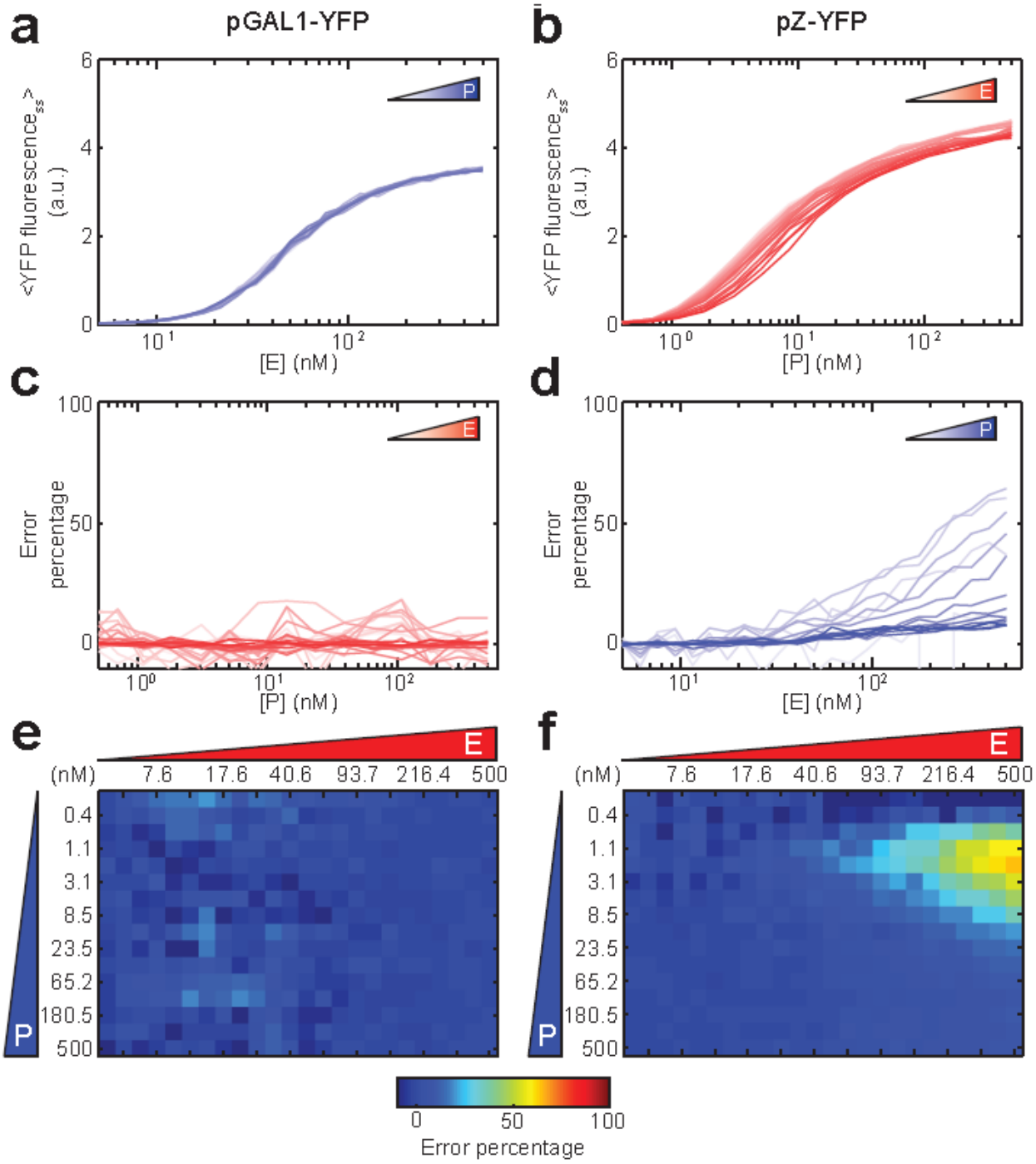

Figure 2.7: Characterization of the independent operation of the TRs in the 2D parallel circuit

(**a**) Dose response of pGAL1-YFP as a function of estradiol for different concentrations of progesterone. (**b**) Dose response of pZ-YFP as a function of progesterone for different concentrations of estradiol. Fluorescence in (a) and (b) is measured 4 hours after induction. (**c-f**) Quantification of crosstalk between the two TRs. For every estradiol concentration, we calculated the error percentage of pGAL1-YFP as difference in expression for this output between cells stimulated with estradiol or estradiol and progesterone, normalized by the estradiol alone data. This value can be computed and

plotted for every progesterone concentration (**c,e).** The error percentage for pZ-YFP can be computed in the same way (**d,f**).

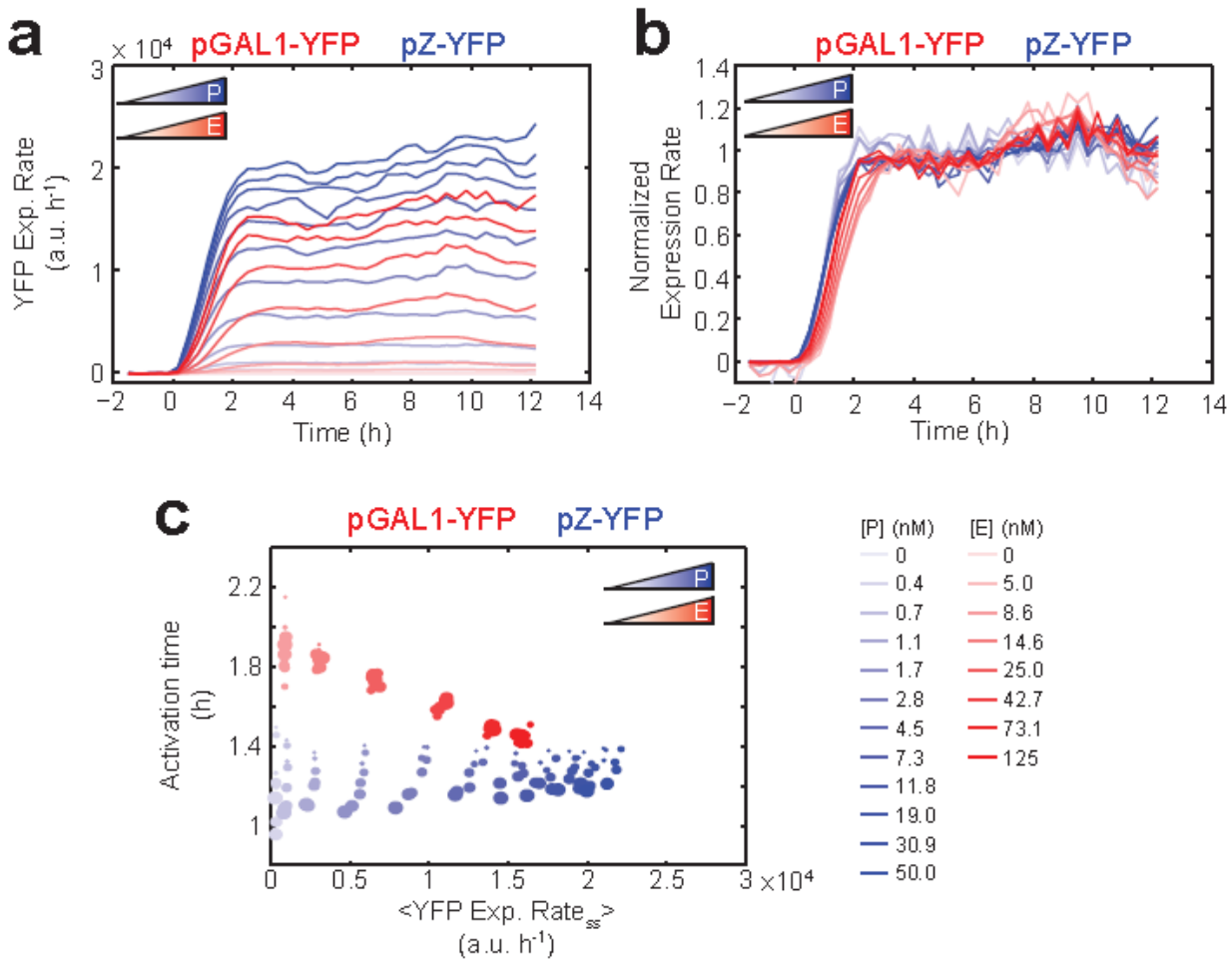

Figure 2.8: Time-resolved and graded control of gene expression by the 2D-parallel circuit

(a) Time-dependent expression rate for pGAL1-YFP (red) and pZ-YFP (blue) for different doses of estradiol (shades of red) and progesterone (shades of blue). pGAL1-YFP and pZ-YFP expression rates are averaged over progesterone or estradiol concentrations, respectively. (b) Mean expression rates normalized by the median steady state (3.3 to 12.3 h) value for each hormone concentration. (c) Quantification of data in (a) showing the activation time for the pGAL1-YFP at different doses of estradiol (shades of red) and progesterone (increasing circle size) and for the pZ-YFP at different doses of progesterone (shades of blue) and estradiol (increasing circle size). Activation time is defined as the time it takes to reach half-steady state induction. Expression rates were averaged from times from 3.3 to 12.3 h after induction.

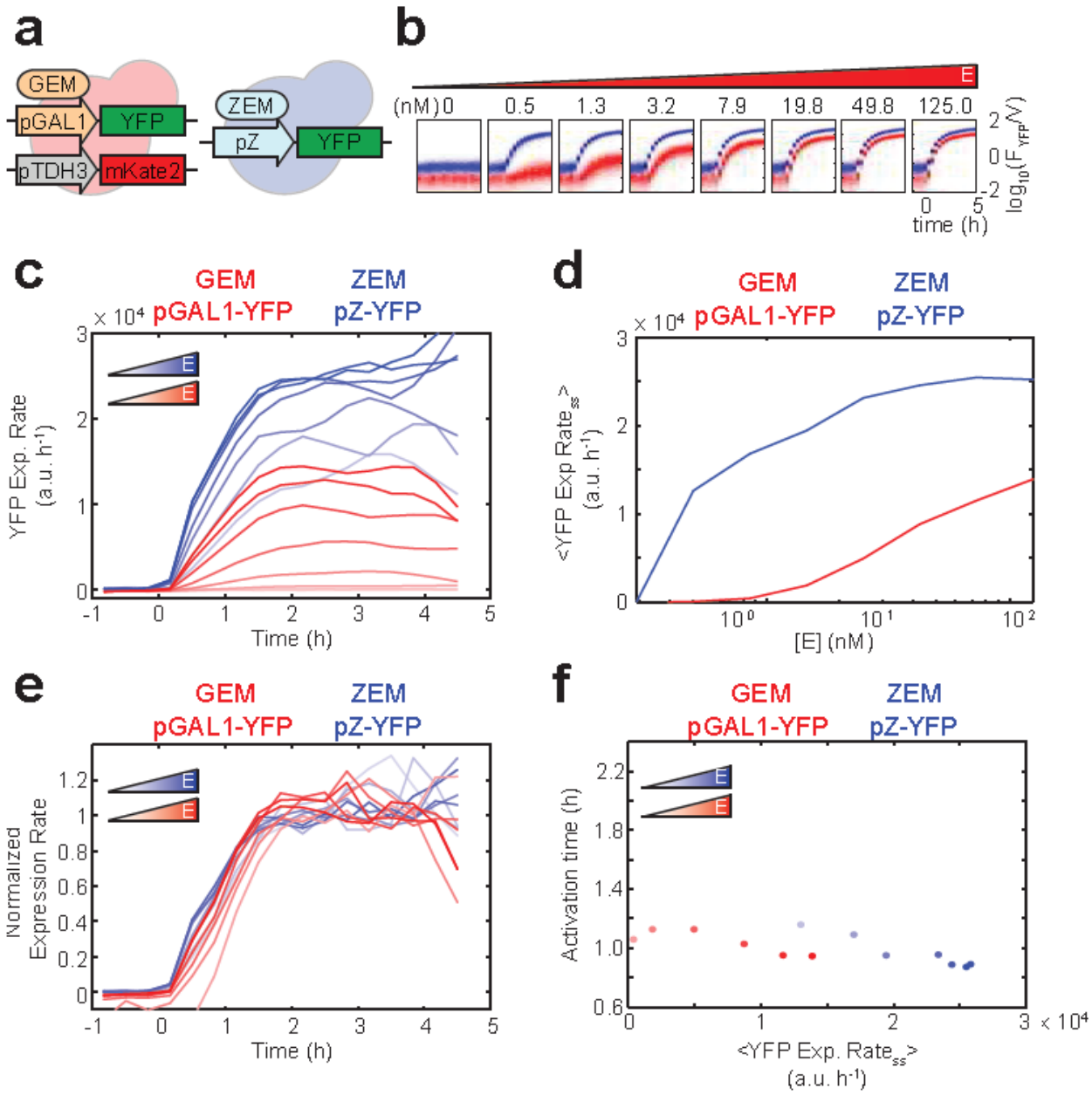

Figure 2.9: Dissection of the roles of the DBD-promoter pair in determining the quantitative parameters of the TRs

(**a**) Two co-cultured strains containing the GEM TR (left) or a Zif268-DBD-containing variant (ZEM, right), both estradiol-responsive but with DNA binding domains that bind to pGAL1 or pZ respectively. A red-fluorescent protein was used to label the GEM, pGAL1-YFP-containing strain (left). (**b**) Time-dependent volume-corrected fluorescence of pGAL1-YFP controlled by GEM (**red**) or pZ-YFP controlled by ZEM (**blue**) for different doses of estradiol (E). (**c**) Time-dependent expression rate for pGAL1-YFP (**red**) or pZ-YFP (**blue**) for different doses of estradiol (shades of red and blue). (**d**) Steady-state average expression rates for GEM (**red**) and ZEM (**blue**). (**e**) Mean expression rates normalized by the maximum value for each hormone concentration. (**f**) Activation time for pGAL1-YFP (red) and pZ-YFP (blue) at different doses of estradiol

(shades of red and blue). Expression rates in (d) and (f) were averaged from 1.3 to 5.3 h after induction.

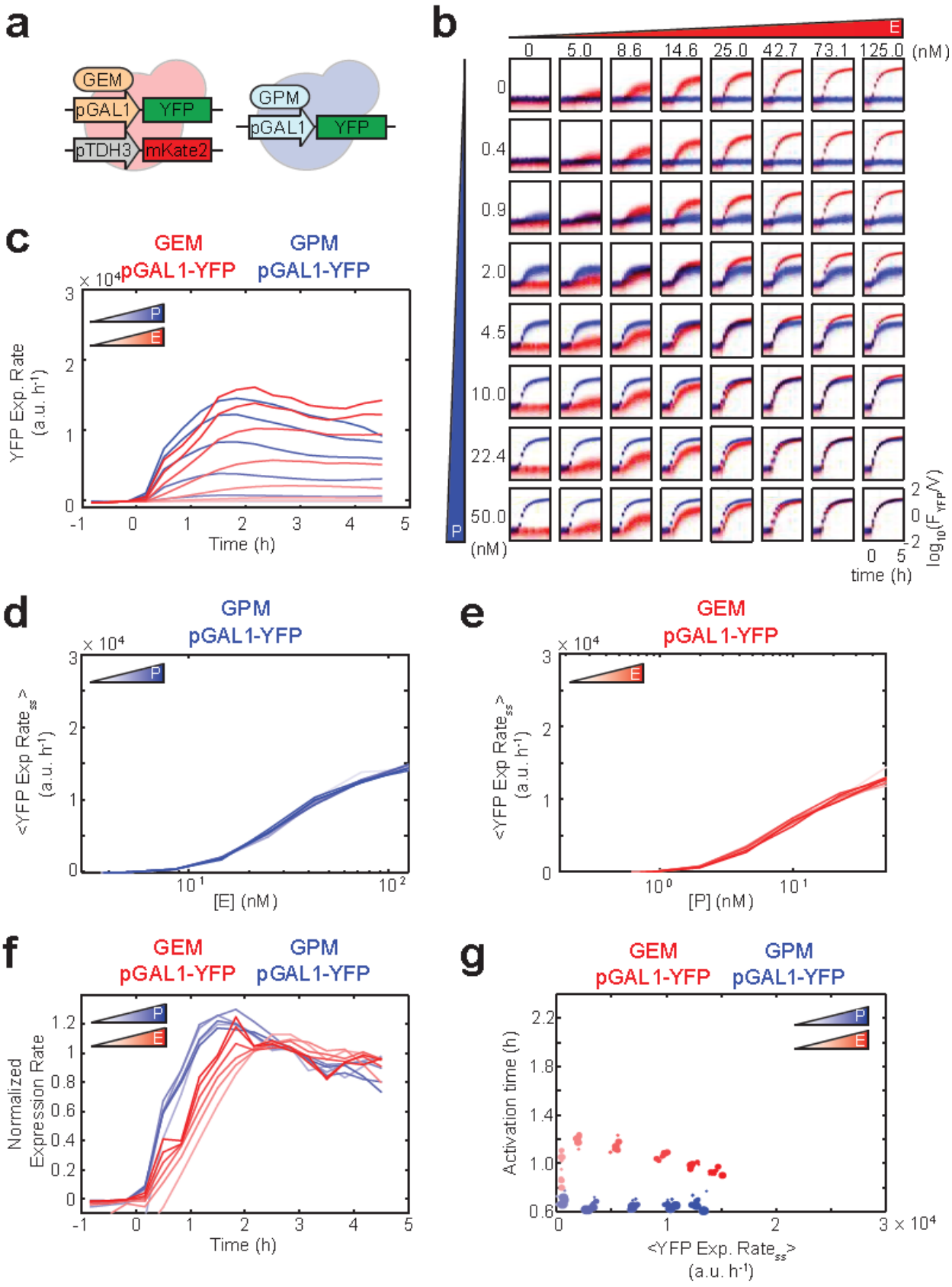
a
GEM
pGAL1
YFP
pTDH3
mKate2
GPM
pGAL1
YFP
b
E
0
5.0
8.6
14.6
25.0
42.7
73.1
125.0
(nM)
0
0.4
0.9
2.0
4.5
10.0
22.4
50.0
P
(nM)
time (h)
log10(FYFP/V)
c
GEM
pGAL1-YFP
GPM
pGAL1-YFP
× 10^4
YFP Exp. Rate
(a.u. h-1)
Time (h)
d
GPM
pGAL1-YFP
<YFP Exp Rate ss>
(a.u. h-1)
[E] (nM)
e
GEM
pGAL1-YFP
<YFP Exp Rate ss>
(a.u. h-1)
[P] (nM)
f
GEM
pGAL1-YFP
GPM
pGAL1-YFP
Normalized
Expression Rate
Time (h)
g
GEM
pGAL1-YFP
GPM
pGAL1-YFP
Activation time (h)
<YFP Exp. Rate ss>
(a.u. h-1)

Figure 2.10: Dissection of the roles of the LBD-hormone pair in determining the quantitative parameters of the TRs
(**a**) Two co-cultured strains containing either the estradiol-responsive GEM TR (left), or a progesterone-responsive hPR-LBD-containing variant (GPM, right). Both TRs bind to and activate expression of a pGAL1-YFP reporter. A red-fluorescent protein was used to label the GEM, pGAL1-YFP-containing strain (**left**). (**b**) Time-dependent volume-corrected fluorescence of pGAL1-YFP controlled by GEM (**red**) or ZPM (**blue**) for different doses of estradiol (E) and progesterone (P). (**c**) Time-dependent expression rate for pGAL1-YFP controlled by GEM for different doses of estradiol (**shades of red**) and by ZPM for different doses of progesterone (**shades of blue**). GEM and GPM-dependent expression rates are averaged over progesterone or estradiol concentrations, respectively. (**d,e**) Dose response of pGAL1-YFP expression rate from GEM (**d**) as a function of estradiol for different doses of progesterone (**shades of blue**) and of GPM (**e**) as a function of progesterone for different doses of estradiol (**shades of red**). (**f**) Mean expression rates normalized by the maximum value for each hormone concentration. (**g**) Activation time for GEM at different doses of estradiol (**shades of red**) and progesterone (**increasing circle size**) and for GPM at different doses of progesterone (**shades of blue**) and estradiol (**increasing circle size**). Expression rates in (d), (e) and (g) were averaged from 2.3 to 5.3 h after induction.

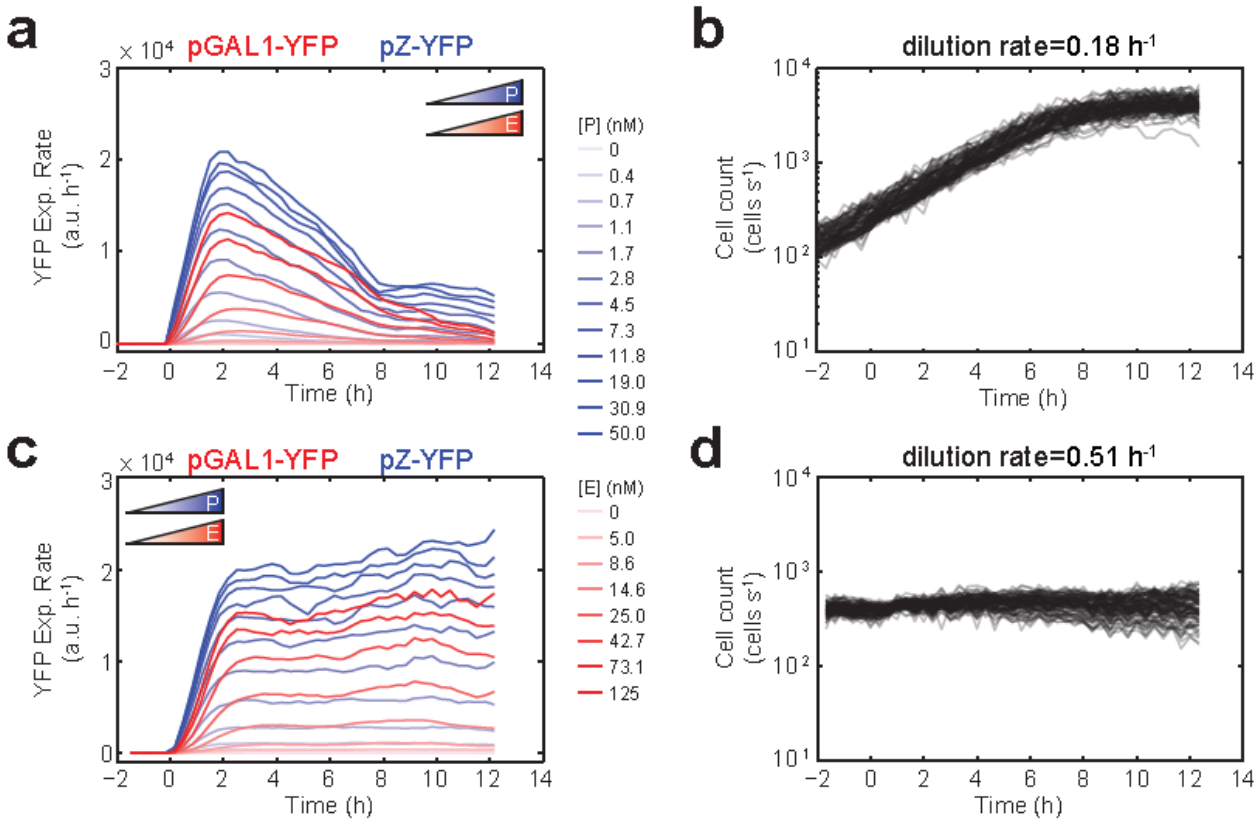

Figure 2.11: The 2D-parallel circuit can achieve either pulse-like or sustained activation of target genes based on population density

(a) Time-dependent expression rate for pGAL1-YFP (red) and pZ-YFP (blue) for different doses of estradiol (shades of red) and progesterone (shades of blue), at a low dilution rate (0.18 h^{-1}). pGAL1-YFP and pZ-YFP expression rates are averaged over progesterone or estradiol concentrations, respectively. (b) Cell density as a function of time for the experiment in (a). (c) Time-dependent expression rate for pGAL1-YFP (red) and pZ-YFP (blue) for different doses of estradiol (shades of red) and progesterone (shades of blue), at a high dilution rate (0.51 h^{-1}). Same data as in Supplementary Fig. 3a. (d) Cell density as a function of time for the experiment in (c).

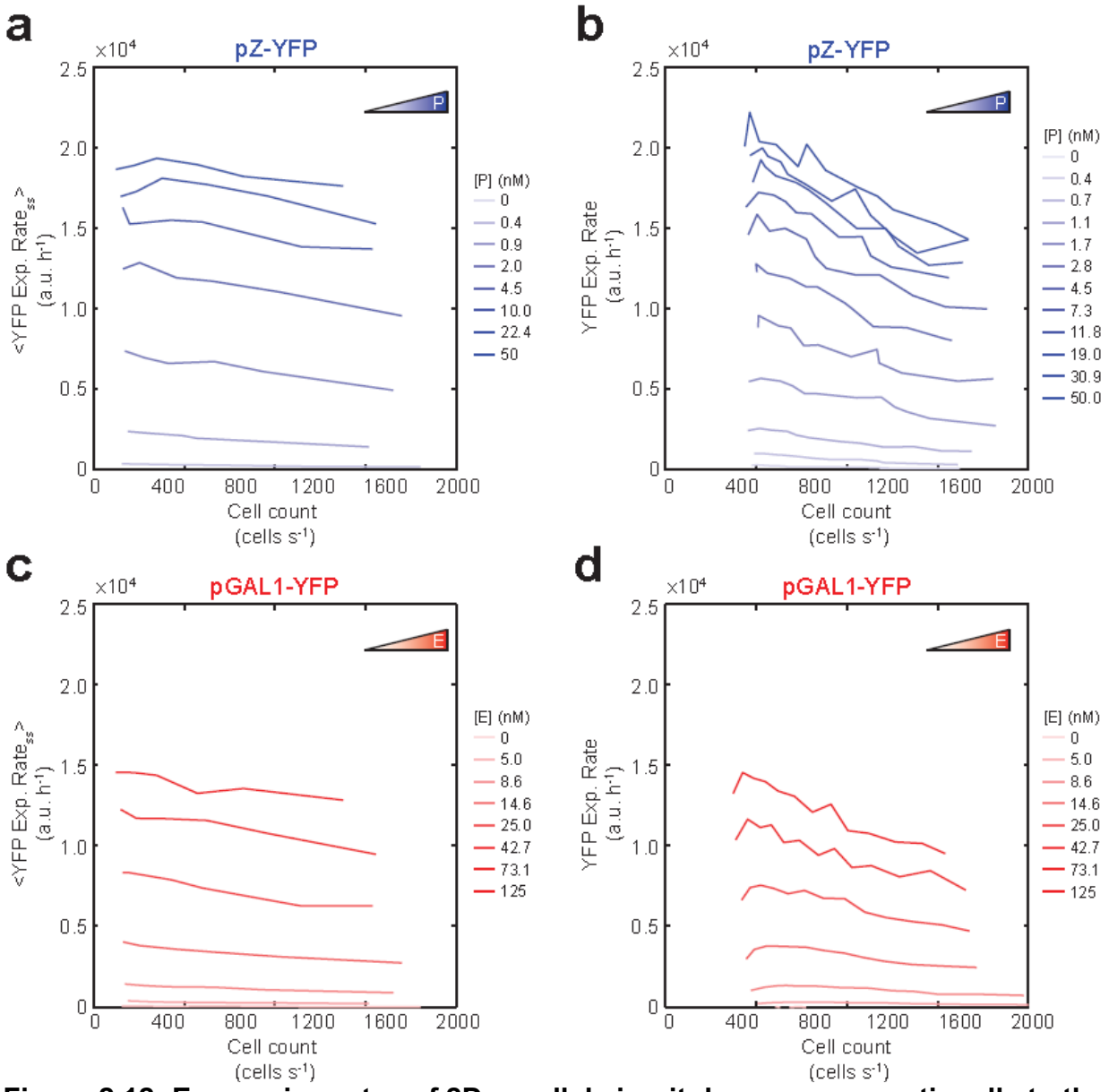

Figure 2.12: Expression rates of 2D-parallel circuit decrease proportionally to the total density of the culture

a,c) pZ-YFP and pGAL1-YFP steady-state expression rates as a function of cell count for different concentrations of progesterone and estradiol (shades of blue and red, respectively). In these experiments, cells were inoculated at a given density, which was then maintained over time by matching the dilution rate of the automated cytometry setup to the proliferation rate of the strains. For the fixed cell density, cultures were exposed to different concentrations of estradiol or progesterone. This experiment was done in duplicate and expression rates were averaged from 2 to 6.3 h after induction. (b,d) pZ-YFP and pGAL1-YFP steady-state expression rates as a function of cell count for different concentrations of progesterone (shades of blue and red, respectively). In this experiment, after progesterone or estradiol input, cell density was allowed to increase over time (same data as in Supplementary Fig. 6a,b).

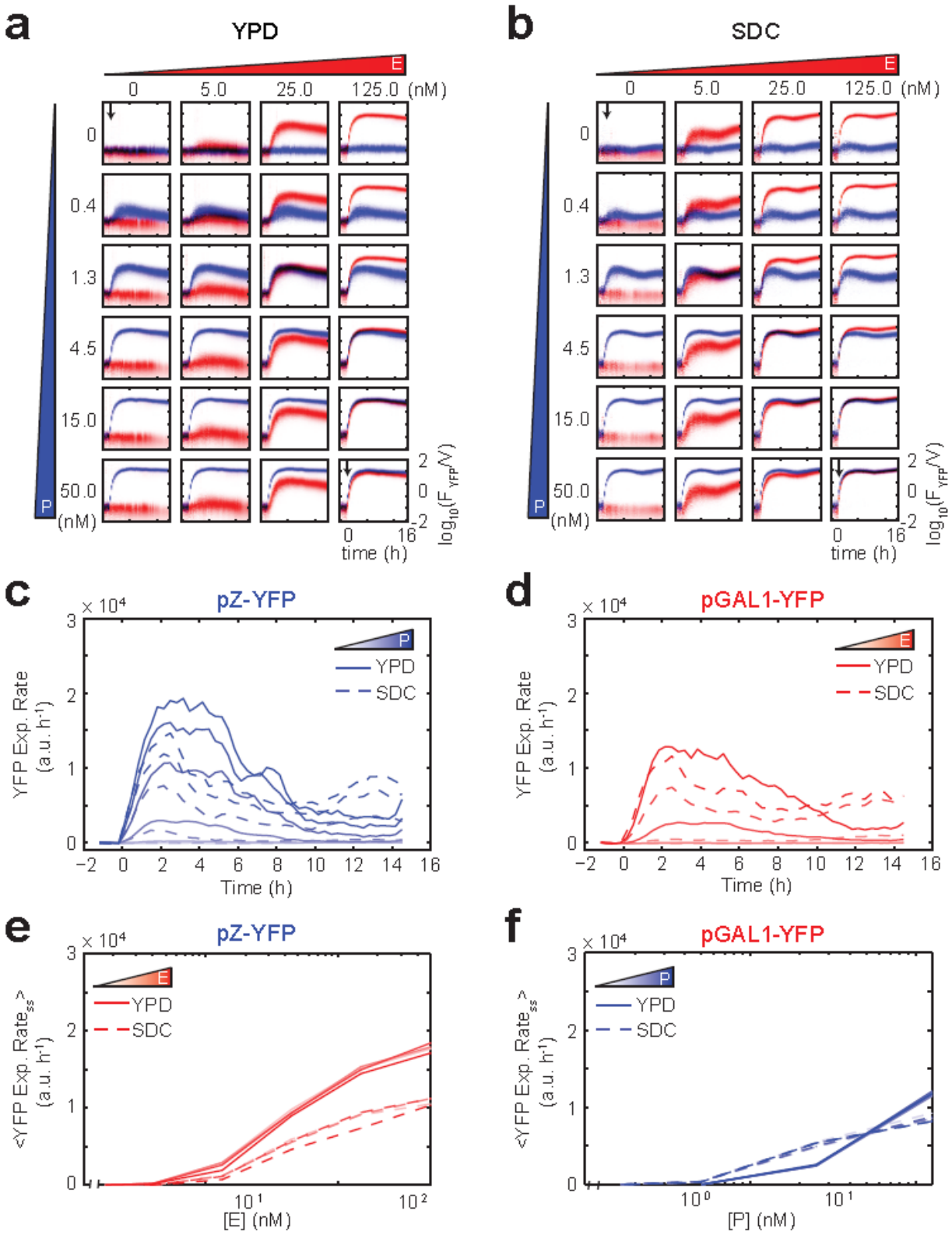

Figure 2.13: Characterization of the 2D-parallel circuit in complete (YPD) and minimal media (SDC)

Time-dependent volume-corrected distributions of pGAL1-YFP (**red**) and pZ-YFP (**blue**) fluorescence for different combinations of logarithmically-spaced doses of estradiol and

progesterone in (**a**) complete (YPD) and (**b**) minimal (SDC) media. (**c,d**) Time-dependent expression rate for pZ-YFP (**c**) or pGAL1-YFP (**d**) for different doses of estradiol (**shades of blue**) or progesterone (**shades of blue**), respectively, in YPD (full lines) or SDC (dashed lines). pGAL1-YFP and pZ-YFP expression rates are averaged over progesterone or estradiol concentrations, respectively. (**e**) Dose response of pGAL1-YFP expression rate as a function of estradiol for different doses of progesterone (**shades of blue**) in YPD (**full lines**) and SDC (**dotted lines**). (**f**) Dose response of pZ-YFP expression rate as a function of progesterone for different doses of estradiol (**shades of red**) in YPD (**full lines**) and SDC (**dotted lines**). Expression rates in (e) and (f) were averaged from 2 to 7 h after induction. For these experiments, cell cultures were diluted at a rate of 0.18 h^{-1}, not exactly matching their growth rate.

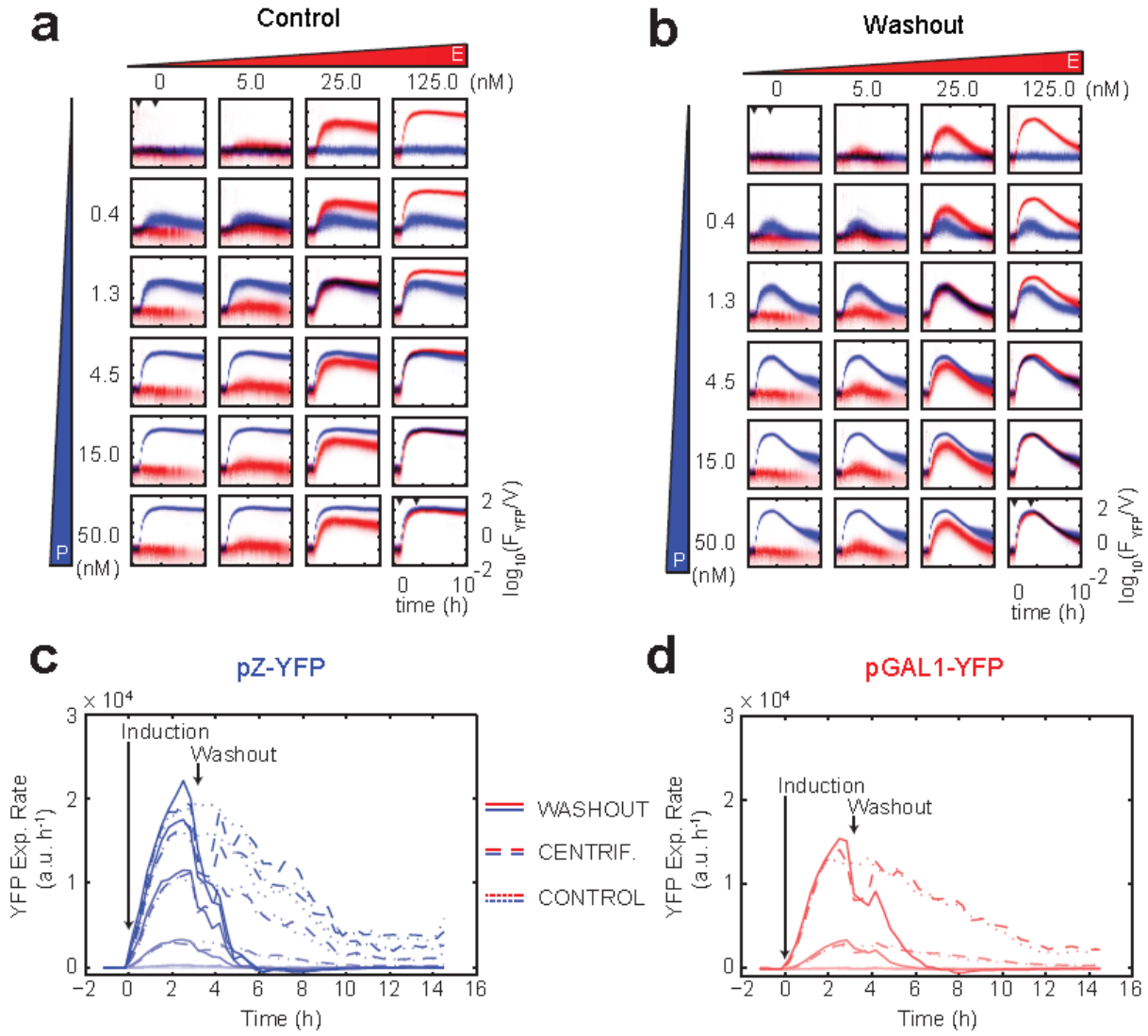

Figure 2.14: Reversibility of the 2D-parallel circuit
(**a,b**) Time-dependent volume-corrected distributions of pGAL1-YFP (**red**) and pZ-YFP (**blue**) fluorescence for different combinations of logarithmically spaced doses of estradiol and progesterone. Cultures were induced at time 0, spun-down after 3.7 hours and resuspended in media containing hormones (control, **a**) or fresh media (washout, **b**). (**c,d**) Time-dependent expression rates of pZ-YFP for different doses of progesterone (**shades of blue**) (**c**) and pGAL1-YFP for different doses of estradiol (**shades of red**) (**d**). Solid lines depict the washout experiments, the dotted lines depict the control. We also added a control where the cells were resuspended in media containing the hormones but without centrifugation (dashed lines). pGAL1-YFP and pZ-YFP expression rates are averaged over progesterone or estradiol concentrations, respectively. For these experiments, cell cultures were diluted at a rate of 0.18 h^{-1}, not exactly matching their growth rate.

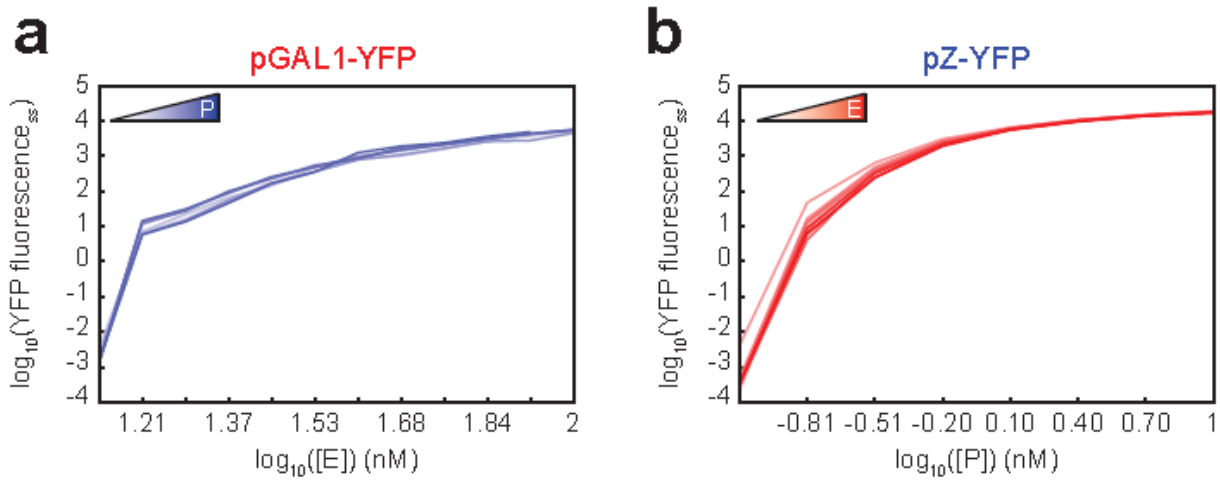

Figure 2.15: Mean volume-corrected YFP fluorescence at 4h for transcriptional reporters

(**a-b**) Mean volume-corrected YFP fluorescence at 4h for transcriptional reporters pGAL1-YFP (**a**) and pZ-YFP (**b**). This is a quantification of the transcriptional output of GEM and ZPM for the same hormone doses reported in Fig. 2 of the main text.

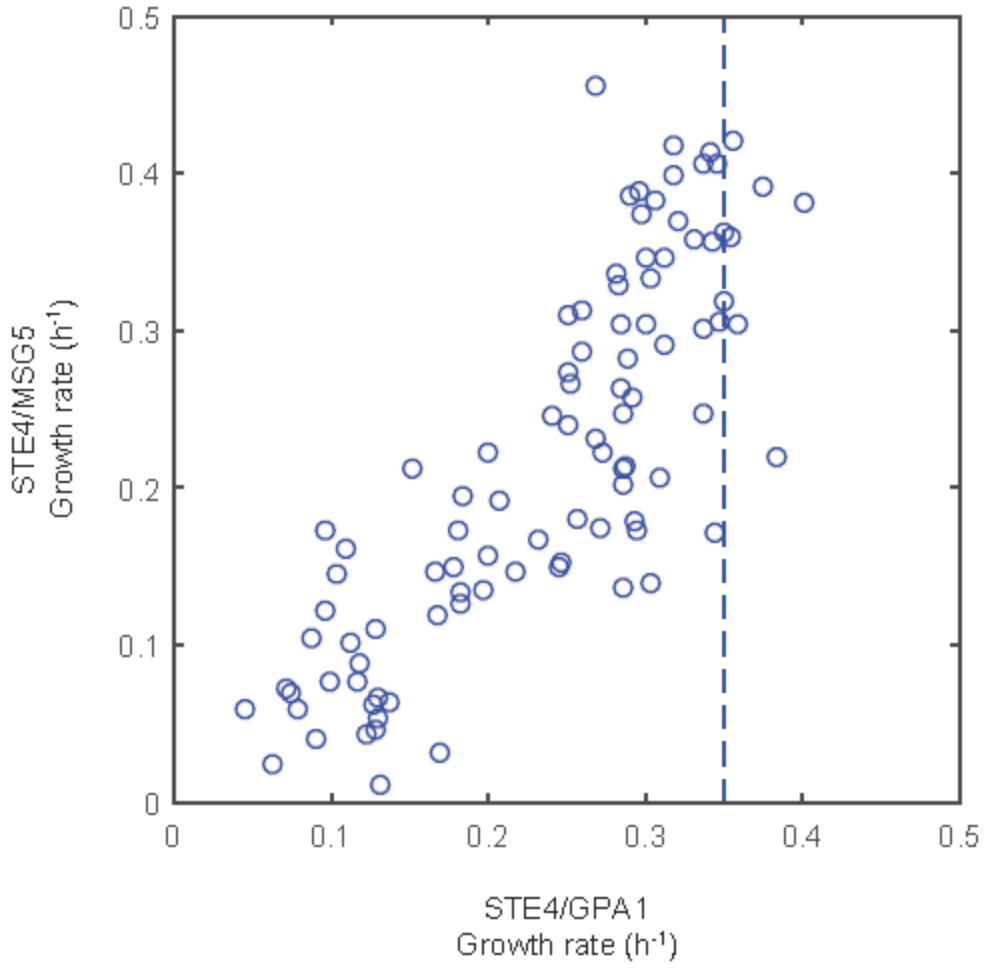

Figure 2.16: Quantitative differences of influence ofGPA1 and MSG5 on growth
Mean steady-state growth rate of strains expressing STE4 under the control of ZPM and GPA1 (x axis) or MSG5 (y axis) under the control of GEM. Each data point represents the growth rate of both strains at the same concentration of estradiol and progesterone. The vertical dashed line represents the growth rate of the MSG5 expressing strain in the absence of both hormones showing that at intermediate growth rates, for the same hormone concentrations, GPA1 expressing cells achieve close to unperturbed growth rates while MSG5 expressing cells are still impaired. Same data as in Fig. 2 b and c, lower panels.

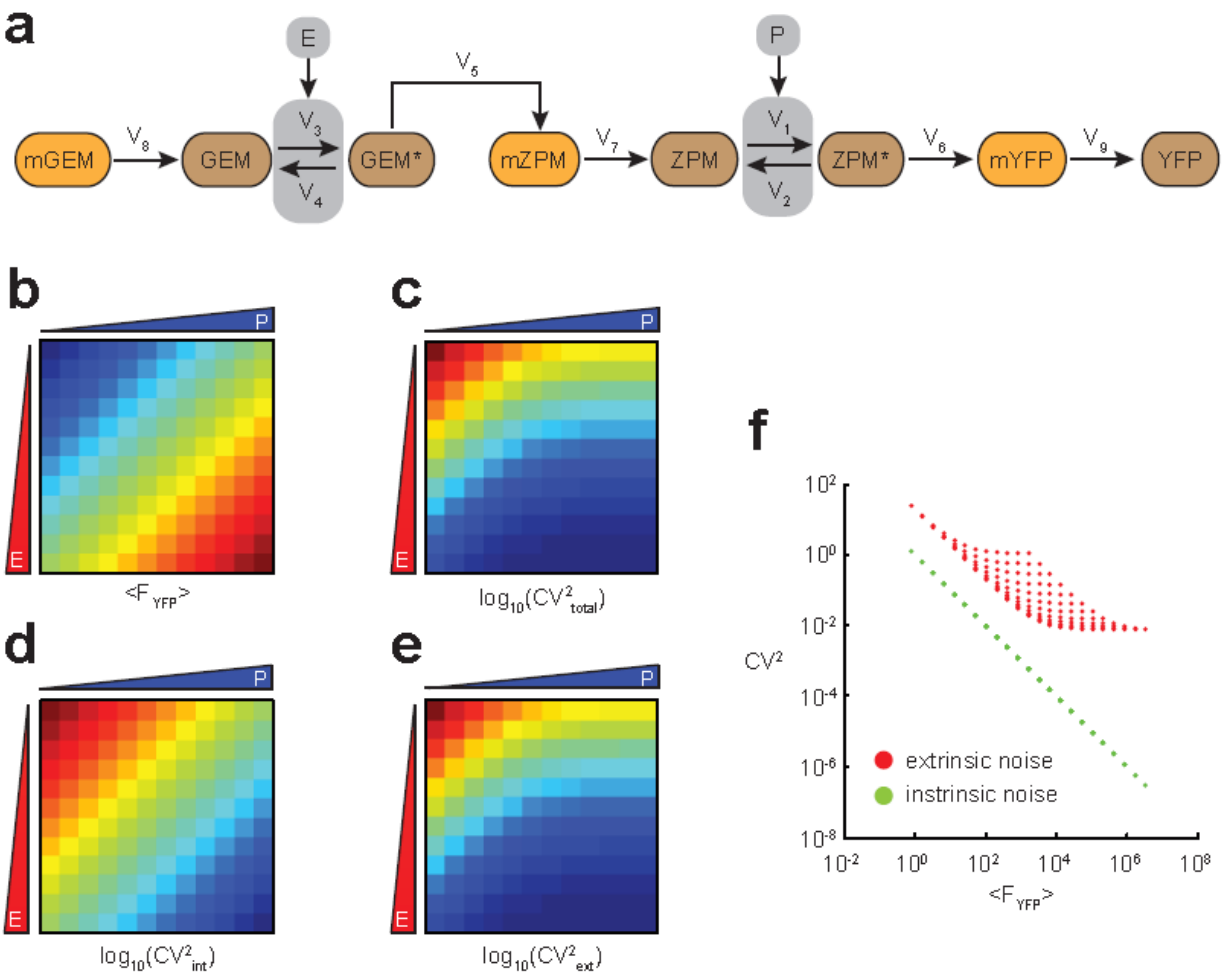

Figure 2.17: Computational design of a noise rheostat based on the connection of the two hormone inducible TRs in series

(a) A diagram of the reactions used in a model of the noise rheostat design. GEM TR is constitutively produced but its activation is dependent on estradiol (E). Active GEM TR induces the production of the ZPM TR. But production of an active ZPM TR is dependent on the presence of progesterone (P). Active ZPM TR in turn activates the production of a fluorescent reporter (YFP). (b) Steady-state YFP expression for different combinations of E and P generated by a computational model encapsulating the reactions depicted in a (see Supplementary Note for details of modeling). (c) Total noise (CV^2), and (d) intrinsic and (e) extrinsic noise components for all combinations of E and P generated by computational model. (f) Model generated intrinsic (green) and extrinsic (red) components of noise as a function of mean fluorescence.

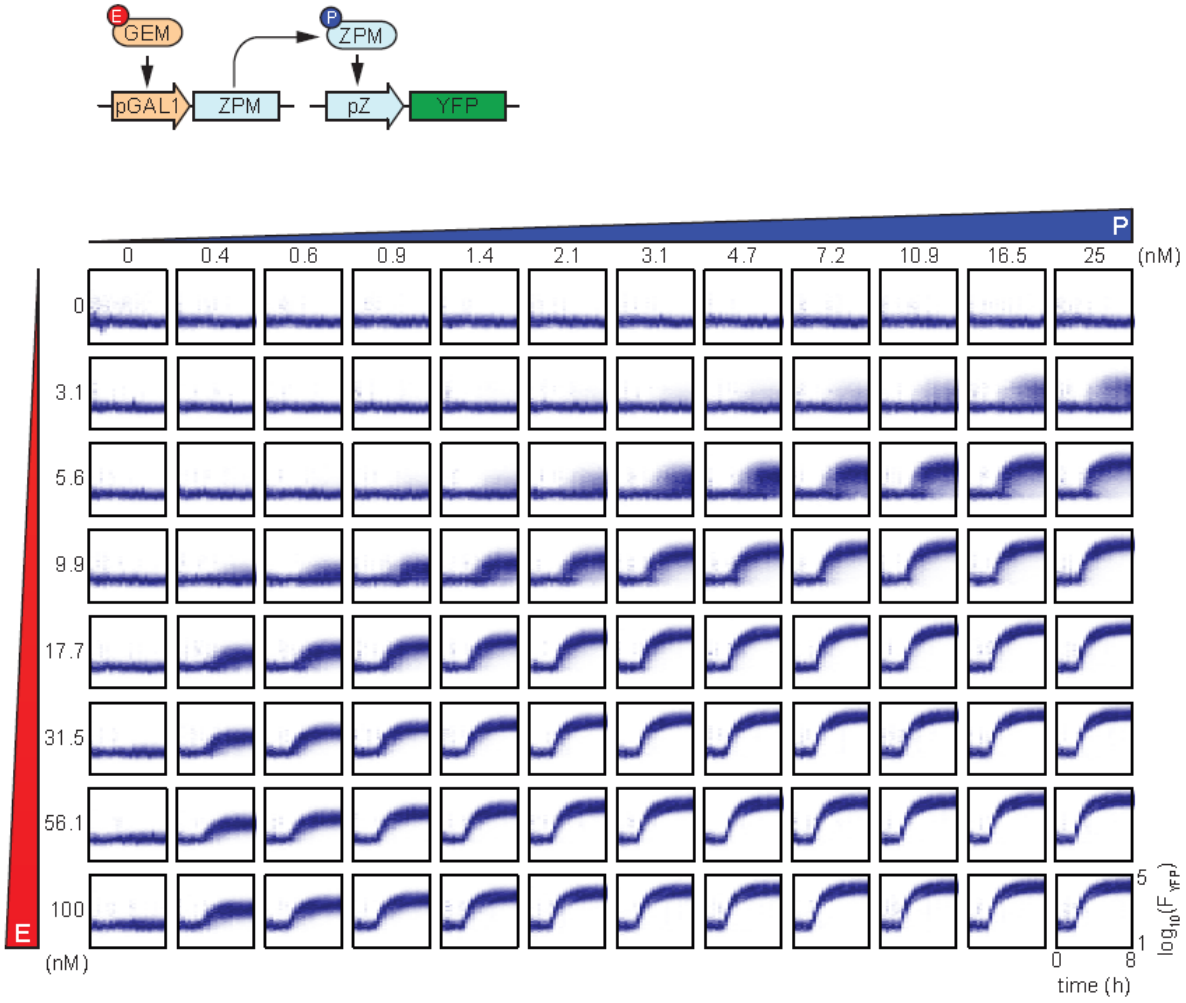

Figure 2.18: pZ-YFP Noise Dynamics in the 2D-series circuit
Single-cell fluorescence output distributions for the pZ-YFP reporter of the noise rheostat for different combinations of estradiol and progesterone.

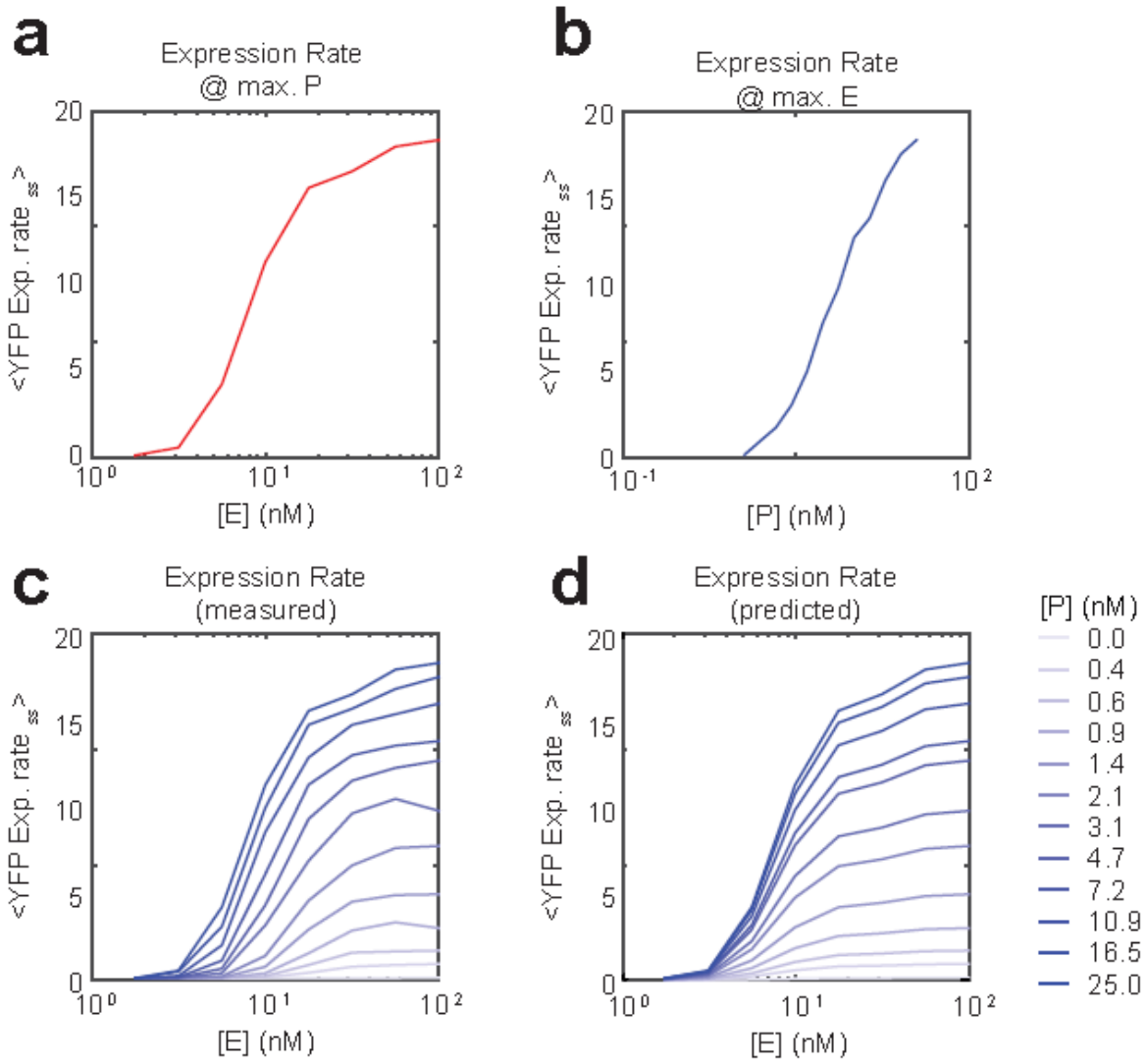

Figure 2.19: Multiplicative nature of the 2D-series noise rheostat
(**a**) Measured dose response of YFP expression rate as a function of estradiol (E) at maximum saturating progesterone (P) concentration. (**b**) Measured dose response of YFP expression rate as a function of progesterone (P) at maximum saturating estradiol (E) concentration. (**c**) Measured dose response of YFP expression rate as a function of estradiol (E) for different concentrations of progesterone (P, shades of blue). Expression rates in (a), (b) and (c) are an average for the last 10 time-points in the experiment. (**d**) Predicted dose response of YFP expression rate as a function of estradiol (E) for different concentrations of progesterone. The values in this plot are computed as the scaled product of the dose responses at either maximum progesterone (**a**) or estradiol (**b**) (see Supplementary Note).

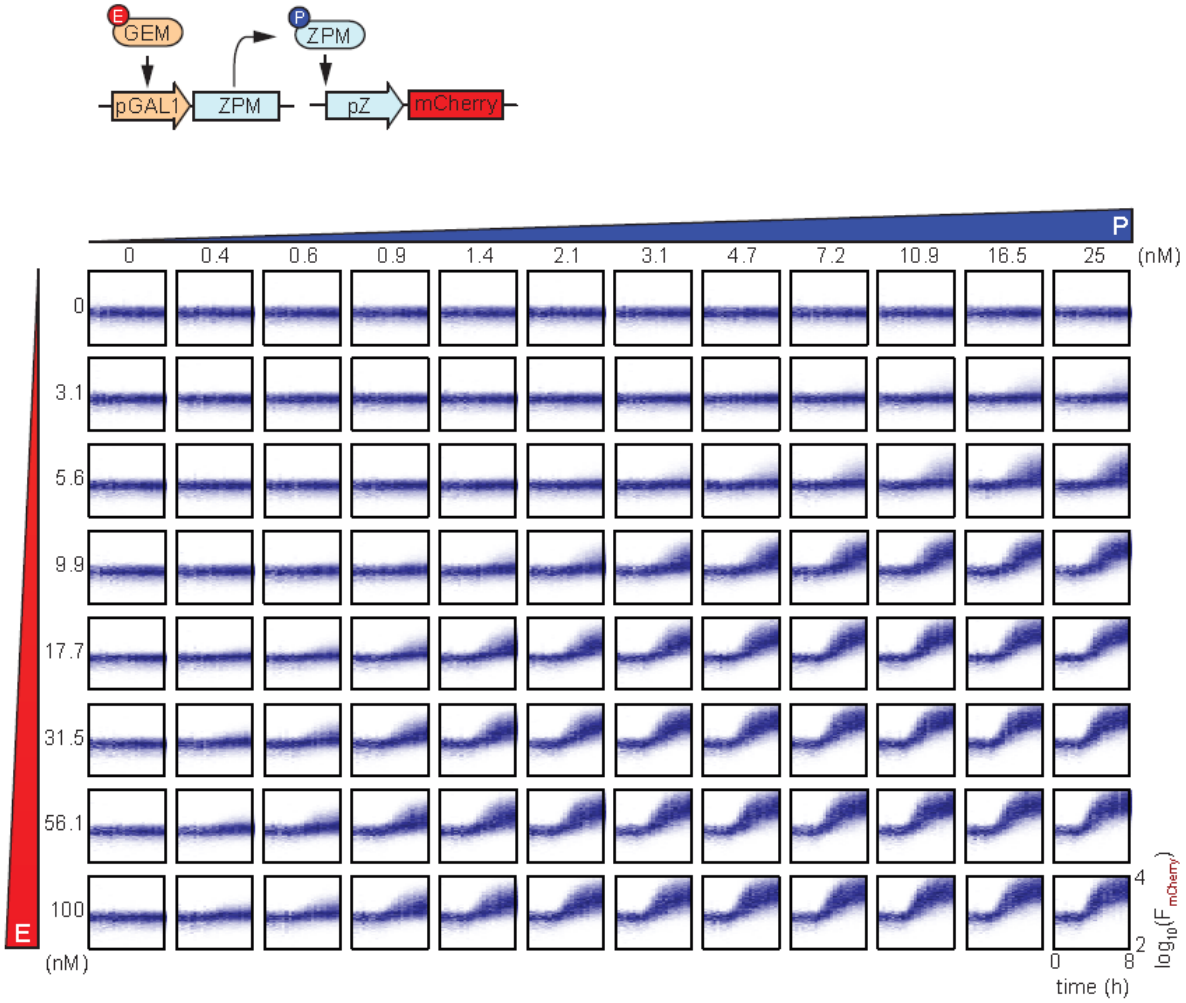

Figure 2.20: Noise modulation in the 2D-series noise rheostat is reproducible irrespective of the fluorescent protein used
pZ-mCherry single-cell fluorescence output distributions for different combinations of estradiol and progesterone.

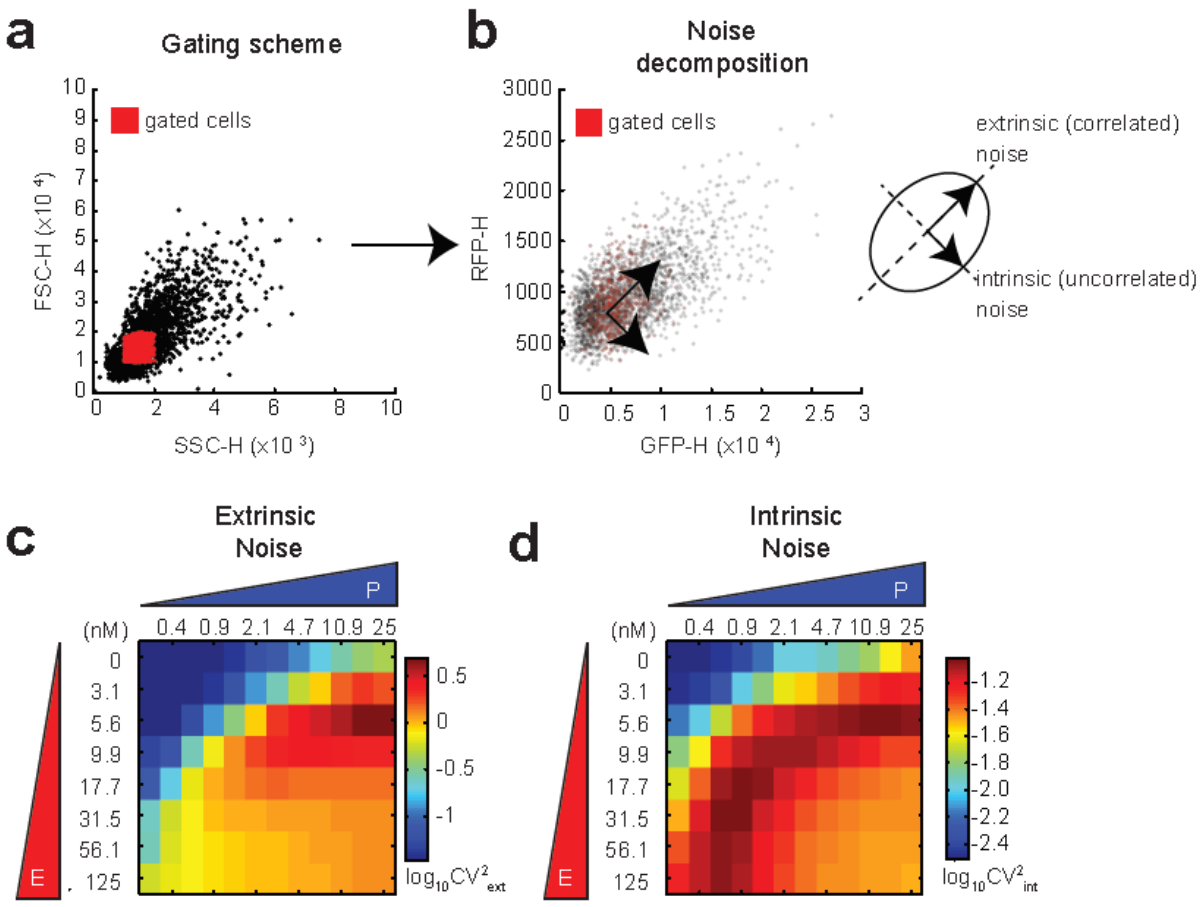

Figure 2.21: Noise decomposition into correlated and uncorrelated components in the 2D-series noise rheostat

Two different copies of pZ are used to drive either YFP or mCherry inside a single cell. (**a**) A size-uniform subpopulation of cells (**red**) was selected for analysis to remove the effect of deterministic cell size variations on protein noise. (**b**) Principal component analysis (PCA) was used to decompose the variance of this subpopulation into two orthogonal contributions (correlated and uncorrelated) at every condition and point in time. (**c**) Extrinsic (correlated) and (**d**) intrinsic (uncorrelated) noise for different doses of estradiol and progesterone. Calculations were made with the last time-point data.

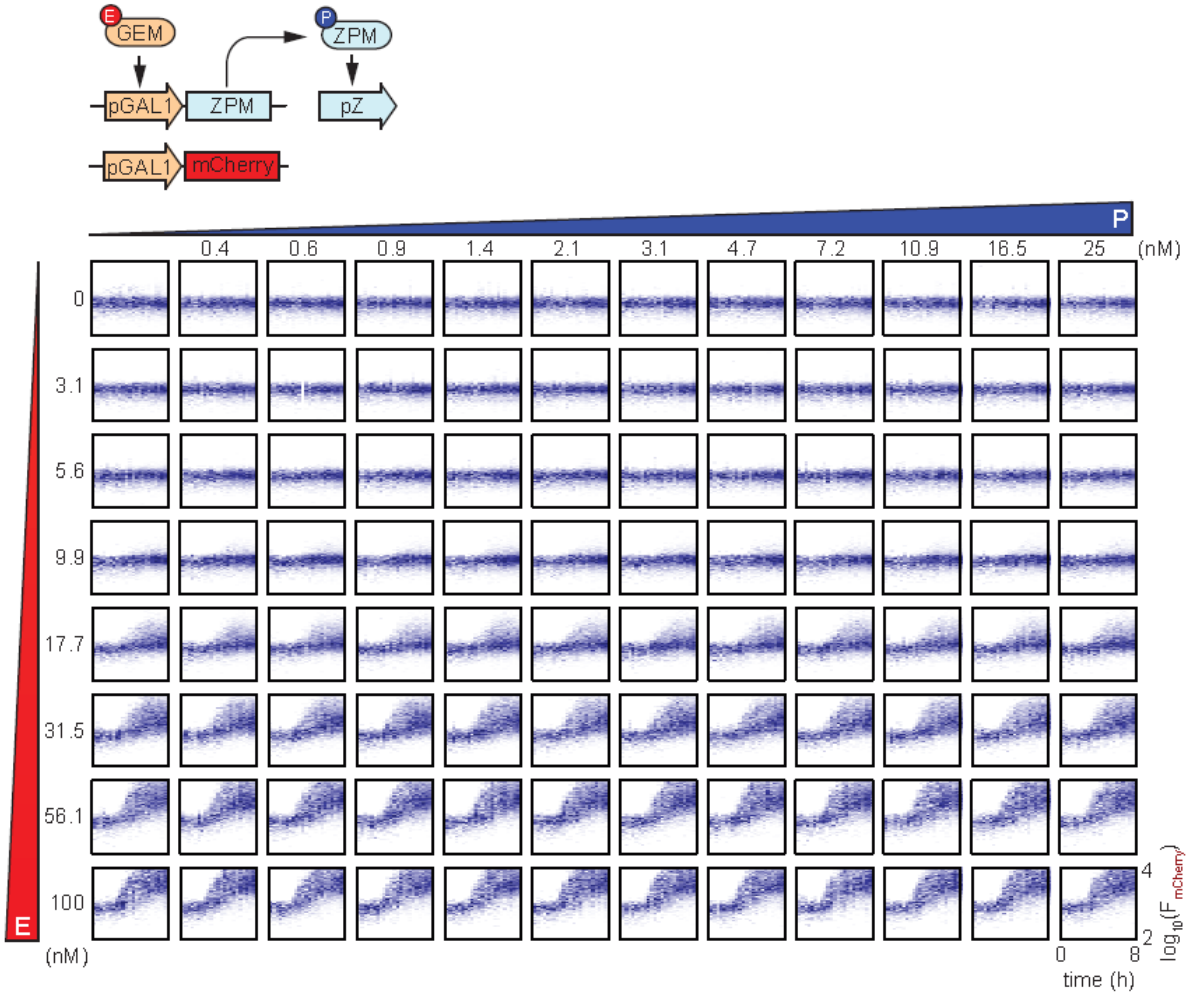

Figure 2.22: Single-cell fluorescence output distributions as a function of time of pGAL1-mCherry for different combinations of estradiol and progesterone in the 2D-series noise rheostat

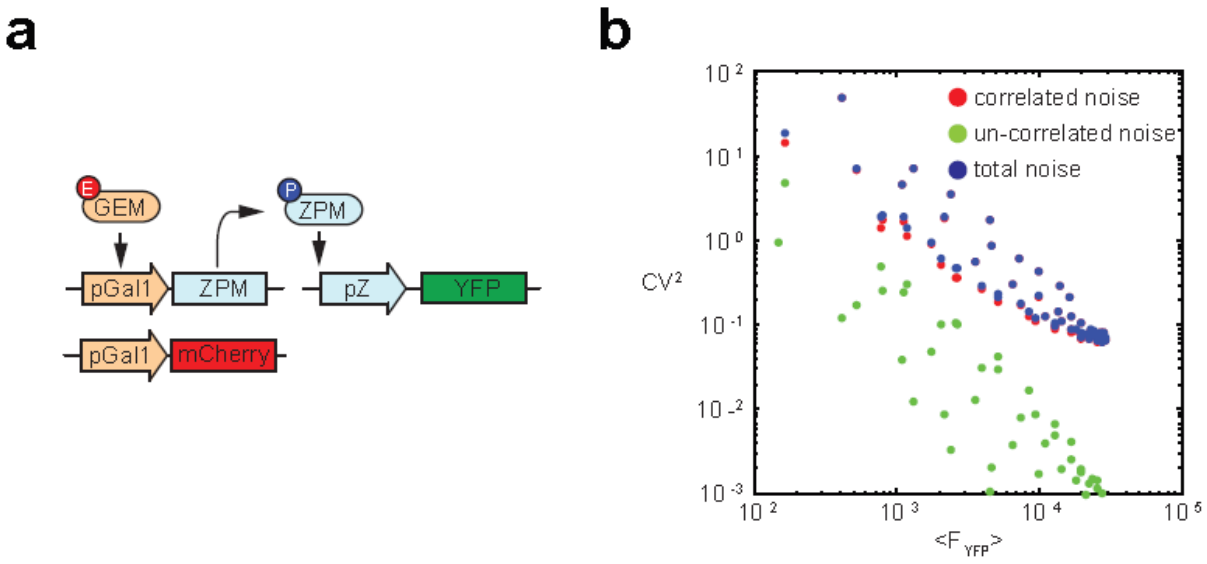

Figure 2.23: Noise decomposition of correlated and uncorrelated noise between upstream and downstream signals in the 2D-series noise rheostat noise
(a) A GEM-regulated pGAL1-mCherry reporter is used as a measurement of ZPM transcription noise. (b) Coefficient of variation associated to upstream-downstream correlated (green), uncorrelated (red) and total (blue) noise, as a function of mean fluorescence. Calculations were made with the last time-point data.

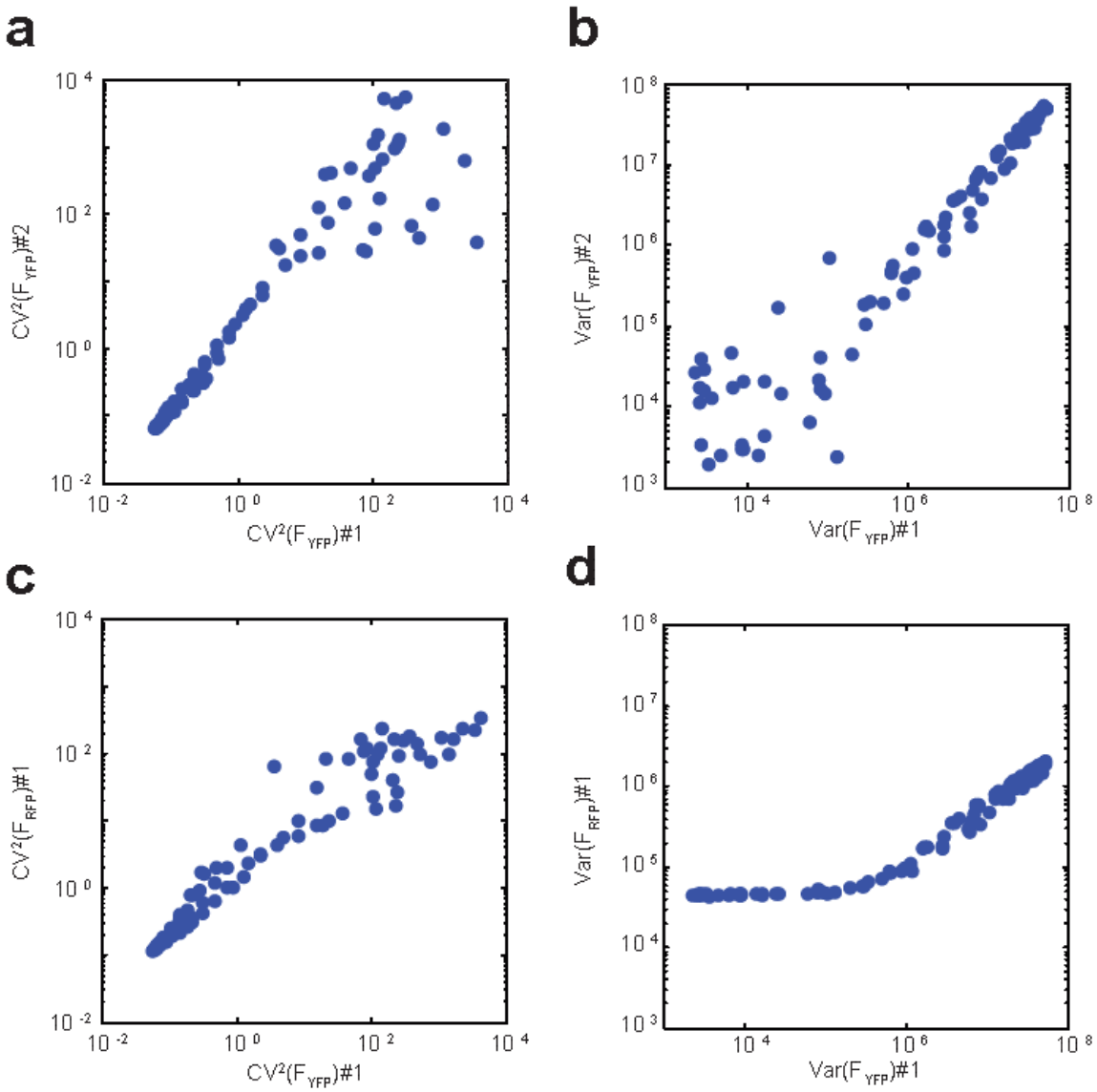

Figure 2.24: Noise profiles are reproducible across experiments and fluorescent reporters

(**a**) Coefficient of variation and (**b**) variance of the pZ-YFP reporter in the 2D-series noise rheostat for two different experiments (#1 and #2). Dots represent the value of each measurement for the same concentration of P and E in each experiment. (**c**) Coefficient of variation and (**d**) variance of the pZ-YFP and pZ-mCherry reporters. Dots represent the value of each measurement for the same concentration of P and E calculated with either reporter in the same experiment.

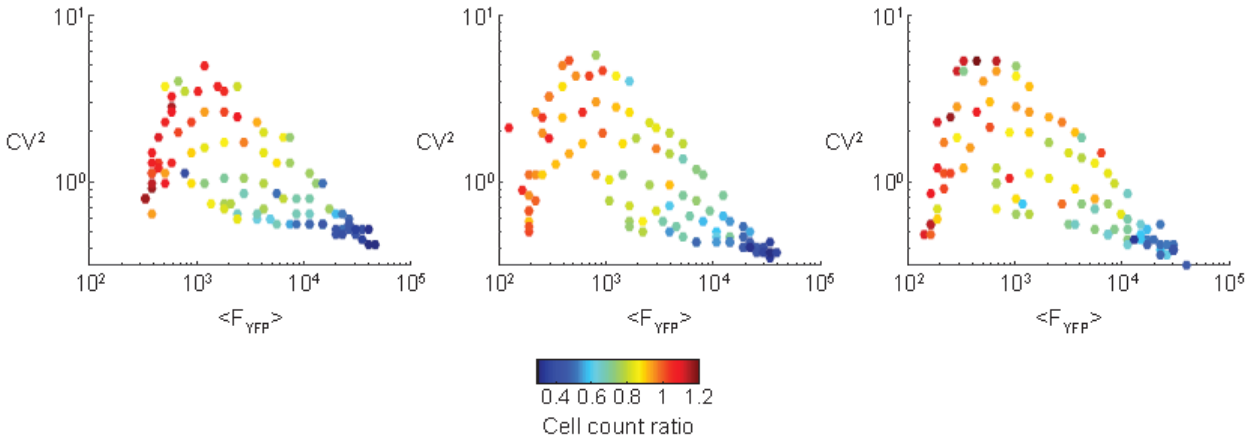

Figure 2.25: SIC1 noise profiles and growth phenotypes are reproducible across experiments

Coefficient of variation as a function of mean of the single-cell YFP fluorescence distribution for different combinations of estradiol and progesterone in a strain containing the noise rheostat regulating the expression of SIC1. Colors of the data points correspond to the cell count ratio, computed as the number of cells in 10 µL of each sample normalized to that of the control (no estradiol or progesterone) and used as a surrogate of differences in growth rate. The plots correspond to three independent experiments. Mean values from these replicates are reported in Figure 4c of the main text.

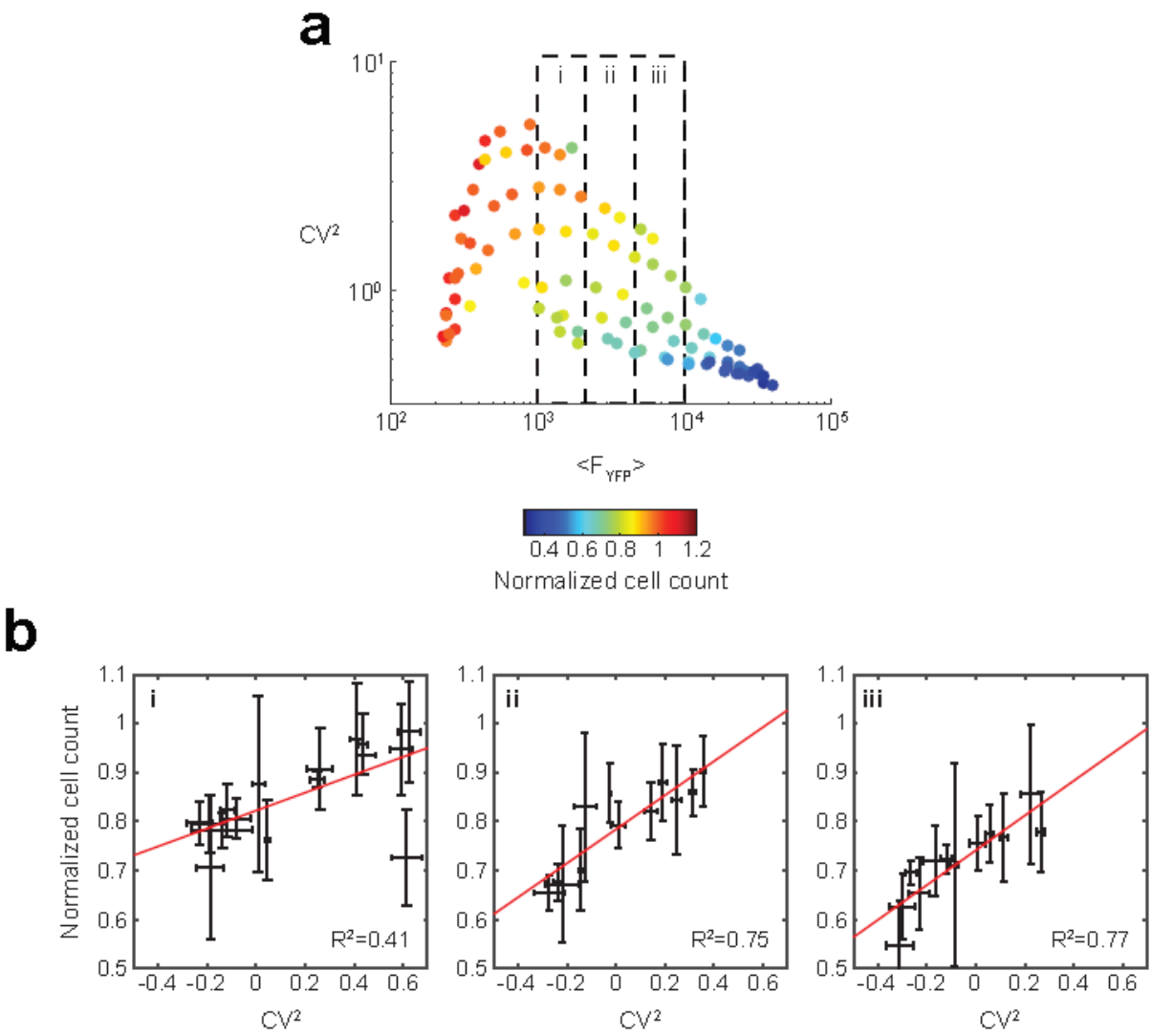

Figure 2.26: Noise rheostat achieves different variability in equi-mean expression regions of Sic1, and differences in variability lead to different growth phenotypes
(a) Coefficient of variation as a function of mean of the single-cell YFP fluorescence distribution for different combinations of estradiol and progesterone in a strain containing the noise rheostat regulating the expression of SIC1. Same as Figure 4c left. (b) Normalized cell count as a function of coefficient of variation for estradiol and progesterone conditions eliciting similar mean expression levels (boxed regions in a). Error bars represent standard deviation across the 3 experiments in Supplementary Fig 21.

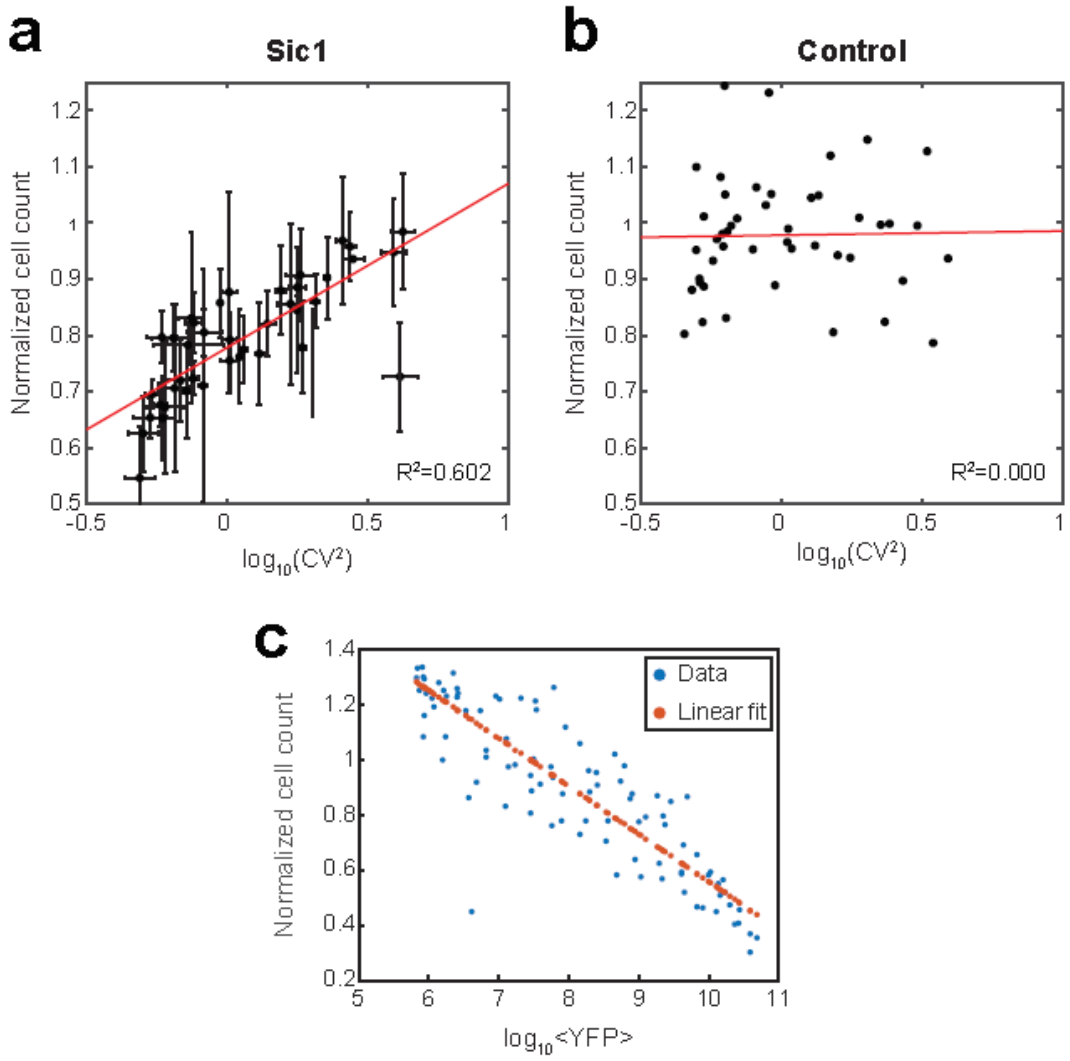
a
Sic1
Normalized cell count
log10(CV²)
R²=0.602
b
Control
Normalized cell count
log10(CV²)
R²=0.000
c
Data
Linear fit
Normalized cell count
log10<YFP>
d
Sic1
Residuals
log10(CV²)
R²=0.278
e
Control
Residuals
log10(CV²)
R²=0.004

Figure 2.27: SIC1 noise correlation with growth is independent of the mean
(**a-b**) Normalized cell count as a function of coefficient of variation for estradiol and progesterone combinations eliciting mean YFP expression levels between 1000 and 10000 a.u. (boxes i-iii in Fig. 2.26 together) in a strain harboring a SIC1 copy driven by the noise rheostat (**a**) and a control containing the noise rheostat without SIC1 construct (**b**). (**c**) Normalized cell count as a function of mean expression levels in a SIC1 construct-harboring strain. A linear fit (red dots) models the effect of the mean on cell density. (**d-e**) Residuals (calculated as distance of each data point to linear fit) as a function of coefficient of variation shows positive correlation between fitness and noise independent of the mean in SIC1 construct harboring strain (**d**) but not a control strain (**e**). Data for SIC1 noise rheostat experiment represent mean of three replicates. Error bars represent standard deviation.

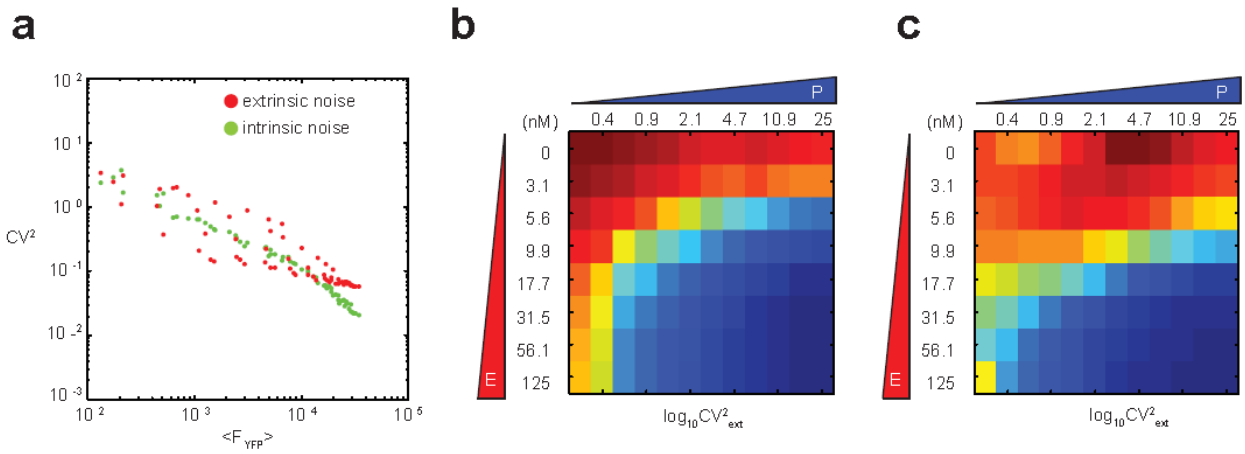

Figure 2.28: Qualitative noise features of the 2D-series noise rheostat to noise decomposition method
(**a**) Correlated (extrinsic) and uncorrelated (intrinsic) components of the noise in the output of the 2D-series circuit computed using the decomposition formalism of Elowitz et al[54]. The plot shows the squared CV as a function of fluorescence. (**b**) Intrinsic and (**c**) extrinsic components of the output noise at steady-state for doses of estradiol and progesterone.

2.11 TABLES

Table 2.1: Growth rates
Mean growth rates for each strain measured during the first 4 hours after induction. [a]: ± standard deviations (n=6 for each condition). [b]: p-value on a 2 sample t-test against the respective control. [c]: Strains used in main Figure 1.

Strain	Control	P 25nM		E 125 nM		P 25nM + E 125nM	
	Mean (h^{-1})[a]	Mean (h^{-1})[a]	p-value[b]	Mean (h^{-1})[a]	p-value[b]	Mean (h^{-1})[a]	p-value[b]
pGal-YFP[c]	0.40±0.05	0.40±0.04	0.91	0.39±0.03	0.74	0.40±0.03	0.86
pZ-YFP[c]	0.41±0.05	0.42±0.03	0.71	0.40±0.04	0.60	0.41±0.05	0.98

Table 2.2: Plasmids used in this study

Plasmid ID	Backbone (Marker)	Contents
pHES839	pNH605 (leu2)	pADH1(cr)->GAL4DBD-hERLBD-MSN2AD (GEM)
pHES941	pNH606 (ura3)	pADH1(cr)->GAL4DBD-hPRLBD-MSN2AD (GPM)
pHES795	pAAD606 (ura3)	pADH1(cr)->Zif268DBD-hERLBD-MSN2AD (ZEM)
pHES830	pAAD606 (ura3)	pADH1(cr)->Zif268DBD-hPRLBD-MSN2AD (ZPM)
pHES873	pAAD606 (ura3)	pGAL1->Zif268DBD-hPRLBD-MSN2AD (ZPM)
pHES820	pNH604 (trp1)	pGAL1->YFP
pHES840	pNH605 (leu2)	pGAL1->YFP
pHES834	pNH603 (his3)	pGAL1->mKate2
pHES875	pNH604 (trp1)	pGAL1-mCherry
pHES835	pNH603 (his3)	pZ->YFP
pHES822	pNH604 (trp1)	pZ->YFP
pHES841	pNH605 (leu2)	pZ->YFP
pHES836	pNH603 (his3)	pZ-mKate2
pHES874	pNH604 (trp1)	pZ-mCherry
pHES854	pNH603 (his3)	pTDH3-mKate2
pHES941	pNH605 modified (leu2/G418)	pAGA1-YFP-terminator-Kan^{R}
pHES936	pNH604 (trp1)	pGAL1-DIG1
pHES938	pNH604 (trp1)	pGAL1-MSG5
pHES939	pNH604 (trp1)	pGAL1-GPA1
pHES940	pNH603 (his3)	pZ-STE4
pHES942	pNH604 (trp1)	pZ-SIC1

Table 2.3 Strains used in this study

All strains background was w303a (leu2, his3, trp1, ura3, can1, ade2::ADE2)

Strain ID	Genotype
yHES1021	ura3::pADH1(cr)->ZPM, leu2::pADH1(cr)->GEM, trp1::pZ-YFP
yHES1022	ura3::pADH1(cr)->ZPM, leu2::pADH1(cr)->GEM, trp1::pGal1-YFP, his3::pTdh3-mKate2
yHES1063	leu2::pADH1(cr)->GEM, trp3::pGAL1-YFP, his3::pTDH3-mKate2
yHES914	ura3::pADH1(cr)->ZEM, leu2::pZ-YFP
yHES857	ura3::pADH1(cr)->GPM, leu2::pGAL1-YFP
yHES910	ura3::pADH1(cr)->ZPM, leu2::pADH1(cr)->GEM, his3::pGal1-mKate2, trp3::pZ-YFP
yHES1070	ura3::pADH1(cr)->ZPM, leu2::pADH1(cr)->GEM, his3::pZ-mKate2, trp3::pGal1-YFP
yHES1072	ura3::pADH1(cr)->ZPM, leu2::pADH1(cr)->GEM, can1::pAGA1-YFP-Kan^R, his3::pZ-Ste4, trp1::pGAL1-Gpa1
yHES1073	ura3::pADH1(cr)->ZPM, leu2::pADH1(cr)->GEM, can1::pAGA1-YFP-Kan^R, his3::pZ-Ste4, trp1::pGAL1-Msg5
yHES1074	ura3::pADH1(cr)->ZPM, leu2::pADH1(cr)->GEM, can1::pAGA1-YFP-Kan^R, his3::pZ-Ste4, trp1::pGAL1-Dig1
yHES1075	ura3::pADH1(cr)->ZPM, leu2::pADH1(cr)->GEM, can1::pAGA1-YFP-Kan^R, his3::pZ-Ste4, trp1::pGAL1-Dig2
yHES980	leu2::pADH1(cr)->GEM, ura3::pGAL1->ZPM, his3::pZ-YFP
yHES981	leu2::pADH1(cr)->GEM, ura3::pGAL1->ZPM, his3::pZ-YFP, trp1::pZ-mCherry
yHES982	leu2::pADH1(cr)->GEM, ura3::pGAL1->ZPM, his3::pZ-YFP, trp1::pGAL1-mCherry

Strain ID	Genotype
yHESXXX	leu2::pADH1(cr)->GEM, ura3::pGAL1->ZPM, his3::pZ-YFP, trp1::pZ-SIC1

Table 2.4: Species used in noise model

Species	Shorthand	Description
1	ZPM	ZPM protein (cytosol)
2	ZPM*	ZPM protein (nuclear)
3	GEM	GEM protein (cytosol)
4	GEM*	GEM protein (nuclear)
5	YFP	Yellow Fluorescent Protein
6	mZPM	ZPM mRNA
7	mGEM	GEM mRNA
8	mYFP	Yellow Fluorescent Protein mRNA

Table 2.5 Rate parameters for noise model

	$-k_1-k_{11}$	k_2	0	0	0	K_7	0	0		0
	k_1	$-k_2-k_{12}$	0	0	0	0	0	0		0
	0	0	$-k_3-k_{13}$	k_4	0	0	k_8	0		0
	0	0	k_3	$-k_4-k_{14}$	0	0	0	0		0
A=	0	0	0	0	$-k_{15}$	0	0	k_9	*B*=	0
	0	0	0	k_5	0	$-k_{16}$	0	0		0
	0	0	0	0	0	0	$-k_{17}$	0		k_{10}
	0	k_6	0	0	0	0	0	$-k_{18}$		0

Table 2.6: Noise model reactions

Reaction	Propensity	Parameters	Description
ZPM → ZPM*	$u_1=k_1x_1$	$k_1=P_{on}^{ZPM}\lambda$	*ZPM activation*
ZPM* → ZPM	$u_2=k_2x_2$	$k_2=(1-P_{on}^{ZPM})\lambda$	*ZPM inactivation*
GEM → GEM*	$u_3=k_3x_3$	$k_3=P_{on}^{GEM}\lambda$	*GEM activation*
GEM* → GEM	$u_4=k_4x_4$	$k_4=(1-P_{on}^{GEM})\lambda$	*GEM inactivation*
GEM* → GEM* + mZPM	$u_5=k_5x_4$	$k_5=2$	*ZPM transcription*
ZPM* → ZPM* + mYFP	$u_6=k_6x_2$	$k_6=2$	*YFP transcription*
mZPM → mZPM + ZPM	$u_7=k_7x_6$	$k_7=1$	*ZPM translation*
mGEM → mGEM + GEM	$u_8=k_8x_7$	$k_8=1$	*GEM translation*
mYFP → mYFP + YFP	$u_9=k_9x_8$	$k_9=1$	*YFP translation*
∅ → mGEM	$u_{10}=k_{10}$	$k_{10}=1$	*GEM transcription*
ZPM → ∅	$u_{11}=k_{11}x_1$	$k_{11}=0.01$	degradation/dilution
ZPM* → ∅	$u_{12}=k_{12}x_2$	$k_{12}=0.01$	degradation/dilution
GEM → ∅	$u_{13}=k_{13}x_3$	$k_{13}=0.01$	degradation/dilution
GEM* → ∅	$u_{14}=k_{14}x_4$	$k_{14}=0.01$	degradation/dilution
YFP → ∅	$u_{15}=k_{15}x_5$	$k_{15}=0.01$	degradation/dilution
mZPM → ∅	$u_{16}=k_{16}x_6$	$k_{16}=1$	degradation/dilution
mGEM → ∅	$u_{17}=k_{17}x_7$	$k_{17}=1$	degradation/dilution
mYFP → ∅	$u_{18}=k_{18}x_8$	$k_{18}=1$	degradation/dilution

Table 2.7: Stoichiometry matrix for reactions

$$S = \begin{vmatrix} -1 & 1 & 0 & 0 & 0 & 0 & 1 & 0 & 0 & 0 & -1 & 0 & 0 & 0 & 0 & 0 & 0 & 0 \\ 1 & -1 & 0 & 0 & 0 & 0 & 0 & 0 & 0 & 0 & 0 & -1 & 0 & 0 & 0 & 0 & 0 & 0 \\ 0 & 0 & -1 & 1 & 0 & 0 & 0 & 1 & 0 & 0 & 0 & 0 & -1 & 0 & 0 & 0 & 0 & 0 \\ 0 & 0 & 1 & -1 & 0 & 0 & 0 & 0 & 0 & 0 & 0 & 0 & 0 & -1 & 0 & 0 & 0 & 0 \\ 0 & 0 & 0 & 0 & 0 & 0 & 0 & 0 & 1 & 0 & 0 & 0 & 0 & 0 & -1 & 0 & 0 & 0 \\ 0 & 0 & 0 & 0 & 1 & 0 & 0 & 0 & 0 & 0 & 0 & 0 & 0 & 0 & 0 & -1 & 0 & 0 \\ 0 & 0 & 0 & 0 & 0 & 0 & 0 & 0 & 0 & 1 & 0 & 0 & 0 & 0 & 0 & 0 & -1 & 0 \\ 0 & 0 & 0 & 0 & 0 & 1 & 0 & 0 & 0 & 0 & 0 & 0 & 0 & 0 & 0 & 0 & 0 & -1 \end{vmatrix}$$

Chapter 3

Multi-kinase control of environmental stress responsive transcription

3.1 ABSTRACT

Cells respond to changes in environmental conditions by activating signal transduction pathways and gene expression programs. Here we present a dataset to explore the relationship between environmental stresses, kinases, and global gene expression in yeast. We subjected 28 drug-sensitive kinase mutants to 10 environmental conditions in the presence of inhibitor and performed mRNA deep sequencing. With these data, we reconstructed canonical stress pathways and identified examples of crosstalk among pathways. The data also implicated numerous kinases in novel environment-specific roles. However, rather than regulating dedicated sets of target genes, individual kinases tuned the magnitude of induction of the environmental stress response (ESR) – a gene expression signature shared across the set of perturbations – in environment-specific ways. This suggests that the ESR integrates inputs from multiple sensory kinases to modulate gene expression and growth control. As an example, we provide experimental evidence that the high osmolarity glycerol pathway is an upstream negative regulator of protein kinase A, a known inhibitor of the ESR. These results elaborate the central axis of cellular stress response signaling.

3.2 INTRODUCTION

Natural selection confers fitness to organisms that are able to adapt to environmental fluctuations. Changes in temperature, osmolarity and nutrient availability are recurrent stresses, and cells have evolved mechanisms to specifically sense and react to these and a variety of other environmental and internal perturbations. Such adaptive processes, collectively known as stress responses, have been extensively characterized at the transcriptional level in the model eukaryote *Saccharomyces cerevisiae* (budding yeast) [57–61]. Classical genetic and biochemical studies defined dedicated signaling pathways that sense and transmit several stress cues, including hyperosmotic shock, glucose starvation, and endoplasmic reticulum (ER) stress [62,63]. More recently, genome-wide genetic interaction studies have comprehensively quantified the effects of gene deletions on several stress response pathways including the ER unfolded protein response (UPR) and cytosolic heat shock response – not only identifying core signaling components but also modifiers of the responses [64,65]. Most stress signaling pathways contain kinases that relay extracellular and subcellular information to transcription factors that control gene expression in the nucleus. However, stresses such as heat shock and oxidative damage – well characterized transcriptionally – have no kinase networks associated exclusively with them.

There are 129 kinases encoded in the *S. cerevisiae* genome, and high-throughput investigations have defined the protein-protein and genetic interactions among the members of the yeast “kinome” [66]. These analyses established the functional organization of the global kinase network and revealed mechanisms of redundancy and

crosstalk in cell cycle regulation and developmental pathways [66–68]. However, the wiring of the kinome is not static. Under hyperosmotic stress conditions, genetic interactions among kinases are reconfigured, suggesting a plasticity to the underlying biochemical interactions [69]. Thus, two motivations – to identify kinases involved in transmitting stress signals and to explore roles for kinases that are contingent on the environment – prompted us to generate a dataset in which we measured global gene expression in a panel of kinase mutant yeast strains across a battery of environmental conditions.

3.3 RESULTS

3.3.1 Measurement of global gene expression in 28 kinase mutants in ten environmental conditions

With the goal of understanding how environmental stress signals propagate through kinase pathways to alter gene expression, we constructed a set of 28 yeast strains harboring mutations in kinases implicated in stress response signaling (Fig 3.1A, B). In each strain, an endogenous kinase gene was replaced with an analog sensitive (AS) allele. The AS alleles encode a key “gatekeeper” mutation designed to preserve catalytic function while enabling the kinase to be inhibited by addition of a cell-permeable ATP analog [70]. For eight of the kinases, the gatekeeper mutant had not been previously generated or validated (Ksp1, Mrk1, Rim11, Rim15, Ssn3, Ste11, Yak1 and Ygk3). We did not develop assays to validate these conditional mutations in this study, so it is possible that the bioinformatically-defined gatekeeper mutations may not confer analog sensitivity to these kinases.

We grew the panel of mutant kinase strains along with four wild type replicates to exponential phase in rich media, added a cocktail of three ATP analogs to ensure efficient inhibition of the various kinases, and subjected this set of 32 strains to 10 different environments: rich media (YPD), synthetic media (SDC), heat shock (39ºC), hyperosmotic shock (0.5 M NaCl), glucose depletion (YP osmo-balanced with sorbitol), endoplasmic reticulum (ER) stress (5 µg/ml tunicamycin), oxidative stress (250 µM menadione), proteotoxic stress (10 mM azetidine 2-carboxylic acid (AZC)), target of rapamycin (TOR) inhibition (1 µg/ml rapamycin), and antifungal drug exposure (250 µg/ml fluconazole). We harvested cells following 20 minutes in each environment, purified total RNA, and performed polyA+ RNA sequencing, generating a total of 301 deeply sequenced transcriptome-wide datasets (> 25X genome coverage for all samples). Since stress responses are inherently transient, we chose the 20-minute timepoint to allow for enough time for the stress to be perceived and lead to transcriptional changes, but before the responses were attenuated. Due to sequencing constraints, we did not perform experiments in the absence of inhibitor cocktail nor were we able to perform biological replicates for the mutant strains in each condition, limiting our statistical power for any one gene in any mutant in a given condition. However, the four replicates of wild type in each condition provided us with high statistical power for the expression of each gene in the genome in all conditions in the reference strain. While we sequenced RNA from each mutant strain 10 times across the conditions, our choice to sacrifice biological replicates for the mutants in each environment enabled us to broadly survey conditions.

We aligned reads, quantified read counts per gene [71] and used DESeq2 to generate normalized expression values (see methods) [72]. With this processed data, we calculated the $\log_2$ fold change of each gene in each sample with respect to wild type cells in YPD plus inhibitor cocktail. Hierarchical clustering revealed a structured matrix ordered with respect to environmental perturbations in the horizontal direction (Fig 3.1C). The genes formed ten clusters in the vertical direction, with the top two clusters enriched for stress response genes and ribosome biogenesis genes, respectively (see Table S1 for gene ontology terms associated with each cluster). Inhibition of certain kinases also induced structured patterns in certain environments. For example, zooming into the top cluster enriched for stress response genes, it is evident that inhibition of Pbs2-as, Sch9-as, Tpk1/2/3-as, and Ypk1-as altered expression of many genes in the absence of any environmental perturbation (Fig 3.1D-i). In the cluster enriched for ribosome biogenesis genes, inhibition of Cdc15-as, Pbs2-as, and Tpk1/2/3-as followed by treatment with rapamycin resulted in dysregulation of many genes (Fig 3.1D-ii). Another example is Ire1-as, inhibition of which had an effect on genes involved in ER stress specifically in tunicamycin (Fig 3.1D-iii).

To visualize similarity among the samples across the full dataset, we performed principal component analysis and t-distributed stochastic neighbor embedding (t-SNE) (Fig 3.1E) [73]. In this low dimensional representation of the data, samples that are correlated across the transcriptome should group together. In general, we observe that clusters form among samples exposed to the same environmental perturbations. However, additional clusters formed among several groups of samples in which a common kinase was inhibited – irrespective of environment – such as Tpk1/2/3-as

(homologs of protein kinase A) and the TOR pathway kinases Sch9-as and Ypk1-as. The t-SNE analysis serves to underscore the above observation that environmental perturbations have a dominant effect on gene expression. Notably, however, inhibition of Tpk1/2/3 and TOR pathway kinases resulted in transcriptome-wide effects with comparable magnitude to environmental perturbations.

3.3.2 Identification of kinase mutants that alter environment-specific gene expression

We next interrogated the dataset to determine which kinases contribute to gene expression in each environmental condition. Specifically, we asked which AS kinase strains displayed gene expression patterns that differed from wild type in each environment. To this end, we used the wild type replicates to define sets of differentially expressed genes in each environment compared to YPD (Table S2, see methods). For these sets of differentially expressed genes, we determined the fold change of each gene in the AS kinase strains relative to the average wild type value under the same environmental perturbation.

First, we plotted these two quantities against each other for every AS mutant in ER stress (tunicamycin) (Fig 3.2A). We then used linear regression to apply a line of best fit to indicate trends in the levels of the differentially expressed genes. For the set of >1000 genes differentially expressed in tunicamycin, many AS kinases such as Cdc7-as, Ctk1-as and Fus3-as produce a response that is indistinguishable from that of wild type (flat regression line, few outliers). However, mutants such as Cdc15-as and Ire1-as show an attenuated response compared to that of the wild-type (regression lines with negative

slopes), while Cdc5-as, Kin1-as and Ksp1-as show enhanced differential expression (regression lines with positive slopes). The attenuated tunicamycin response in the Ire1-as cells is consistent with a known role for Ire1 in the unfolded protein response [74], but the other implicated kinases have not been previously associated with ER stress. An additional group of AS kinases including Tpk1/2/3-as and Ypk1-as have flat slopes but large numbers of outliers, indicating low correlation with wild type across the set of differentially expressed genes. This apparent global dysregulation suggests that inhibition of these kinases may impair the ability of the cell to sense or respond to tunicamycin.

Similar analysis for hyperosmotic stress (NaCl) revealed that Pbs2-as, Hog1-as, Ste11-as and Cdc15-as have negative slopes, while Cdc7-as and Tpk1/2/3-as have positive slopes (Fig 3.2B). Ste11, Pbs2 and Hog1 form a linear mitogen activated protein kinase (MAPK) cascade that is activated by hyperosmotic stress, while Tpk1/2/3 is known to be inactivated under a variety of stress conditions including hyperosmotic shock [57]. The mitotic cell cycle regulators Cdc15 and Cdc7 have not been previously studied in the context of osmo-signaling.

We plotted the slopes for relationships as above for all inhibited kinases in each of the environmental perturbations as a heat map (Fig 3.2C). The set of kinases included in this study was enriched for those likely to be involved in the heat shock response. Indeed, while several AS mutants altered expression in many of the environments, 14/28 AS mutants attenuated the response to heat shock. However, only two mutants, Cdc15-as and Snf1-as, displayed significantly altered expression of the set of 42 genes

controlled by the heat shock transcription factor Hsf1 (Fig 3.2D)[75]. Cdc15 has no known link to Hsf1, but Snf1 has been previously reported to phosphorylate and activate Hsf1 [76]. This relative dearth of interactions between Hsf1 targets and kinases is consistent with the observation that a mutant of Hsf1 lacking all phosphorylation sites can still be induced by heat shock [77]. Thus, rather than influencing Hsf1 activity, the other 12 kinases that modulate the heat shock transcriptome do so by affecting the levels of the >400 mRNAs that are differentially expressed during heat shock in an Hsf1-independent manner [75].

3.3.3 Kinase mutants alter environmental responses by affecting overlapping and distinct sets of genes

The above analysis revealed that multiple kinase mutants alter differential gene expression in most environments (Fig 3.2C). However, it is unclear if these kinases are acting on the same sets of target genes. To ascertain this for the case of tunicamycin, we performed hierarchical clustering of the differentially expressed genes defined in Fig 3.2A and identified seven clusters (Fig 3.3A). Gene ontology analysis revealed enriched categories in five clusters. We examined Cdc15-as and Ire1-as since they both attenuated the response to tunicamycin (Fig 3.2A). While both mutants showed reduced expression of the “regulatory processes” and increased expression of the “ribosome biogenesis” clusters, only Ire1-as showed reduced expression of the “response to ER stress” cluster. In contrast to Ire1-as, inhibition of Cdc15-as did not exclusively alter any set of genes. However, while not unique to Cdc15-as, inhibition of Cdc15 showed strong repression of the amino acid metabolism genes in both tunicamycin and heat shock (Fig 3.3A). With respect to the genes differentially expressed in tunicamycin, when

compared to each other across the set of environmental conditions, Cdc15-as and Ire1-as closely mirrored each other except for the “response to ER stress” cluster in response to tunicamycin (Fig 3.3A, right). This suggests that Cdc15 and Ire1 may impinge on a common generic pathway, but that only Ire1 plays a specific role in response to tunicamycin.

In the hyperosmotic stress environment, we found that the Pbs2-as, Hog1-as, Ste11-as and Cdc15-as, display a common pattern of altered expression across the genes differentially expressed in NaCl (Fig 3.3B). With the exception of Cdc15-as, these kinases are known to form a linear MAPK cascade [78–81]. In addition, Cdc7-as uniquely shows altered expression of cell wall biogenesis genes (Fig 3.3B). When compared to each other across all the environments using the genes differentially expressed in NaCl, Hog1-as and Pbs2-as were similar but not identical, with the magnitude of the effect stronger for Pbs2-as (Fig 3.3B, right). This could be due to Hog1-independent roles for Pbs2 or to differential penetrance of the AS alleles.

3.3.4 Nonlinear interactions between environmental perturbations and inhibited kinases

To systematically identify interactions between particular environments and inhibition of specific kinases that affect the expression of individual genes, we constructed a mathematical model for the expression of each gene in the genome. In the model, the expression level of a gene is determined by the sum of two effects assumed to be independent: the environmental perturbation and the kinase inhibition ($\Delta e = c_i + k_j$, where **e** is the expression of a given gene, **c** is the contribution of the environmental

condition (indexed i) to the expression of the gene, and **k** is contribution of the inhibited kinase (indexed j) to the expression of a gene. When a predicted Δe from this model – i.e., a value for the $\log_2$ fold change for a given gene in a specific environmental condition with a particular kinase inhibited – is significantly different from the measured $\log_2$ fold change, this indicates a nonlinear interaction between the perturbation and the inhibition. This nonlinearity implies that the activity of the kinase may be somehow involved in the environmental response in a manner analogous to genetic interaction epistasis analysis [82,83].

To apply the model to the data, we decomposed the full gene expression dataset using ordinary least squares regression (Fig 3.4A, left, see methods). To compute the contribution of an environmental condition (c_i) to expression, we determined the fold change for each gene for the wild type strain in this environment relative to expression in YPD for the wild type strain (Fig 3.4A, middle). To compute the contribution of a kinase (k_j), we determined the fold change in every gene in the corresponding AS kinase strain in YPD relative to wild type in YPD (Fig 3.4A, right). For every gene, we correlated the sum of these two terms to the experimentally measured fold change value for each of the >300 measurements made for that gene across the dataset, estimating the R^2 value of this correlation. This analysis generated R^2 values for >6000 genes, whose distribution can be examined to assess the extent to which such a linear model broadly applies. (Fig 3.4B). The mean of this distribution is 0.74, indicating that, on average, the linear model can explain 74% of the variance for a given gene (see Residual and Model performance tab on online applet for all gene models: https://mace.shinyapps.io/kinase-app/).

Gene expression measurements that the model predicts well require no further explanation. However, large error between a model prediction and an experimental measurement suggests that the environmental perturbation is not independent of the inhibited kinase. We compared the distribution of the model errors to a normal distribution using a quantile-quantile plot, which demonstrated that the error was approximated well by normal distribution until the error in the model exceeded 2 standard deviations of the mean (Fig 3.4C). This error – the difference between predicted and measured expression values – is termed the "residual" and will be quantified in units of standard deviation from the mean (σ). We calculated the residual for all >2 x 10^6 data points and plotted the distribution as a density contour plot to demonstrate that the vast majority of the data points (>98%) are within 2.5σ and that the residuals are not correlated to average gene expression (Fig 3.4D). We set a threshold for residuals > 2.5σ to identify candidate transcripts regulated by a particular kinase in a given environment (Table S3).

3.3.5 Instances of residuals with putative biological significance

One of the genes that was among those best fit by the model across the full dataset was *HSP12* (R^2 > 0.9), a stress-induced gene predominately activated by the paralogous general stress transcription factors Msn2 and Msn4 (Msn2/4) [57,58,84,85]. However, one data point was an outlier that was poorly explained by the model and had a residual > 2.5σ: Tpk1/2/3-as cells treated with NaCl (Fig 3.4E). In this case, the model predicted higher *HSP12* expression than what we measured. This indicates that

Tpk1/2/3-as inhibition and NaCl do not exert independent effects on *HSP12* expression and suggests that NaCl may induce *HSP12* in wild type cells via inactivation of Tpk1/2/3, as has been previously shown experimentally[86]. We would expect the same result for glucose depletion in Tpk1/2/3-as cells, but this sample was not in our dataset.

We next extracted all genes with residual of > 2.5σ and performed gene ontology analysis (go slim terms) (Table S4). One of the top categories produced by this analysis was “response to pheromone”. We averaged expression for all genes with this designation and plotted the predicted versus measured expression for all data points (Fig 3.4F). Two points were poorly predicted by the model: Hog1-as and Pbs2-as in NaCl. In both cases, the measured expression of the pheromone response regulon was greater than predicted by the model. This result recapitulates a classical finding of crosstalk between MAPK signaling pathways. The pheromone and high osmolarity glycerol (HOG) pathways share a common upstream regulator (Ste11) [78,79,81,87]; in the presence of hyperosmotic shock, Hog1 is required to prevent spurious activation of the mating program [79].

A second enriched gene set contained genes encoding proteasome subunits in cells exposed to menadione (oxidative stress). As we did for the pheromone response genes, we averaged expression of all genes with a “proteasome” GO term and plotted the predicted expression in each of the samples as a function of experimentally measured expression (Fig 3.4G). This plot reveals that the proteasome is highly induced by menadione across all samples, consistent with prior studies[88]. Moreover, proteasome gene expression was very poorly predicted in response to menadione for two AS

kinases: Sch9-as and Ypk1-as. When these kinases are inhibited, the proteasome genes are even more highly induced by menadione than predicted. This suggests that Sch9 and Ypk1 may serve to dampen proteasome gene induction in response to menadione in wild type cells.

3.3.6 Prediction of links between kinases and transcription factors

To implicate transcription factors in responding to specific kinases in particular environments, we determined all genes with significant residuals in each sample and used MEME [89] to search for transcription factor (TF) binding motifs that are enriched upstream of these genes (Table S5). Across this gene set – which contains the outliers from the linear model – we identified enriched binding motifs associated with 33 different TFs using the JASPAR database [90]. For 21/28 mutant kinases in our dataset, this analysis identified a putative connection to at least one TF in at least one condition. Kinases such as Ypk1, Ypk3 and Rim11 connect to multiple TFs under heat shock conditions, while Snf1 connects only to a single TF during heat shock (Fig 3.5A). Similarly, Sch9 and Ssn3 connect to many TFs under oxidative stress, while Ctk1 and Ire1 have a single TF link (Fig 3.5B). It remains to be determined how many of these links represent direct kinase-substrate interactions.

While most of the conditions had sparse connections between kinases and TFs, heat shock and menadione had complex interaction networks consistent with the pleiotropic nature of temperature and oxidative stresses (Fig 3.5A, B). Heat shock had six kinases interacting with ten TFs, while menadione had nine kinases interacting with 15 TFs. Notably, while both heat shock and menadione led to enrichment of TFs known to be

involved in environmental stress responses (Msn2/4, Dot6/Tod6, Stb3, Sfp1) [57,84,91], the kinases that connect to these TFs are largely non-overlapping (with the exception of Ypk1-as and Cdc15-as). This analysis also recapitulated known interactions, such as that between Ire1 and the UPR TF Hac1 in tunicamycin [62,74], and predicted novel regulatory connections, such as that between Cdc15 and Msn2 in response to tunicamycin. Taken together, these results demonstrate that residual analysis can be used to suggest previously unknown pathways that connect environmental conditions to gene expression through kinases and their responsive TFs.

3.3.7 The HOG pathway is an upstream negative regulator of Tpk1/2/3 under all conditions

In contrast to the instances of environment-specific interactions between kinase inhibition and gene expression described above, we observed that across all conditions, Tpk1/2/3-as and Pbs2-as affect the same genes across the dataset, but do so in opposite directions for many genes (Fig 3.6A). Tpk1/2/3 is the master kinase of the environmental stress response (ESR) [57]. The ESR is comprised of two branches: the pan-stress induced (iESR) and pan-stress repressed (rESR) gene modules [57]. Mechanistically, Tpk1/2/3 has been shown to directly control phosphorylation of two sets of paralogous TFs – Msn2/4 and Dot6/Tod6 – that induce the iESR and repress the rESR, respectively [57,92–94]. Phosphorylation by Tpk1/2/3 inactivates all four of these TFs by preventing their nuclear localization[84,91]. To compare the effects of inhibition of Tpk1/2/3 to inhibition of Pbs2 with respect to the ESR, we extracted the $\log_2$ fold change of the iESR and rESR genes for all experiments where Tpk1/2/3-as was inhibited; we did the same for the values of the iESR and rESR genes when Pbs2-as was inhibited.

For reference, we extracted the $\log_2$ fold change for the iESR and rESR genes when all other kinases in dataset were inhibited. An overlay of the distributions of the Tpk1/2/3-as, Pbs2-as, and reference sets shows that: 1) inhibition of Tpk1/2/3-as led to induction of the iESR and repression of the rESR; 2) inhibition of Pbs2-as had the opposite effect: repression of the iESR and induction of the rESR; 3) inhibition of other kinases minimally affected the iESR and rESR genes (Fig 3.6B, C). This suggests that Tpk1/2/3 and Pbs2 regulate the same pathway but in an antagonistic way.

To experimentally test this prediction and to order the pathway, we utilized flow cytometry to measure a canonical fluorescent reporter of the iESR, *HSP12pr*-GFP [95–97]. We first validated that addition of 0.5 M NaCl and inhibition of Tpk1/2/3-as with 5 μM 1NM-PP1 induced the *HSP12pr*-GFP reporter (Fig 3.6D). If Pbs2 is involved in regulation of *HSP12pr*-GFP, then its deletion should alter *HSP12pr*-GFP levels. Indeed, we observed that in *pbs2*Δ cells, the basal level of *HSP12pr*-GFP was reduced 4-fold. Moreover, *pbs2*Δ obviated the ability of NaCl to induce the reporter, indicating that Pbs2 plays positive role in both setting the basal level of *HSP12pr*-GFP and inducing it in response to NaCl (Fig 3.6D). If Pbs2 is acting downstream of Tpk1/2/3, then direct inhibition of Tpk1/2/3-as with 1NM-PP1 should not be able to rescue induction of *HSP12pr*-GFP in *pbs2*Δ cells. However, we observed that addition of 1NM-PP1 led to full induction of the reporter, suggesting that Pbs2 must be acting upstream of Tpk1/2/3. To verify this, we expressed a constitutively active version of Ras2 (Ras2-G19V), a known upstream activator of Tpk1/2/3. Activation of Pbs2 by NaCl failed to induce *HSP12pr*-GFP in the presence of Ras2-G19V, while direct inhibition of Tpk1/2/3-as with

1NM-PP1 rescued induction of the reporter in the presence of Ras2-G19V. Thus, Pbs2 must be acting to inhibit Tpk1/2/3 at or above the level of Ras activation.

Tpk1/2/3 regulation is implemented by tuning the ratio of free kinase to repressor-bound kinase via the second messenger cAMP [98]. Since Pbs2 is acting at or above the level of Ras2, we hypothesized that in the absence of Pbs2, the ratio of free Tpk1/2/3 to repressed Tpk1/2/3 would be higher, and it would therefore take a higher concentration of inhibitor to inactivate Tpk1/2/3-as in *pbs2*Δ cells compared to otherwise wild-type cells. To test this, we performed a 1NM-PP1 dose response assay and measured the *HSP12pr*-GFP reporter in Tpk1/2/3-as/*pbs2*Δ cells (Fig 3.6E). Consistent with our hypothesis, Tpk1/2/3-as/*pbs2*Δ cells were desensitized to 1NM-PP1 relative to Tpk1/2/3-as cells (otherwise wild type). Moreover, Tpk1/2/3-as/*hog1*Δ cells phenocopied the Tpk1/2/3-as/*pbs2*Δ cells and were equally desensitized to 1NM-PP1. Taken together, these data indicate that the HOG pathway is a general upstream negative regulator of Tpk1/2/3 (Fig 3.6F).

3.4 CONCLUSIONS

The kinase domain evolved a highly plastic structure that enables it to maintain its core catalytic function (transferring a phosphate group from ATP onto a substrate protein) while radiating into a family that includes > 500 members encoded in human cells, each receiving a specific set of inputs and relaying information to a distinct set of substrates [99,100]. Like wires in electronic devices, kinases transmit information using a common currency – phosphorylation – that enables them form serial and parallel relays. But

unlike static wires, kinases form dynamic networks that rearrange their spatial localization and interaction partners in complex patterns that are contingent on the environment. To gain insight into the plasticity of a subset of the cellular “kinome”, we generated transcriptomic data from yeast cells exposed to 10 different environments in the context of mutations in 28 different kinases (21% of total kinases in yeast). We chose this set of kinases to be enriched for those with known or putative functions in stress pathways.

Transcriptional responses to a large number of environmental perturbations have been measured in yeast cells. A major conclusion from these studies is that across nearly all environmental stress conditions, cells display a common gene expression signature known as the environmental stress response (ESR) [57,92,93,101]. The ESR is comprised of two sets of genes that cells coordinately regulate across stresses: one that gets repressed (enriched for ribosomal protein and biogenesis genes), and one that gets induced (enriched for genes involved in alternative carbon and nitrogen metabolism) [57,101]. Subsequent studies have traced the regulation of the ESR to two major signaling axes: Ras/PKA and TOR. Key regulatory kinases in these pathways (Tpk1/2/3 and Tor1/2, respectively) phosphorylate and directly regulate the activity of transcription factors that control the ESR genes [102,103]. Consistent with this body of work, we observed both the induced and repressed ESR signatures in our environmental perturbation data (Fig 3.1C). Moreover, unlike most kinases, we observed that inhibition of Tpk1/2/3-as and the TOR-pathway kinases Sch9-as and Ypk1-as had strong transcriptional signatures in the absence of any environmental perturbation and tended to cluster together regardless of environment (Fig 3.1D, E). This result underscores the centrality of these kinases in the stress signaling network.

With the exceptions of the UPR target genes in tunicamycin in Ire1-as cells, and the pheromone responsive genes in NaCl in Hog1-AS and Pbs2-AS cells, we did not identify dedicated sets of target genes regulated by a particular kinase in a specific condition. This is not unexpected, as these connections would have likely already been made in genetic studies. However, as in the case of heat shock, we identified many kinases whose inhibition altered the gene expression response compared to wild type. But rather than modulating the targets of the specific heat shock transcription factor Hsf1 (Fig 3.2D), these kinase mutants changed the amplitude of the ESR. This is the rule rather than the exception: across the different conditions, different subsets of kinases modulate the ESR. This suggests that the inputs received by Ras/PKA and TOR are diverse and contingent.

The statistical model we employed to analyze the dataset – linear regression – is based on an assumption that the environmental perturbations and kinases each affect the expression of a given gene independently (Fig 3.4A). When this model fails to explain an experimental measurement, there is a “residual” amount of gene expression that is unaccounted for. In this case, we can infer that the kinase is involved in regulating the gene in the particular environment. By applying this residual analysis globally, we recapitulated known examples of signaling crosstalk and identified putative novel connections (Fig 3.4). Based on dysregulated genes, we mapped kinases to putative transcription factors (Fig 3.5). Identifying interactions in this manner was inspired by high-throughput genetic interaction studies [67,69,95,104,105]. Like these previous works, there are many putative connections that we have not validated. The dataset can be parsed to find these interactions on the accompanying internet application (https://mace.shinyapps.io/kinase-app/).

Finally, we focused on a global antagonistic relationship – previously proposed – that we observed in the data between Tpk1/2/3 and Pbs2, a canonical member of the high osmolarity glycerol (HOG) MAPK pathway [95]. Across all experiments, we found that Pbs2-as cells had reduced ESR output in both directions (Fig 3.6B, C). Explaining this, we found experimentally that the HOG pathway is a constitutive negative regulator acting upstream of Tpk1/2/3. While we did not reveal the precise molecular mechanism, we traced it to operating at or upstream of Ras-GTP (Fig 3.6F). These results reveal a new organization to the global stress response signaling network and elaborate the pathway at the center of the ESR.

3.5 MATERIALS AND METHODS

3.5.1 Yeast strain construction

The 28 kinases genes, including ≥800 bp of promoter/5'UTR sequence were cloned from yeast genomic DNA into single integration vectors and sequence verified. Kinases were rendered analog sensitive (AS) by site-directed mutagenesis by introducing "gatekeeper" mutations as previously described [70,106]. Yeast strains deleted for the nonessential kinases were transformed with the corresponding AS kinase mutant vector and genomic integration was verified by PCR. Essential kinases were replaced by by first being transformed with an episomal plasmid harboring a *URA3*-marked second copy of the essential kinase, then the genomic copy was deleted, then the AS allele was transformed and verified, and finally the episomal plasmid was counter-selected by 5-FOA resistance. *HSP12pr*-GFP was built by amplifying 800 bp upstream of the *HSP12* ORF from genomic DNA and cloned upstream of the GFP. All strains are in the W303

genetic background. Gene deletions were performed by one-step PCR as described [107]. Site-directed mutagenesis was performed with QuickChange according to the manufacturer's direction (Agilent). Strains used in this work are described in Table S6.

3.5.2 Inhibitor cocktail

AS kinase mutants and wild type controls were treated with a cocktail of cell-permeable ATP analogs consisting of 2 μM 1NM-PP1, 2 μM 3MB-PP1 and 2 μM BEZ235 to enable inhibition of kinases with diverse structural features near the ATP binding pocket.

3.5.3 Cell culture and treatment

Cells were inoculated from single colonies into liquid media (YPD or SDC) and grown for at least 20 hours phase at 30°C arriving in exponential phase at $OD_{600} \approx 0.5$ at the start of the experiment. Cell growth and treatment were done in deep well 96 well plates. YPD consists of 10 g/L yeast extract, 20 g/L Bactopeptone (Becton Dickinson) and 0.2 g/L dextrose (Sigma-Aldrich). Complete synthetic media (SDC) consists of 6.7 g/L nitrogen base without amino acids, 2 g/L dextrose (Sigma-Aldrich) and 0.79 g/L complete supplement mixture (MP Biomedicals). Cells were then treated with inhibitor cocktail for 5 min, followed by the given environmental perturbation for 20 min. Heat shock was performed by mixing 1 ml of cells at 30ºC with 1 ml of media pre-heated to 50ºC followed by incubation at 39ºC. Glucose depletion was performed by two consecutive whole-plate centrifugation steps (4000g for 3 minutes), decanting off media and replacing with osmo-balanced, glucose-free media (YPSorbitol). All other treatments were applied as 10x stocks made in YPD. Following treatment, cells were

then spun (4000g for 3 minutes) in the deep well plates, media decanted and plates were snap frozen in liquid nitrogen. Samples were kept in storage at -80℃.

3.5.4 Total RNA extraction

Frozen cell pellets were thawed on ice, resuspended in 1 ml water, transferred to fresh 1.5 ml tubes and harvested by spinning as above. Washed cell pellets were resuspended in 200 µl AE (50 mM NaOAc, pH 5.2, 10 mM EDTA) and vortexed. 20 µl of 10% SDS was added, followed by 250 µl acid phenol, and samples were incubated at 65℃ with shaking for 10 minutes. After an additional 5 minutes on ice, samples were spun at 15,000 rpm for 5 minutes at 4℃. Supernatants were transferred to pre-spun heavy phase lock tubes (5 Prime) and 250 µl chloroform was added. Tubes were spun at full speed for 5 minutes at 15,000 rpm and aqueous layers (above the wax) were transferred to fresh 1.5 ml tubes. 30 µl of 3M NaOAc, pH 5.2 was added followed by 750 µL ice cold 100% ethanol. RNA was precipitated at -80℃ for 30 minutes and samples were spun at 15,000 rpm for 30 minutes at 4℃. Pellets were washed with 1 ml 70% ethanol, spun at 15,000 rpm for 10 minutes at 4℃. The supernatant was removed and pellets were air dried. Pellets were resuspended in 30 µl DEPC water and the RNA concentrations of the resulting solutions measured by Nano Drop.

3.5.5 Library preparation and deep sequencing

Sequencing libraries were prepared and sequenced on an Illumina HighSeq 2500 with single end sequencing at 40 base reads. Total RNA samples were submitted to the Whitehead Institute Genome Technology Core where polyA + RNA was purified,

fragmented and sequencing libraries barcoded to enable multiplexing in an Illumina Hi-Seq 2500. Reads were assigned by the barcode to the appropriate sample.

3.5.6 Read alignment and normalization

Genomic alignment was performed using STAR [71], using the UCSC *S. cerevis*iae annotation file. Log counts were calculated using the variance stabilizing transform from DESeq2 [72]. See Computational Pipeline section for more information.

3.5.7 Differential Gene expression analysis

Differential gene expression calling for each stress-environment were defined using DESeq2 and using an adjusted p-value cutoff of 0.05 using wild type cells with YPD as the baseline condition [72].

3.5.8 GO Enrichment

GO term enrichment was assessed using the Yeastmine API [108]

3.5.9 Motif enrichment and TF association

Gene's promotor regions were defined as 500bp upstream of the canonical start sequence of the gene. Motif enrichment analysis was conducted with MEME [89], and TF motifs were defined using all the motifs in the JASPAR 2016 Yeast database [90].

3.5.10 Flow cytometry

Flow cytometry was performed on a BD Fortessa with a high throughput sampler. For each sample, 10000 cells were collected and GFP fluorescence was quantified. The median of the distribution of the GFP signal was determined for three biological replicates, the average and standard deviation of the replicates are presented.

3.5.11 Strain and Data availability

The strains are available to the research community upon request, the raw sequencing data is publicly available for download, and the processed data is presented in several interactive forms included as “applets” on the accompanying website [GSE115556, https://mace.shinyapps.io/kinase-app/].

3.5.12 Computational Pipeline

All data analysis code and figure generation steps are available at: github.com/kmace/kinase.

3.6 FIGURES

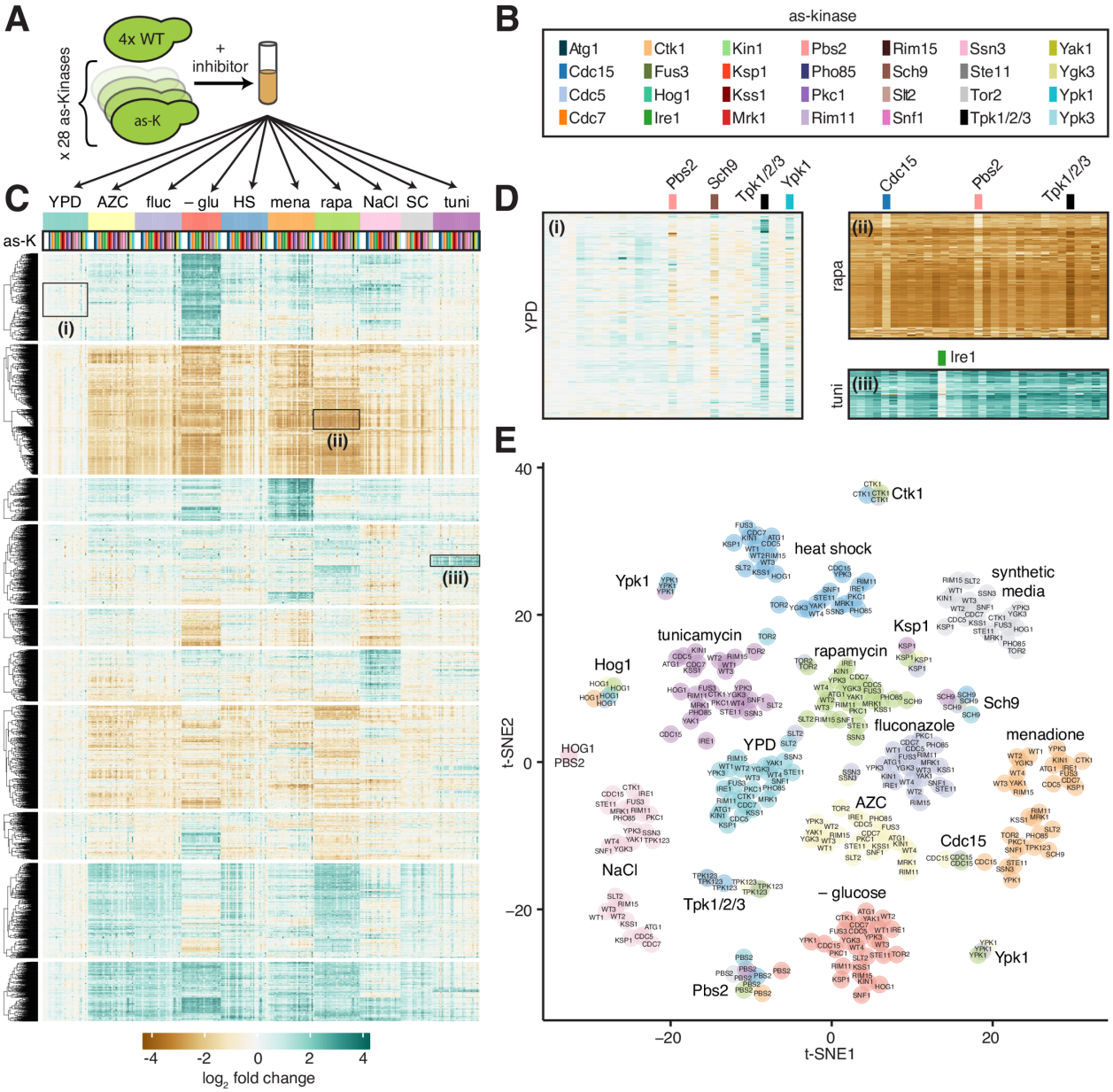

Figure 3.1: Measurement of global gene expression in 28 kinase mutants in ten environmental conditions

A) Schematic of experimental protocol. Four replicates of a wild type yeast strain and 28 isogenic strains harboring point mutations in genes encoding kinases that render the kinases “analog sensitive” (AS, see methods) were grown to exponential phase, treated with inhibitor cocktail for 5 min, and subjugated to one of 10 environmental conditions for 20 minutes.
B) Color key indicating AS kinase strains in (c), (d) and (e).
C) Expression heatmap of all genes across all samples in the dataset relative to the level of each gene in wild type cells in YPD. Gene rows are clustered hierarchically,

samples are ordered by environmental condition and by AS kinase within each condition alphabetically.
D) Expanded expression heatmaps for three regions: i) inhibition of Pbs2, Sch9, Tpk1/2/3, and Ypk1 resulted in altered expression of genes enriched for ribosome biogenesis factors in YPD; ii) inhibition of Cdc15, Pbs2 and Tpk1/2/3 altered levels of a set of genes induced by rapamycin enriched for alternative metabolic enzymes; iii) inhibition of Ire1 attenuated induction of genes enriched for ERAD components and UPR targets in tunicamycin.
E) Clustering of RNA-seq samples following dimensionality reduction by PCA followed by t-SNE plotted on a two-dimensional projection. Environments are color-coded.

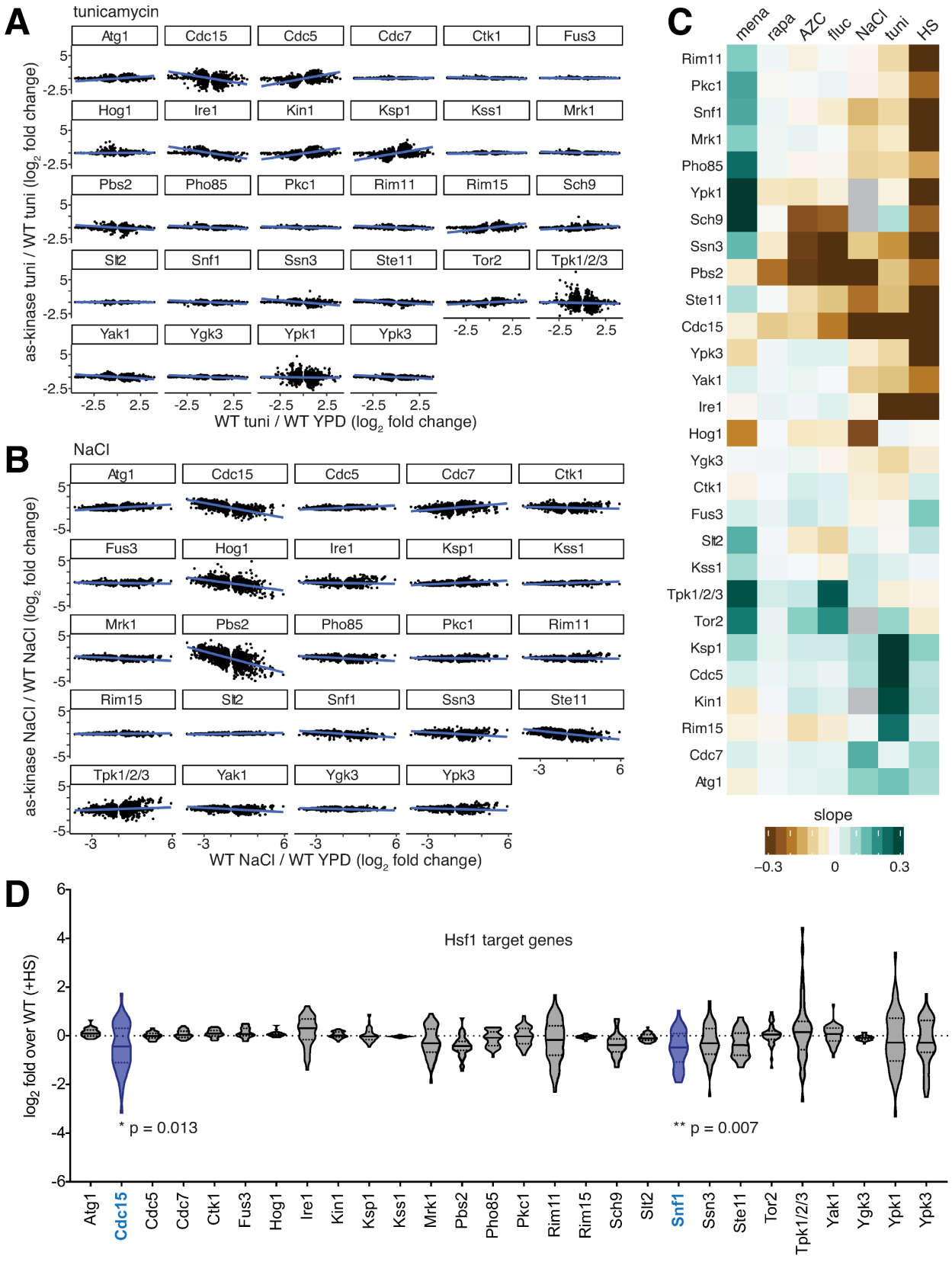

Figure 3.2: Identification of kinase mutants that alter environment-specific gene expression

A) Genes differentially expressed in tunicamycin relative to YPD in wild type cells plotted for each inhibited kinase. The x-axis is the $\log_2$ fold change for the wild type in tunicamycin; the y-axis is the $\log_2$ fold change for the inhibited kinase strain relative to wild type. **B)** the same as (A), but for the NaCl.
C) Slopes of regression lines fitted to plots like those in (A) and (B) for all inhibited kinases in all environments (missing samples in gray).
D) Expression level following heat shock of the 42 genes controlled by Hsf1. Violin plots show the $\log_2$ fold change of the 42 genes in heat shock relative to wild type in heat shock for the set of inhibited kinases. Distributions of expression levels were analyzed pairwise by two-way ANOVA, revealing that Cdc15-as and Snf1-as show statistically significant attenuation of the Hsf1 operon in heat shock.

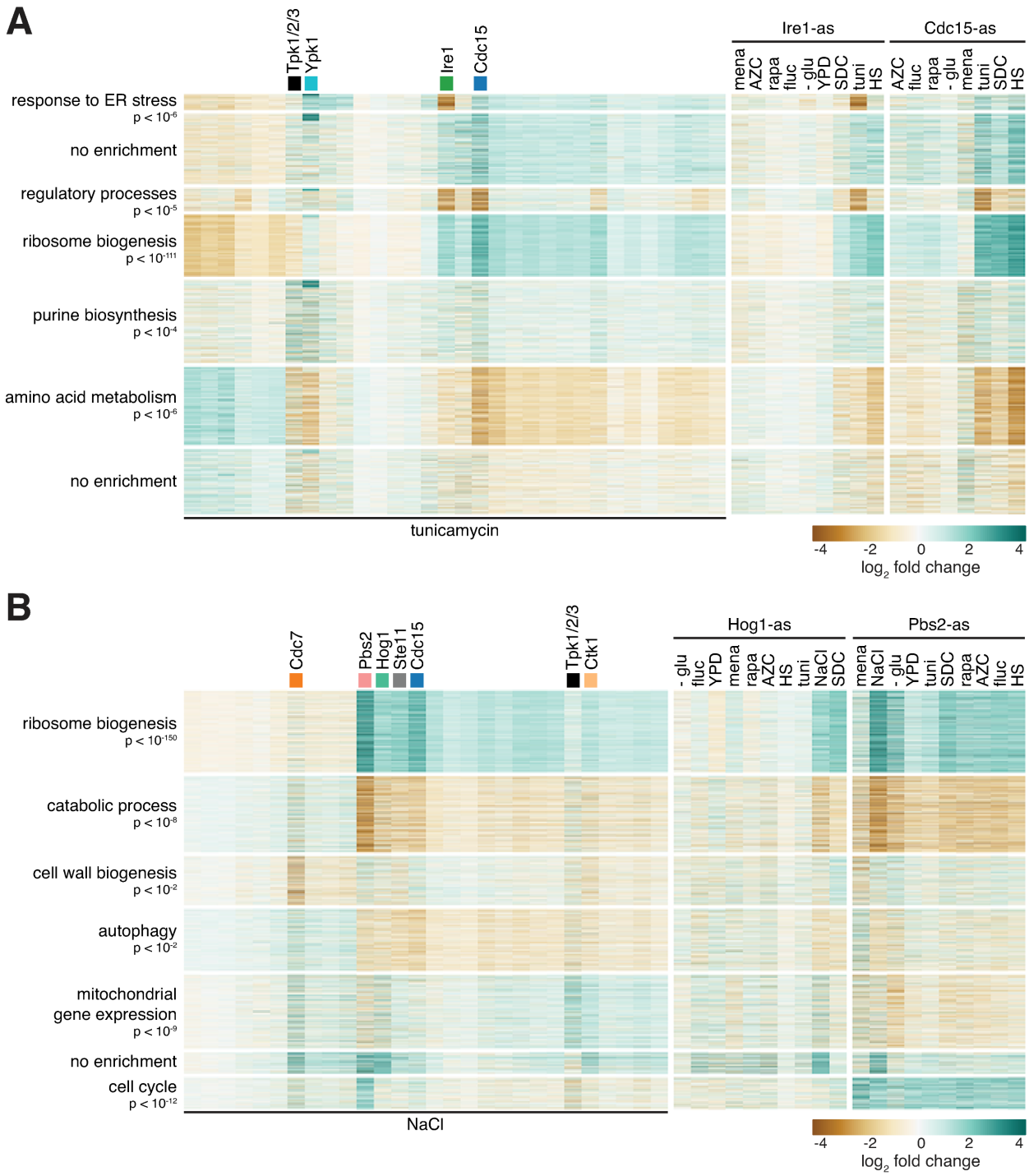

Figure 3.3 Kinase mutants that alter common environmental responses do so by affecting overlapping and distinct sets of genes

A) Heatmaps showing the set of genes differentially expressed in tunicamycin in wild type cells, clustered into seven groups labeled by the most significant gene ontology term enriched in the group. Left panel: $\log_2$ fold change relative to wild type in

tunicamycin for the set of kinase mutants treated with tunicamycin. Middle and right panels: For Ire1-as and Cdc15-as, $\log_2$ fold change of the same set of genes across all environments, shown relative to wild type in each environment.
B) As in (A) but for set of genes differentially expressed in in NaCl.

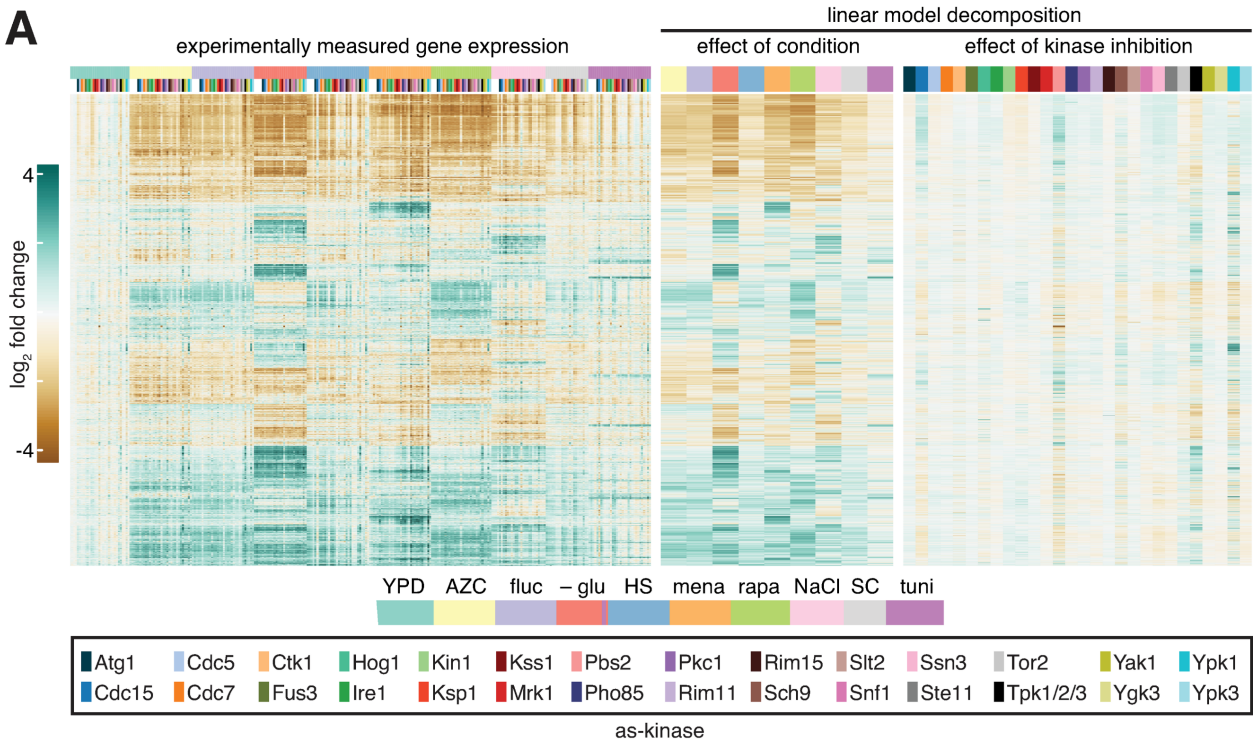
A
linear model decomposition
experimentally measured gene expression
effect of condition
effect of kinase inhibition
log2 fold change
4
-4
YPD AZC fluc – glu HS mena rapa NaCl SC tuni
Atg1 Cdc5 Ctk1 Hog1 Kin1 Kss1 Pbs2 Pkc1 Rim15 Slt2 Ssn3 Tor2 Yak1 Ypk1
Cdc15 Cdc7 Fus3 Ire1 Ksp1 Mrk1 Pho85 Rim11 Sch9 Snf1 Ste11 Tpk1/2/3 Ygk3 Ypk3
as-kinase

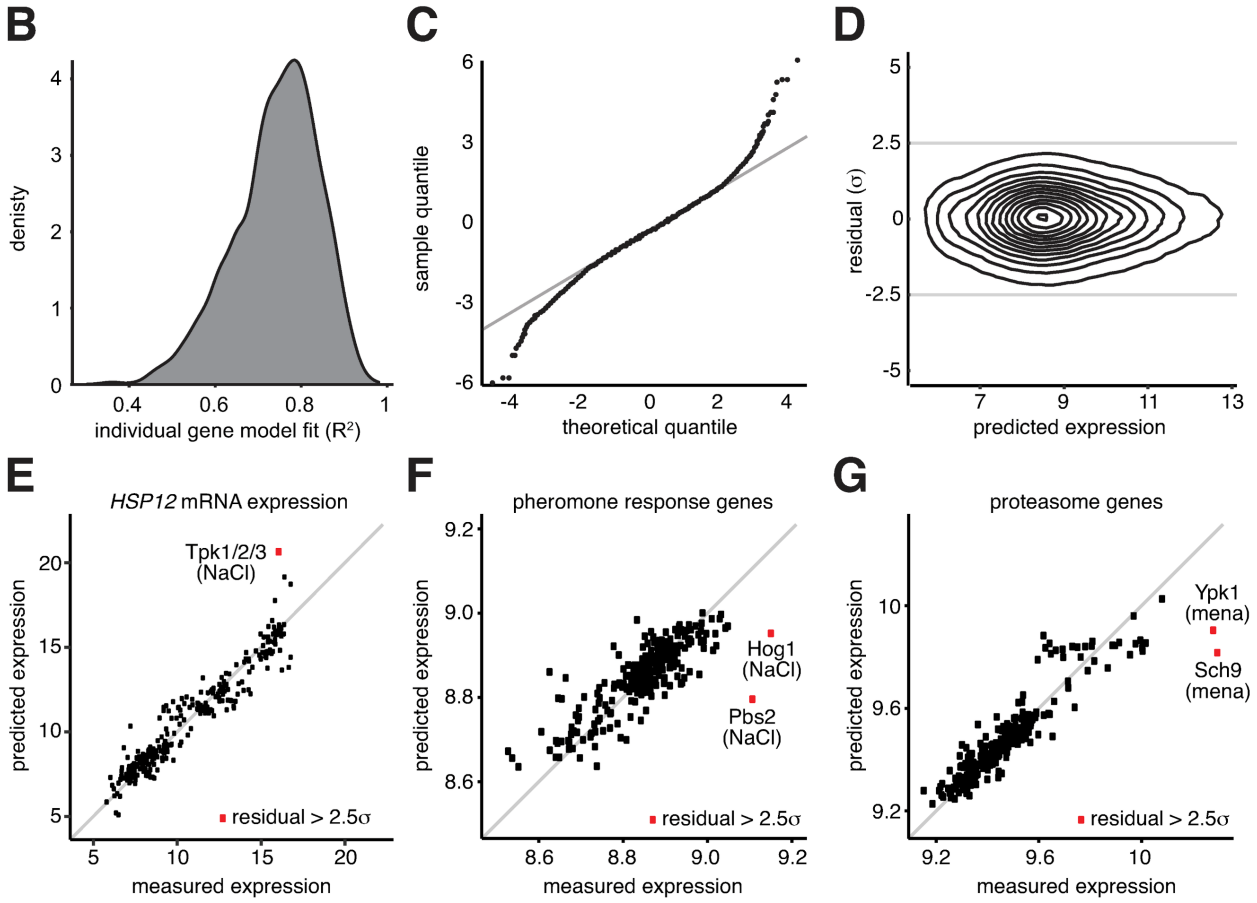
B
denisty
individual gene model fit (R²)
C
sample quantile
theoretical quantile
D
residual (σ)
predicted expression
E
HSP12 mRNA expression
Tpk1/2/3 (NaCl)
predicted expression
measured expression
residual > 2.5σ
F
pheromone response genes
Hog1 (NaCl)
Pbs2 (NaCl)
predicted expression
measured expression
residual > 2.5σ
G
proteasome genes
Ypk1 (mena)
Sch9 (mena)
predicted expression
measured expression
residual > 2.5σ

Figure 3.4 . Identification of nonlinear interactions between environmental perturbations and inhibited kinases

A) Linear decomposition of the gene expression matrix. Left panel: Measured gene expression matrix (log_2 fold change of each gene in each environment relative to the expression in wild type in YPD; same data as Fig 3.1C). Middle: A linear model was fit to each gene to estimate the contribution of each environment on expression in the wild type. The heat map shows the estimated log_2 fold change for each gene relative to expression in wild type in YPD. Right: A linear model was fit to each gene to estimate the contribution of inhibiting each kinase in YPD. The heat map shows the estimated log_2 fold change for each gene relative to expression in wild type in YPD. Kinases and environments are color-coded as depicted in the key at the bottom.

B) Frequency distribution of the set of individual gene models, binned by the quality of the fit across the full set of measurements – i.e., how well each model matches the measured expression of the given gene across the set of >300 samples – quantified as the R^2.

C) Quantile-quantile plot comparing the distribution of the residuals (the differences between the model predictions and measured values) against a theoretical normal distribution. 98% of the data points lie on the x=y line, suggesting that these residuals are normally distributed and therefore unlikely to be meaningful (just modeling and measurement error). The residuals of the remaining 2% of samples are no longer normally distributed, suggesting the linear model is insufficient in these cases.

D) Density contour plot of all two million model residuals as a function of absolute gene expression, demonstrating low correlation between residuals and expression level.

E) Scatter plot of all measurements of the expression of *HSP12*. For each sample, measured *HSP12* expression is plotted versus the predicted expression value. For a single sample, Tpk1/2/3-as under NaCl, the absolute value of the difference between the predicted and measured expression values exceeded 2.5 standard deviations. Note: *HSP12* was not measured in Tpk1/2/3-as following glucose depletion.

F) Scatter plot of all measurements of the mating pheromone response genes versus model predictions. For each sample, the expression of all genes with the gene ontology term “pheromone response” was averaged. For Hog1-as and Pbs2-as under NaCl, the measured expression of the pheromone response genes exceeded the model predictions by greater than 2.5 standard deviations.

G) As in (F), but for genes with the gene ontology term “proteasome”. For Ypk1-as and Sch9-as under menadione, the residuals exceeded 2.5 standard deviations.

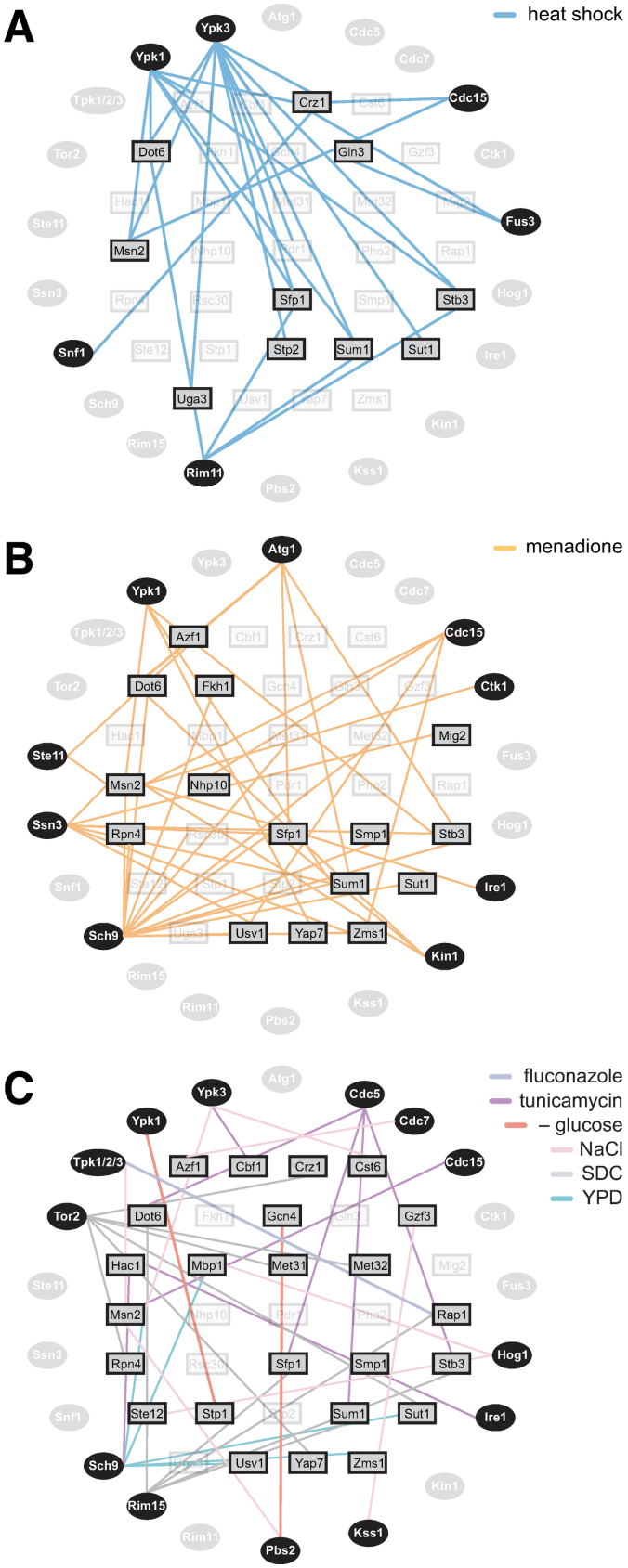
A
heat shock
Ypk3
Ypk1
Crz1
Cdc15
Dot6
Gln3
Fus3
Msn2
Sfp1
Stb3
Snf1
Stp2
Sum1
Sut1
Uga3
Rim11
B
menadione
Atg1
Ypk1
Azf1
Cdc15
Dot6
Fkh1
Ctk1
Mig2
Ste11
Msn2
Nhp10
Ssn3
Rpn4
Sfp1
Smp1
Stb3
Sum1
Sut1
Ire1
Sch9
Usv1
Yap7
Zms1
Kin1
C
fluconazole
tunicamycin
– glucose
NaCl
SDC
YPD
Ypk3
Cdc5
Ypk1
Cdc7
Tpk1/2/3
Azf1
Cbf1
Crz1
Cst6
Cdc15
Tor2
Dot6
Gcn4
Gzf3
Ctk1
Hac1
Mbp1
Met31
Met32
Mig2
Ste11
Fus3
Msn2
Rap1
Ssn3
Rpn4
Sfp1
Smp1
Stb3
Hog1
Ste12
Stp1
Sum1
Sut1
Ire1
Sch9
Usv1
Yap7
Zms1
Kin1
Rim15
Kss1
Pbs2

Figure 3.5 Prediction of links between kinases and transcription factors

A) The set of all genes with expression measurements with model residuals greater than an absolute value of 2.5 standard in any sample was analyzed for enriched TF binding sites in their promoter regions. The edges on the graph connect peripheral AS kinases with interior TFs. Connections indicate that when the given kinase is inhibited during heat shock, the genes with significant residuals are enriched for binding sites for the given TF.
B) As in (A), but for menadione.
C) As in (A), but for all environments except heat shock and menadione.

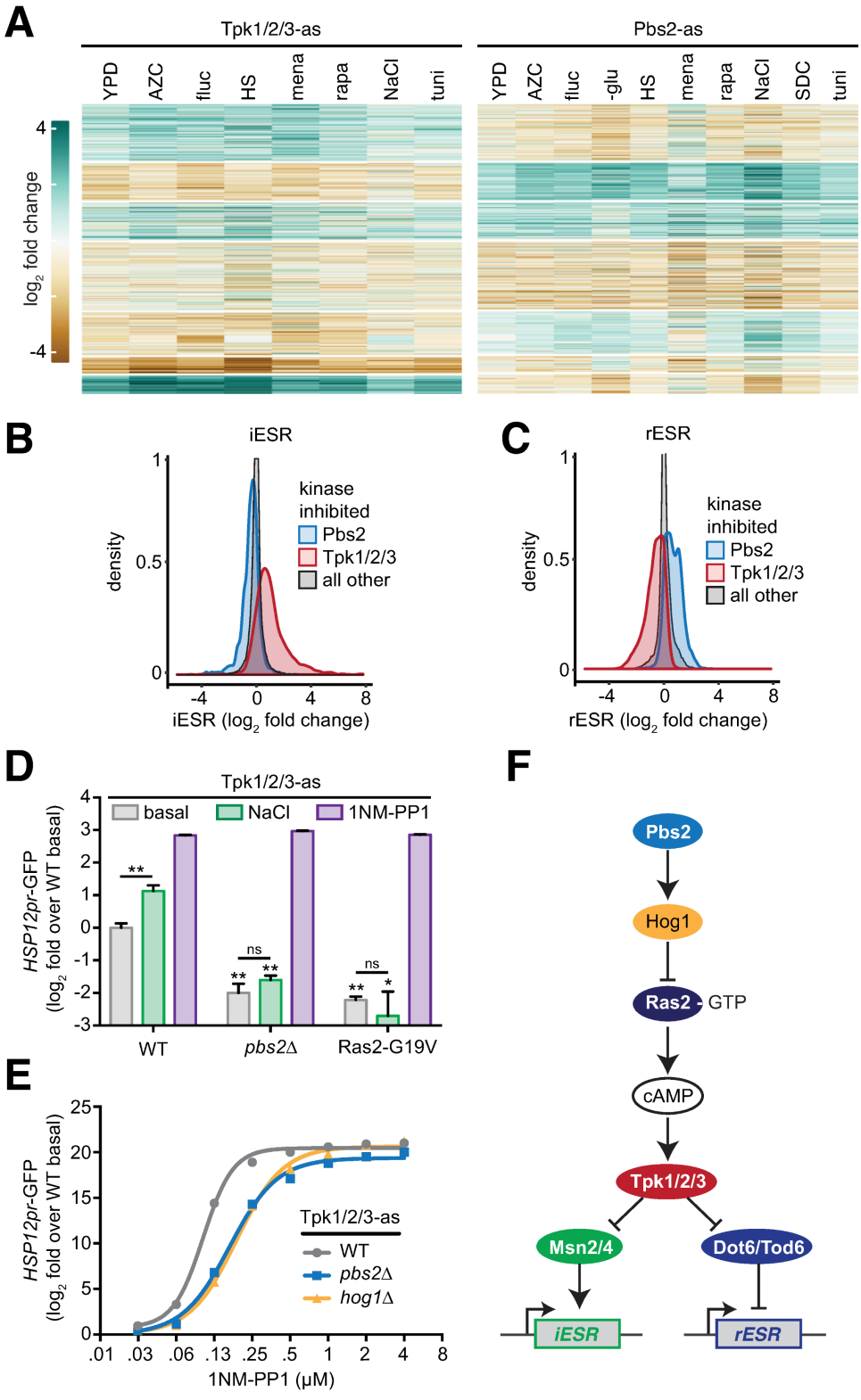

Figure 3.6: The HOG pathway is an upstream negative regulator of Tpk1/2/3 under all conditions

A) Heatmaps showing the genome-wide effects of inhibition of Tpk1/2/3-as and Pbs2-as relative to wild type across the set of environments.

B) Distribution of fold changes for all genes in the iESR in Pbs2-as cells, Tpk1/2/3-as cells and all other strains.
C) As in (B), but for the rESR.
D) A GFP reporter driven by the HSP12 promoter was measured by flow cytometry under basal conditions, following 0.8 M NaCl for 1 hour and following addition of 5 μM 1NM-PP1 for 1 hour in Tpk1/2/3-as cells, Tpk1/2/3-as/pbs2Δ cells and Tpk1/2/3-as/Ras2-G19V cells. The median of 104 cells was measured in triplicate for each condition, and the error bar represents the standard deviation of the replicates.
E) Tpk1/2/3-as, Tpk1/2/3-as/pbs2Δ and Tpk1/2/3-as/hog1Δ cells were subjected to a 1NM-PP1 dose response assay, using the HSP12pr-GFP as a readout. Each concentration of inhibitor was incubated with cells for 1 hour. Measurements performed analyzed as in (D).
F) Proposed architecture of the upstream signaling pathway controlling the ESR.

3.7 TABLES

Table 3.1 Strains used in this study

DPY number	Description	Genotype
1	WT	W303 MATa ADE2
716	Atg1-as	W303 MATa ADE2 atg1Δ::HYG atg1-as::HIS3
1119	Cdc5-as	W303 MATa ADE2 cdc5Δ::HYG cdc5-as::HIS3
1120	Cdc7-as	W303 MATa ADE2 cdc7Δ::HYG cdc7-as::HIS3
1121	Cdc15-as	W303 MATa ADE2 cdc15Δ::HYG cdc1-as::HIS3
1122	Ctk1-as	W303 MATa ADE2 ctk1Δ::HYG ctk1-as::HIS3
719	Fus3-as	W303 MATa ADE2 fus3Δ::HYG fus3-as::HIS3
727	Hog1-as	W303 MATa ADE2 hog1Δ::HYG hog1-as::HIS3
718	Ire1-as	W303 MATa ADE2 ire1Δ::HYG ire1-as::HIS3
1078	Kin1-as	W303 MATa ADE2 kin1Δ::HYG kin1-as::HIS3
1079	Ksp1-as	W303 MATa ADE2 ksp1Δ::HYG ksp1-as::HIS3
720	Kss1-as	W303 MATa ADE2 kss1Δ::HYG kss1-as::HIS3
1088	Mrk1-as	W303 MATa ADE2 mrk1Δ::HYG mrk1-as::HIS3
1089	Pbs2-as	W303 MATa ADE2 pbs2Δ::HYG pbs2-as::HIS3
1213	Pho85-as	W303 MATa ADE2 pho85Δ::HYG pho85-as::HIS3
723	Pkc1-as	W303 MATa ADE2 pkc1Δ::HYG pkc1-as::HIS3
1214	Rim11-as	W303 MATa ADE2 rim11Δ::HYG rim11-as::HIS3
722	Rim15-as	W303 MATa ADE2 rim15Δ::HYG rim15-as::HIS3
724	Sch9-as	W303 MATa ADE2 sch9Δ::HYG sch9-as::HIS3
1198	Slt2-as	W303 MATa ADE2 slt2Δ::HYG slt2-as::HIS3
726	Snf1-as	W303 MATa ADE2 snf1Δ::HYG snf1-as::HIS3
1090	Ssn3-as	W303 MATa ADE2 ssn3Δ::HYG ssn3-as::HIS3

DPY number	Description	Genotype
1091	Ste11-as	W303 MATa ADE2 ste11Δ::HYG ste11-as::HIS3
1069	Tor2-as	W303 MATa ADE2 tor2Δ::HYG tor2-as::HIS3
312	Tpk1/2/3-as	W303 MATa ADE2 tpk1/2/3-as
1066	Yak1-as	W303 MATa ADE2 yak1Δ::HYG yak1-as::HIS3
1067	Ygk3-as	W303 MATa ADE2 ygk3Δ::HYG ygk3-as::HIS3
1068	Ypk1-as	W303 MATa ADE2 ypk1Δ::HYG ypk1-as::HIS3
1101	Ypk3-as	W303 MATa ADE2 ypk3Δ::HYG ypk3-as::HIS3
1378	Tpk1/2/3-as HSP12pr-GFP	W303 MATa ADE2 tpk1/2/3-as HSP12pr-GFP::LEU2
1396	Tpk1/2/3-as hog1Δ HSP12pr-GFP	W303 MATa ADE2 tpk1/2/3-as hog1Δ::HYG HSP12pr-GFP::LEU2
1379	Tpk1/2/3-as pbs2Δ HSP12pr-GFP	W303 MATa ADE2 tpk1/2/3-as pbs2Δ::HYG HSP12pr-GFP::LEU2

REFERENCES

1. Beltrao, P., Cagney, G. & Krogan, N. J. Quantitative genetic interactions reveal biological modularity. *Cell* **141**, 739–45 (2010).
2. Schuldiner, M. *et al.* Exploration of the function and organization of the yeast early secretory pathway through an epistatic miniarray profile. *Cell* **123**, 507–19 (2005).
3. Setty, Y., Mayo, a E., Surette, M. G. & Alon, U. Detailed map of a cis-regulatory input function. *Proc. Natl. Acad. Sci. U. S. A.* **100**, 7702–7 (2003).
4. Anderson, J. C., Voigt, C. a & Arkin, A. P. Environmental signal integration by a modular AND gate. *Mol. Syst. Biol.* **3**, 133 (2007).
5. Louvion, J. F., Havaux-Copf, B. & Picard, D. Fusion of GAL4-VP16 to a steroid-binding domain provides a tool for gratuitous induction of galactose-responsive genes in yeast. *Gene* **131**, 129–134 (1993).
6. McIsaac, R. S. *et al.* Fast-acting and nearly gratuitous induction of gene expression and protein depletion in Saccharomyces cerevisiae. *Mol. Biol. Cell* **22**, 4447–59 (2011).
7. Stewart-Ornstein, J., Weissman, J. S. & El-Samad, H. Cellular noise regulons underlie fluctuations in Saccharomyces cerevisiae. *Mol. Cell* **45**, 483–93 (2012).
8. Ottoz, D. S. M., Rudolf, F. & Stelling, J. Inducible, tightly regulated and growth condition-independent transcription factor in Saccharomyces cerevisiae. *Nucleic Acids Res.* 1–11 (2014).
9. Labow, M. A., Baim, S. B., Shenk, T. & Levine, A. J. Conversion of the lac repressor into an allosterically regulated transcriptional activator for mammalian

cells. *Mol. Cell. Biol.* **10**, 3343–56 (1990).

10. Gossen, M. & Bujard, H. Tight control of gene expression in mammalian cells by tetracycline-responsive promoters. *Proc. Natl. Acad. Sci. U. S. A.* **89**, 5547–51 (1992).
11. Gossen, M. *et al.* Transcriptional activation by tetracyclines in mammalian cells. *Science* **268**, 1766–9 (1995).
12. Qi, L. S. *et al.* Repurposing CRISPR as an RNA-guided platform for sequence-specific control of gene expression. *Cell* **152**, 1173–83 (2013).
13. Hovland, P., Flick, J., Johnston, M. & Sclafani, R. A. Galactose as a gratuitous inducer of GAL gene expression in yeasts growing on glucose. *Gene* **83**, 57–64 (1989).
14. Shimizu-Sato, S., Huq, E., Tepperman, J. M. & Quail, P. H. A light-switchable gene promoter system. *Nat. Biotechnol.* **20**, 1041–4 (2002).
15. Konermann, S. *et al.* Optical control of mammalian endogenous transcription and epigenetic states. *Nature* **500**, 472–6 (2013).
16. Rao, C. V, Wolf, D. M. & Arkin, A. P. Control, exploitation and tolerance of intracellular noise. *Nature* **420**, 231–7 (2002).
17. Samoilov, M. S., Price, G. & Arkin, A. P. From fluctuations to phenotypes: the physiology of noise. *Sci. STKE* **2006**, re17 (2006).
18. Balaban, N. Q., Merrin, J., Chait, R., Kowalik, L. & Leibler, S. Bacterial persistence as a phenotypic switch. *Science* **305**, 1622–5 (2004).
19. Sourjik, V. & Wingreen, N. S. Responding to chemical gradients: bacterial chemotaxis. *Curr. Opin. Cell Biol.* **24**, 262–8 (2012).
20. Spencer, S. L., Gaudet, S., Albeck, J. G., Burke, J. M. & Sorger, P. K. Non-

genetic origins of cell-to-cell variability in TRAIL-induced apoptosis. *Nature* **459**, 428–32 (2009).

21. Delbrück, M. The Burst Size Distribution in the Growth of Bacterial Viruses (Bacteriophages). *J. Bacteriol.* **50**, 131–5 (1945).

22. Burnett, J. C., Miller-Jensen, K., Shah, P. S., Arkin, A. P. & Schaffer, D. V. Control of stochastic gene expression by host factors at the HIV promoter. *PLoS Pathog.* **5**, e1000260 (2009).

23. Tanouchi, Y. *et al.* A noisy linear map underlies oscillations in cell size and gene expression in bacteria. *Nature* **523**, 357–60 (2015).

24. Ozbudak, E. M., Thattai, M., Kurtser, I., Grossman, A. D. & van Oudenaarden, A. Regulation of noise in the expression of a single gene. *Nat. Genet.* **31**, 69–73 (2002).

25. Murphy, K. F., Balázsi, G. & Collins, J. J. Combinatorial promoter design for engineering noisy gene expression. *Proc. Natl. Acad. Sci. U. S. A.* **104**, 12726–12731 (2007).

26. Tabor, J. J., Bayer, T. S., Simpson, Z. B., Levy, M. & Ellington, A. D. Engineering stochasticity in gene expression. *Mol. Biosyst.* **4**, 754–61 (2008).

27. Hooshangi, S., Thiberge, S. & Weiss, R. Ultrasensitivity and noise propagation in a synthetic transcriptional cascade. *Proc. Natl. Acad. Sci. U. S. A.* **102**, 3581–6 (2005).

28. Murphy, K. F., Adams, R. M., Wang, X., Balázsi, G. & Collins, J. J. Tuning and controlling gene expression noise in synthetic gene networks. *Nucleic Acids Res.* **38**, 2712–26 (2010).

29. Hung, M. *et al.* Modulating the frequency and bias of stochastic switching to

control phenotypic variation. *Nat. Commun.* **5**, 4574 (2014).

30. Braselmann, S., Graninger, P. & Busslinger, M. A selective transcriptional induction system for mammalian cells based on Gal4-estrogen receptor fusion proteins. *Proc. Natl. Acad. Sci. U. S. A.* **90**, 1657–61 (1993).
31. Wang, Y., O'Malley, B. W. & Tsai, S. Y. A regulatory system for use in gene transfer. *Proc. Natl. Acad. Sci. U. S. A.* **91**, 8180–4 (1994).
32. Wang, Y., Xu, J., Pierson, T., O'Malley, B. W. & Tsai, S. Y. Positive and negative regulation of gene expression in eukaryotic cells with an inducible transcriptional regulator. *Gene Ther.* **4**, 432–41 (1997).
33. Pratt, W. B. The hsp90-based chaperone system: involvement in signal transduction from a variety of hormone and growth factor receptors. *Proc. Soc. Exp. Biol. Med.* **217**, 420–434 (1998).
34. Smith, D. F. & Toft, D. O. Minireview: the intersection of steroid receptors with molecular chaperones: observations and questions. *Mol. Endocrinol.* **22**, 2229–2240 (2008).
35. McIsaac, R. S. *et al.* Synthetic gene expression perturbation systems with rapid, tunable, single-gene specificity in yeast. *Nucleic Acids Res.* **41**, e57 (2013).
36. Bram, R. J. & Kornberg, R. D. Specific protein binding to far upstream activating sequences in polymerase II promoters. *Proc. Natl. Acad. Sci. U. S. A.* **82**, 43–47 (1985).
37. Giniger, E., Varnum, S. M. & Ptashne, M. Specific DNA binding of GAL4, a positive regulatory protein of yeast. *Cell* **40**, 767–774 (1985).
38. Zuleta, I., Aranda-Díaz, A., Li, H. & El-Samad, H. Dynamic characterization of growth and gene expression using high-throughput automated flow cytometry.

Nat. Methods **11**, 443–8 (2014).

39. Pichon, M. F. & Milgrom, E. Characterization and Assay of Progesterone Receptor in Human Mammary Carcinoma Characterization and Assay of Progesterone Receptor in Human Mammary Carcinoma1. 464–471 (1977).
40. Bardwell, L. A walk-through of the yeast mating pheromone response pathway. *Peptides* **25**, 1465–76 (2004).
41. Kim, J., Couve, A. & Hirsch, J. P. Receptor inhibition of pheromone signaling is mediated by the Ste4p Gbeta subunit. *Mol. Cell. Biol.* **19**, 441–9 (1999).
42. Tedford, K., Kim, S., Sa, D., Stevens, K. & Tyers, M. Regulation of the mating pheromone and invasive growth responses in yeast by two MAP kinase substrates. *Curr. Biol.* **7**, 228–38 (1997).
43. Doi, K. *et al.* MSG5, a novel protein phosphatase promotes adaptation to pheromone response in S. cerevisiae. *EMBO J.* **13**, 61–70 (1994).
44. Nomoto, S., Nakayama, N., Arai, K. & Matsumoto, K. Regulation of the yeast pheromone response pathway by G protein subunits. *EMBO J.* **9**, 691–6 (1990).
45. McCullagh, E., Seshan, A., El-Samad, H. & Madhani, H. D. Coordinate control of gene expression noise and interchromosomal interactions in a MAP kinase pathway. *Nat. Cell Biol.* **12**, 954–62 (2010).
46. Takahashi, S. & Pryciak, P. M. Membrane Localization of Scaffold Proteins Promotes Graded Signaling in the Yeast MAP Kinase Cascade. *Curr. Biol.* **18**, 1184–1191 (2008).
47. Peter, M., Gartner, A., Horecka, J., Ammerer, G. & Herskowitz, I. FAR1 links the signal transduction pathway to the cell cycle machinery in yeast. *Cell* **73**, 747–60 (1993).

48. Blake, W. J., Kaern, M., Cantor, C. R. & Collins, J. J. Noise in eukaryotic gene expression. *Nature* **422**, 633–7 (2003).

49. Raser, J. M. & O'Shea, E. K. Control of stochasticity in eukaryotic gene expression. *Science* **304**, 1811–4 (2004).

50. Schwob, E., Böhm, T., Mendenhall, M. D. & Nasmyth, K. The B-type cyclin kinase inhibitor p40SIC1 controls the G1 to S transition in S. cerevisiae. *Cell* **79**, 233–44 (1994).

51. Nugroho, T. T. & Mendenhall, M. D. An inhibitor of yeast cyclin-dependent protein kinase plays an important role in ensuring the genomic integrity of daughter cells. *Mol. Cell. Biol.* **14**, 3320–8 (1994).

52. García-Rodríguez, L. J., Valle, R., Durán, A. & Roncero, C. Cell integrity signaling activation in response to hyperosmotic shock in yeast. *FEBS Lett.* **579**, 6186–90 (2005).

53. Pincus, D., Aranda-Díaz, A., Zuleta, I. A., Walter, P. & El-Samad, H. Delayed Ras/PKA signaling augments the unfolded protein response. *Proc. Natl. Acad. Sci. U. S. A.* **111**, 14800–5 (2014).

54. Elowitz, M. B., Levine, A. J., Siggia, E. D. & Swain, P. S. Stochastic gene expression in a single cell. *Science* **297**, 1183–6 (2002).

55. Paulsson, J. Summing up the noise in gene networks. *Nature* **427**, 415–8 (2004).

56. Paulsson, J. Models of stochastic gene expression. *Phys. Life Rev.* **2**, 157–175 (2005).

57. Gasch, A. P. *et al.* Genomic Expression Programs in the Response of Yeast Cells to Environmental Changes. *Mol. Biol. Cell* (2000). doi:10.1091/mbc.11.12.4241

58. Berry, D. B. & Gasch, A. P. Stress-activated Genomic Expression Changes Serve

a Preparative Role for Impending Stress in Yeast. *Mol. Biol. Cell* (2008). doi:10.1091/mbc.E07-07-0680

59. Loewith, R. & Hall, M. N. Target of rapamycin (TOR) in nutrient signaling and growth control. *Genetics* (2011). doi:10.1534/genetics.111.133363

60. Morano, K. A., Grant, C. M. & Moye-Rowley, W. S. The response to heat shock and oxidative stress in saccharomyces cerevisiae. *Genetics* (2012). doi:10.1534/genetics.111.128033

61. Saito, H. & Posas, F. Response to hyperosmotic stress. *Genetics* (2012). doi:10.1534/genetics.112.140863

62. Shamu, C. E. & Walter, P. Oligomerization and phosphorylation of the Ire1p kinase during intracellular signaling from the endoplasmic reticulum to the nucleus. *EMBO J.* (1996). doi:10.1002/j.1460-2075.1996.tb00666.x

63. Kobayashi, N. & McEntee, K. Identification of cis and trans components of a novel heat shock stress regulatory pathway in Saccharomyces cerevisiae. *Mol. Cell. Biol.* (1993). doi:10.1128/MCB.13.1.248.Updated

64. Jonikas, M. C. *et al.* Comprehensive characterization of genes required for protein folding in the endoplasmic reticulum. *Science (80-.).* (2009). doi:10.1126/science.1167983

65. Brandman, O. *et al.* A Ribosome-Bound Quality Control Complex Triggers Degradation of Nascent Peptides and Signals Translation Stress. *Cell* (2012). doi:10.1016/j.cell.2012.10.044

66. Breitkreutz, A. *et al.* A global protein kinase and phosphatase interaction network in yeast. *Science (80-.).* (2010). doi:10.1126/science.1176495

67. Van Wageningen, S. *et al.* Functional overlap and regulatory links shape genetic

interactions between signaling pathways. *Cell* (2010). doi:10.1016/j.cell.2010.11.021

68. Fiedler, D. *et al.* Functional Organization of the S. cerevisiae Phosphorylation Network. *Cell* (2009). doi:10.1016/j.cell.2008.12.039

69. Martin, H. *et al.* Differential genetic interactions of yeast stress response MAPK pathways. *Mol. Syst. Biol.* (2015). doi:10.15252/msb.20145606

70. Bishop, A. C. *et al.* A chemical switch for inhibitor-sensitive alleles of any protein kinase. *Nature* (2000). doi:10.1038/35030148

71. Dobin, A. *et al.* STAR: Ultrafast universal RNA-seq aligner. *Bioinformatics* (2013). doi:10.1093/bioinformatics/bts635

72. Love, M. I., Anders, S. & Huber, W. *Differential analysis of count data - the DESeq2 package*. *Genome Biology* (2014). doi:110.1186/s13059-014-0550-8

73. Van Der Maaten, L. & Hinton, G. Visualizing Data using t-SNE. *J. Mach. Learn. Res.* (2008). doi:10.1007/s10479-011-0841-3

74. Cox, J. S., Shamu, C. E. & Walter, P. Transcriptional induction of genes encoding endoplasmic reticulum resident proteins requires a transmembrane protein kinase. *Cell* (1993). doi:10.1016/0092-8674(93)90648-A

75. Solís, E. J. *et al.* Defining the Essential Function of Yeast Hsf1 Reveals a Compact Transcriptional Program for Maintaining Eukaryotic Proteostasis. *Mol. Cell* (2016). doi:10.1016/j.molcel.2016.05.014

76. Hahn, J. S. & Thiele, D. J. Activation of the Saccharomyces cerevisiae Heat Shock Transcription Factor under Glucose Starvation Conditions by Snf1 Protein Kinase. *J. Biol. Chem.* (2004). doi:10.1074/jbc.M311005200

77. Zheng, X. *et al.* Dynamic control of Hsf1 during heat shock by a chaperone switch

and phosphorylation. *Elife* (2016). doi:10.7554/eLife.18638

78. Westfall, P. J., Ballon, D. R. & Thorner, J. When the stress of your environment makes you go HOG wild. *Science* (2004). doi:10.1126/science.1104879

79. O'Rourke, S. M. & Herskowitz, I. The Hog1 MAPK prevents cross talk between the HOG and pheromone response MAPK pathways in Saccharomyces cerevisiae. *Genes Dev.* (1998). doi:10.1101/gad.12.18.2874

80. Capaldi, A. P. *et al.* Structure and function of a transcriptional network activated by the MAPK Hog1. *Nat. Genet.* (2008). doi:10.1038/ng.235

81. Hersen, P., McClean, M. N., Mahadevan, L. & Ramanathan, S. Signal processing by the HOG MAP kinase pathway. *Proc. Natl. Acad. Sci.* **105**, 7165–7170 (2008).

82. Tong, A. H. Y. *et al.* Global Mapping of the Yeast Genetic Interaction Network. *Science (80-.).* (2004). doi:10.1126/science.1091317

83. Schuldiner, M. *et al.* Exploration of the function and organization of the yeast early secretory pathway through an epistatic miniarray profile. *Cell* (2005). doi:10.1016/j.cell.2005.08.031

84. Görner, W. *et al.* Nuclear localization of the C2H2zinc finger protein Msn2p is regulated by stress and protein kinase A activity. *Genes Dev.* (1998). doi:10.1101/gad.12.4.586

85. Sadeh, A., Movshovich, N., Volokh, M., Gheber, L. & Aharoni, A. Fine-tuning of the Msn2/4-mediated yeast stress responses as revealed by systematic deletion of Msn2/4 partners. *Mol. Biol. Cell* (2011). doi:10.1091/mbc.E10-12-1007

86. Hao, N. & O'Shea, E. K. Signal-dependent dynamics of transcription factor translocation controls gene expression. *Nat. Struct. Mol. Biol.* (2012). doi:10.1038/nsmb.2192

87. Lee, B. N. & Elion, E. A. The MAPKKK Ste11 regulates vegetative growth through a kinase cascade of shared signaling components. *Proc. Natl. Acad. Sci. U. S. A.* (1999). doi:10.1073/PNAS.96.22.12679

88. Aiken, C. T., Kaake, R. M., Wang, X. & Huang, L. Oxidative Stress-Mediated Regulation of Proteasome Complexes. *Mol. Cell. Proteomics* (2011). doi:10.1074/mcp.M110.006924

89. McLeay, R. C. & Bailey, T. L. Motif Enrichment Analysis: A unified framework and an evaluation on ChIP data. *BMC Bioinformatics* (2010). doi:10.1186/1471-2105-11-165

90. Mathelier, A. *et al.* JASPAR 2016: A major expansion and update of the open-access database of transcription factor binding profiles. *Nucleic Acids Res.* (2016). doi:10.1093/nar/gkv1176

91. Huber, A. *et al.* Sch9 regulates ribosome biogenesis via Stb3, Dot6 and Tod6 and the histone deacetylase complex RPD3L. *EMBO J.* (2011). doi:10.1038/emboj.2011.221

92. Martínez-Pastor, M. T. *et al.* The Saccharomyces cerevisiae zinc finger proteins Msn2p and Msn4p are required for transcriptional induction through the stress response element (STRE). *EMBO J.* (1996). doi:10.1002/j.1460-2075.1996.tb00576.x

93. Schmitt, A. P. & McEntee, K. Msn2p, a zinc finger DNA-binding protein, is the transcriptional activator of the multistress response in *Saccharomyces cerevisiae*. *Proc. Natl. Acad. Sci. U. S. A.* (1996). doi:10.1073/pnas.93.12.5777

94. Lippman, S. I. & Broach, J. R. Protein kinase A and TORC1 activate genes for ribosomal biogenesis by inactivating repressors encoded by Dot6 and its homolog

Tod6. *Proc. Natl. Acad. Sci. U. S. A.* (2009). doi:10.1073/pnas.0907027106

95. Gutin, J., Sadeh, A., Rahat, A., Aharoni, A. & Friedman, N. Condition-specific genetic interaction maps reveal crosstalk between the cAMP/PKA and the HOG MAPK pathways in the activation of the general stress response. *Mol Syst Biol* (2015). doi:10.15252/msb.20156451

96. Pincus, D., Aranda-Diaz, A., Zuleta, I. A., Walter, P. & El-Samad, H. Delayed Ras/PKA signaling augments the unfolded protein response. *Proc. Natl. Acad. Sci.* (2014). doi:10.1073/pnas.1409588111

97. Zuleta, I. a, Aranda-Díaz, A., Li, H. & El-Samad, H. Dynamic characterization of growth and gene expression using high-throughput automated flow cytometry. *Nat. Methods* (2014). doi:10.1038/nmeth.2879

98. Thevelein, J. M. & De Winde, J. H. Novel sensing mechanisms and targets for the cAMP-protein kinase A pathway in the yeast Saccharomyces cerevisiae. *Molecular Microbiology* (1999). doi:10.1046/j.1365-2958.1999.01538.x

99. Creixell, P. *et al.* Hierarchical Organization Endows the Kinase Domain with Regulatory Plasticity. *Cell Syst.* (2018). doi:10.1016/j.cels.2018.08.008

100. Raser, J. M. & O'Shea, E. K. Control of stochasticity in eukaryotic gene expression. *Science* **304**, 1811–1814 (2004).

101. Causton, H. C. *et al.* Remodeling of Yeast Genome Expression in Response to Environmental Changes. *Mol. Biol. Cell* (2001). doi:10.1091/mbc.12.2.323

102. Hansen, A. S. & O'Shea, E. K. Promoter decoding of transcription factor dynamics involves a trade-off between noise and control of gene expression. *Mol. Syst. Biol.* **9**, (2013).

103. Smith, A., Ward, M. P. & Garrett, S. Yeast PKA represses Msn2p/Msn4p-

dependent gene expression to regulate growth, stress response and glycogen accumulation. *EMBO J.* (1998). doi:10.1093/emboj/17.13.3556

104. Kemmeren, P. *et al.* Large-scale genetic perturbations reveal regulatory networks and an abundance of gene-specific repressors. *Cell* **157**, 740–752 (2014).
105. Collins, S. R., Schuldiner, M., Krogan, N. J. & Weissman, J. S. A strategy for extracting and analyzing large-scale quantitative epistatic interaction data. *Genome Biol.* (2006). doi:10.1186/gb-2006-7-7-r63
106. Lopez, M. S., Kliegman, J. I. & Shokat, K. M. The logic and design of analog-sensitive kinases and their small molecule inhibitors. *Methods Enzymol.* (2014). doi:10.1016/B978-0-12-397918-6.00008-2
107. Longtine, M. S. *et al.* Additional modules for versatile and economical PCR-based gene deletion and modification in Saccharomyces cerevisiae. *Yeast* (1998). doi:10.1002/(SICI)1097-0061(199807)14:10<953::AID-YEA293>3.0.CO;2-U
108. Cherry, J. M. *et al.* SGD: Saccharomyces genome database. *Nucleic Acids Res.* (1998). doi:10.1093/nar/26.1.73

Publishing Agreement

It is the policy of the University to encourage open access and broad distribution of all theses, dissertations, and manuscripts. The Graduate Division will facilitate the distribution of UCSF theses, dissertations, and manuscripts to the UCSF Library for open access and distribution. UCSF will make such theses, dissertations, and manuscripts accessible to the public and will take reasonable steps to preserve these works in perpetuity.

I hereby grant the non-exclusive, perpetual right to The Regents of the University of California to reproduce, publicly display, distribute, preserve, and publish copies of my thesis, dissertation, or manuscript in any form or media, now existing or later derived, including access online for teaching, research, and public service purposes.

DocuSigned by:
Kieran Mace
D7A346BA2439430...
Author Signature

9/1/2021
Date